“Anything truly worth anything isn’t going to come easily.”

- Ronald Breedon

GRAVE OR GUT: EXPLORATION INTO BACTERIAL BIOEROSION AND BONE DECOMPOSITION IN AN 18TH-19TH CENTURY ATLANTIC CANADIAN CEMETERY

by

Nicole Breedon

Bachelor of Arts (Honours), Trent University, 2018

A Thesis Submitted in Partial Fulfillment of the Requirements for the Degree of

Master of Arts

In the Graduate Academic Unit of Anthropology

Supervisor:	Amy Scott, PhD, Anthropology
Examining Board:	Gabriel Hrynick, PhD, Anthropology (Chair) Tracy Betsinger, PhD, Anthropology Ben Newling, PhD, Physics

This thesis is accepted by the Dean of Graduate Students

THE UNIVERSITY OF NEW BRUNSWICK

June, 2022

ABSTRACT

Bioarchaeology is the study of human skeletal remains from archaeological contexts to explore the lived experience of past populations. Bone is a dynamic, living tissue. Whether growing and developing throughout life, or decomposing after death, changes to the skeleton occur in predictable patterns. Microscopic analyses of how bone structure degrades after death can tell us about the life of the individual, specifically their bacterial load within the digestive tract. This thesis utilized microscopic X-ray Computed Tomography (micro-CT) technology to create a new method in the assessment of skeletal remains as it pertains to a unique type of skeletal degeneration known as bacterial bioerosion. While this type of research has never been conducted within the Canadian Maritimes before, the method created was used to positively identify evidence of bacterial bioerosion in the skeletal remains of five of the seven assessed individuals from an 18th -19th century Atlantic Canadian cemetery.

ACKNOWLEDGMENTS

My deepest and most sincere gratitude goes to my supervisor, Dr. Amy Scott. I am so incredibly grateful for the constant encouragement, support, and understanding during the course of this research. For all her time and guidance, I will be forever appreciative. I would also like to thank Dr. Andrew Nelson for all of his assistance during microscopic Computed Tomography training and access to the resources at the Museum of Ontario Archaeology. My appreciation is also extended to Dr. Tracy Betsinger for her insights regarding research and the friendly nature of academic networking. A thank you for Dr. Gabe Hrynick who was the committee chair during my thesis defence. I would also like to acknowledge Dr. Ben Newling for the time he dedicated to review my thesis. I would like to share my appreciation for Valerie Macdonald and the members of the Presbyterian Church of St. David who granted permissions to conduct this research with the Methodist Church skeletal assemblage. A warm thank you is extended to Judy Babin who always brightened my days in the Anthropology Annex, as well as my fellow friends in the graduate program. I would like to thank Ron and Gwen Breedon, Michael Desjarlais, Coralie Jays, Samantha Cabat and the rest of my family for their constant encouragement (and patience while listening to me read fractions of my thesis aloud). I could not have done this without your unconditional love. I would also extend the warmest regards Mackenzie Condon, Nicole Hughes, Alexandra Mackay, Laura Schmidt, and Alyssa Simms. I am indescribably grateful for their validation and support through these precarious years. Finally, I would like to thank Vince McFadyen for supporting me and my goals, keeping me grounded in times of distress, and reminding me that every day is a gift.

TABLE OF CONTENTS

LIST OF TABLES

LIST OF FIGURES

CHAPTER 3 – Materials and Methods Figures

CHAPTER 4 – Results Figures

CHAPTER 5 – Discussion Figures

LIST OF APPENDICIES

CHAPTER 1 – Introduction

1.1 Background and Significance

The study of human skeletal remains in an archeological context represents an immense resource for understanding and interpreting past populations. As a dynamic living tissue, the human skeleton is in a constant state of growth and development that occurs in a relatively predictable pattern. Therefore, by identifying skeletal variation that deviates from this expected trajectory of maturation, it is possible to determine whether a person was affected by disease, trauma, biological stress, or any other factor disrupting normal skeletal development (Turner-Walker, 2012; Agarwal, 2016; Lewis, 2018; Eriksen et al., 2020). These assessments are vital in the interpretation of the individual lived experience; however, recent research has argued that assessments of skeletal degeneration after death are equally as important in understanding the human skeleton and what it can tell us about the past (Turner-Walker, 2012; Agarwal, 2016; Lewis, 2018; Eriksen et al., 2020).

Osteological tissue degenerates on a relatively predictable trajectory after death. However, various factors such as funerary treatment, the timing of burial after death, and conditions of the burial environment (e.g., soil acidity and hydrology) can interrupt soft and hard tissue decomposition, altering the typical processes of bone degeneration (Pinheiro, 2006; Turner-Walker, 2012; Delannoy et al., 2018; Hemer et al., 2021). Known as the process of diagenesis, research into how osteological tissue physically and chemically degenerates after death has become a significant point of interest in bioarchaeological research (Turner-Walker, 2008; White et al., 2012; Christensen et al., 2019a).

Microbial bioerosion is a type of diagenetic change that manifests as microbial tunnels – also described as deteriorating pores – throughout the cortical tissue of bone due to bacterial or fungal microorganisms (microbes) (Turner-Walker and Syversen, 2002; Turner-Walker, 2012; Jans, 2013; Booth, 2015; Booth et al., 2016; Bronnimann et al., 2018). Since the 19th century, biological anthropologists have studied microbial bioerosion in the hopes of better understanding how morphological variations in internal bone degeneration relate to the burial environment. Bacterial bioerosion is a specific type of microbial bioerosion caused by endogenous bacteria that build up within the digestive tract as an individual consumes food during life. Therefore, the assessment of bacterial bioerosion and diagenetic changes captured within the cortical tissue may help bioarchaeologists better understand bacterial load as it relates to the gut and to patterns of overall health within the population.

Traditionally, the application of histological thin section analysis has been used in bacterial bioerosion research (see Hackett, 1981; Bell et al., 1996; Jans, 2008, 2013; Turner-Walker, 2008, 2012; White and Booth, 2014; Booth, 2015; 2017; Booth et al., 2016); however, this method is destructive and not always preferred when conducting bioarchaeological research. Therefore, this thesis focuses on utilizing non-destructive microscopic X-ray Computed Tomography (micro-CT) technology to assess skeletal diagenesis, specifically bacterial bioerosion, in non-adult skeletal remains.

1.2 Objectives and Research Questions

The goal of this thesis is to determine whether micro-CT technology can be used independently from traditional methods (i.e., histology) to assess bacterial bioerosion, as

well as provide additional interpretive information regarding patterns of microbial tunnel development in cortical bone. The three research questions guiding this thesis are:

1. Can micro-CT methods be used independently from histological analysis to accurately identify and assess bacterial bioerosion in osteological tissue?
2. Is the development of bacterial bioerosion in cortical bone associated with factors such as cortical preservation or the age of the individual?
3. Does bacterial bioerosion develop consistently within specific skeletal elements and/or across the entire skeleton?

1.3 Thesis Outline

This thesis is comprised of six chapters. The Introduction chapter has briefly discussed the value of the proposed research as well as the objectives of this study. The second chapter is a literature review which discusses the history of microbial bioerosion research and how the composition of bone is related to bacterial bioerosion development. A review of micro-CT technology and its application in the study of bacterial bioerosion is also provided. The Literature Review concludes with a brief history of Halifax and the cemetery used in this study. Chapter Three will review the materials and methods used in this research, beginning with an overview of the permissions required to access the skeletal assemblage, as well as what skeletal elements were sampled for micro-CT imaging. Chapter Three will also outline how micro-CT images were captured and rendered, and how osteological tissue was assessed when determining the presence or absence of bacterial bioerosion. Chapter Four presents the results of this research. This will include the metric analyses of microbial tunnel diameter size, morphological analyses of microbial tunnel development, trends identified

in the development of bacterial bioerosion, and individual skeletal assessments. Chapter Five is the Discussion and explores the results of this thesis, specifically the metric and morphological traits assessed and the various patterns that emerged. This chapter will also reflect on the relationship between bacterial bioerosion and various factors that may impact its development such as cortical preservation, age, and pathological conditions. This will lead to a discussion of the results from each individual assessed and conclude with a review of the limitations of micro-CT technology in the study of bacterial bioerosion. Finally, Chapter Six will provide a summary of the data collected throughout this research as well as revisit the thesis objectives and research questions. This chapter will conclude with suggestions for future research as it pertains to bacterial bioerosion analyses.

CHAPTER 2 – Literature Review

2.1 Introduction

This literature review will be comprised of six sections providing the necessary background information on microbial bioerosion and its identification in osteological remains. Section 2.2 will discuss the composition and structure of skeletal tissue as well as introduce the processes of skeletal diagenesis. Section 2.3 will outline the history of microbial bioerosion research in bioarchaeological studies as well as discuss the endogenous model of microbial bioerosion. Section 2.4 will provide a discussion on how microscopic-Computer Tomography (micro-CT) technology works and how it can be used to assess microbial bioerosion. Building on this, section 2.5 will focus on the factors and circumstances which may impact the formation of microbial bioerosion in osteological tissues. Section 2.6 will review the early life development of the human microbiome, followed by an interdisciplinary discussion of the mother-infant nexus. In conclusion, the final section will provide a brief historical overview of Halifax during the 18th and 19th centuries, aimed to build a foundational understanding of what life might have been like for the individuals sampled for this study.

2.2 Skeletal Tissue: Composition and Structure

Bone is a significantly complex material in composition and structure. All osteological tissue is comprised of organic material (i.e., collagen), which allows for bone flexibility and inorganic mineral (i.e., hydroxyapatite), which develops within the collagen matrix to reinforce the structural rigidity of bone (White et al., 2012; Cunningham et al., 2016). There are two types of bone tissue: cortical tissue and

trabecular tissue (White et al., 2012; Milovanovic et al., 2017; Kendall, 2018). Cortical tissue makes up the dense external surface of bone, whereas the sponge-like trabecular tissue makes up the interior component of bone (White et al., 2012; Cunningham et al., 2016; Milovanovic et al., 2017; Kendall, 2018).

For both bone tissues to function properly, they must be supplied with blood and nutrients (White et al., 2012; Milovanovic et al., 2017). In cortical bone, Haversian systems transmit blood and nutrients to the bone cells through an elaborate labyrinth of vertical and horizontal canals connected to the exterior surface of the bone through small nutrient foramina (White et al., 2012; Milovanovic et al., 2017). In contrast, due to the honeycomb structure of trabecular bone, blood and nutrients easily diffuse in this spongy tissue from the vessels incorporated into the Haversian systems in the overlaying cortical bone (White et al., 2012). While these latticework systems play a significant role in the maintenance of skeletal tissues during life, they also influence skeletal diagenesis after death.

Skeletal diagenesis is the study of how bone physically, biologically, and chemically degrades after death (Turner-Walker, 2008; White et al., 2012; Christensen et al., 2019a). Diagenetic trajectories are relatively predictable but vary depending on environmental conditions (Turner-Walker, 2012; Kendall, 2018; Kontopoulos et al., 2019). Therefore, the study of skeletal diagenesis can contribute to our understanding of the relationship between skeletal tissue, the burial environment, and events that may have taken place around the time of death (Hollund et al., 2012; Turner-Walker, 2012; White & Booth, 2014; Booth, 2017; Christensen et al., 2019a; Eriksen et al., 2020). A

specific form of skeletal diagenesis known as biological-erosion or bioerosion will be the focus of this study.

2.3 The History of Microbial Bioerosion Research

Bioerosion refers to all structural alterations to bone caused by biological agents such as micro-organisms (microbes), animals, and plant growth (Turner-Walker, 2012); however, the role of microbes in bone degeneration has dominated much of the diagenetic literature since the late 19th century (see Hackett, 1981; Bell et al., 1996; Jans, 2008; Bronnimann et al., 2018). Microbial bioerosion was first identified in 1864 by Carl Wedl, who identified deteriorating pores extending from the naturally occurring Haversian systems in cortical bone through histological thin section analysis (Wedl, 1864). Wedl argued that these unique deteriorating pores were the result of long-term exposure to environmental microbes and formally titled them as Wedl tunnels, which can also be described as microbial tunnels (Wedl, 1864; Jans, 2008; Turner-Walker, 2012; Bronnimann et al., 2018). This presumed relationship between tunnel development and environmental microbes was accepted for over one hundred years until further research demonstrated that Wedl's hypothesis was only partially correct, and microbial diagenesis was much more complex than previously suspected.

In 1981 the work of Cecile Hackett expanded on Wedl's theory by exploring the variation in microbial tunnel formation (Hackett, 1981). In this research, Hackett determined that there are two distinct classes of microbial tunnels which can be differentiated from one another based on size and morphological structure: Wedl tunnels and non-Wedl tunnels (Hackett, 1981; Nielsen-Marsh and Hedges, 2000). Wedl tunnels were believed to be the result of *fungal* microbes found within the surrounding burial

environment and developed on the external surface of cortical tissue (Hackett, 1981). These tunnels were branch-like in formation and had diameters ranging between 5-15 micrometers (μm) (Hackett, 1981). In contrast, non-Wedl tunnels were believed to be the result of *bacterial* microbes found within the surrounding burial environment and developed throughout the internal structures of cortical tissue (Hackett, 1981). These tunnels could manifest in three different forms: linear-longitudinal, lamellate, or budded microbial tunnels with diameters ranging between 5-60 μm (Hackett, 1981). Based on this distinction, 'microbial' bioerosion was used to describe tunnels caused by any bone degenerating microbe, whereas 'bacterial' bioerosion was used exclusively to describe tunnels caused specifically by bacterial microbes.

Through their work, both Wedl and Hackett asserted that all forms of microbial bioerosion were the result of environmental microbes. Therefore, diagenetic research was conducted using skeletonized remains, rather than the remains from individuals who still had soft tissue intact (Bell, 2012; Jans, 2013; Bronnimann et al., 2018). Lynne Bell and colleagues (1996) were the first to challenge this long-held assumption in the mid-1990s. By studying the diagenetic patterns of bones before the body was completely skeletonized, they determined that traces of non-Wedl tunnels could develop in skeletal remains within the first few days after death (Bell et al., 1996; Bronnimann et al., 2018). This stood in contrast to the work of Wedl and Hackett, as bacteria from the environment would not have been able to reach the skeletal tissue of these non-skeletonized individuals prior to analysis (Bell et al., 1996; Bronnimann et al., 2018).

This finding resulted in a drastic shift in the understanding of microbial bioerosion. Bell and colleagues (1996) argued that Wedl microbial tunneling represented

the exogenous model of microbial bioerosion, where diagenetic changes to skeletal tissue were the result of environmental factors (see Table 1) (i.e., cyanobacteria and fungal microbes) (Bell et al., 1996; Jans, 2008; Sasso et al., 2014; Booth et al., 2016; Bronnimann et al., 2018). In contrast, non-Wedl microbial tunneling represented the endogenous model of microbial bioerosion, where bacteria within the human microbiome were the main catalyst in skeletal diagenesis (see Table 1) (Bell et al., 1996; Jans, 2008; Sasso et al., 2014; Booth et al., 2016; Bronnimann et al., 2018).

Table 1: Microbial bioerosion classification and affiliated tunnel diameter

Microbial Bioerosion Classification	Source of Causative Microbes	Form of Microbial Tunnel	Typical Tunnel Diameter
Wedl	Environmental	Branched	5-15 µm
Non-Wedl	Endogenous	Linear-longitudinal	5-10 µm
		Lamellate	10-60 µm
		Budded	30-60 µm

2.3.1 The Endogenous Model of Microbial Bioerosion

The human microbiome accounts for all micro-organisms that reside within the human body during life (Benezra, 2012; Knight et al., 2017; Kennedy et al., 2021). These bacteria live symbiotically within human hosts and assist in the maintenance of many bodily functions such as immune defence, elasticity of the epidermis, etc. (Althani et al., 2015; Beasley et al., 2015; Kennedy et al., 2021). Different groups of bacteria may be identified in different regions of the body, and the term microbiota is used to differentiate regionally specific communities of microbes (Benezra et al., 2012; Althani et al., 2015; Knight et al., 2017). The gut microbiota refers to all the microbes that reside within the digestive tract, from the esophagus to the anus (Knight et al., 2017). While the gut microbiota contributes to healthy digestive functions such as nutrient absorption and

pathogen displacement during life, it is also the catalyst for bacterial bioerosion after soft tissue decomposition (Bell et al., 1996; Jans, 2008; Daman and Carter, 2013; Benezra et al., 2012; Jans, 2013; Sasso et al., 2014; White and Booth, 2014; Booth et al., 2016; Bronnimann et al., 2018).

There are two major events that occur during decomposition: autolysis and putrefaction (Clark et al., 1996; Daman and Carter, 2013; Finley et al., 2015; Christensen et al., 2019a). Autolysis begins immediately after death when cells begin to digest themselves, breaking down the structural integrity of the soft tissues and giving way to putrefaction (Clark et al., 1996; Daman and Carter, 2013; Finley et al., 2015; Christensen et al., 2019a). Putrefaction begins when the various microbiota are released from their biologically specific systems due to the degeneration of surrounding soft tissues, such as the mucosal lining of the digestive organs (Jans, 2008; White and Booth, 2014; Booth, 2015; Finley et al., 2015; Christensen et al., 2019a). During putrefaction, microbes transmigrate through the circulatory system, multiply and attack the remaining soft tissues (Finley et al., 2015; Booth, 2017; Christensen et al., 2019a). As bacteria move throughout the decomposing body, they can infiltrate the Haversian systems of the cortical bone through the nutrient foramina (Finley et al., 2015; Booth et al., 2016; Booth, 2017; Bronnimann et al., 2018). Certain microbes secrete an enzyme known as collagenase which resorbs the collagen component of bone resulting in distinct non-Wedl microbial tunnels (Turner-Walker and Syversen, 2002; Szostek et al., 2011; White and Booth, 2014; Kontopoulos, 2019; Turner-Walker, 2019).

2.3.2 Bioerosion Terminology

With consideration to the history of microbial bioerosion research and the specific microbes that influence skeletal diagenesis, specific terminology will be used for the remainder of this thesis. The term ‘environmental microbes’ will refer to all microbes from the surrounding burial environment, whereas ‘endogenous microbes’ or ‘endogenous bacteria’ may be used interchangeably to refer to the bacteria residing within the digestive tract (i.e., the gut microbiota). ‘Microbial bioerosion’ will refer to all diagenetic alterations to the internal microstructures of bone due to microbial activity, whether onset by environmental microbes or endogenous microbes. The term ‘microbial tunnel’ will describe any deteriorating pores caused by microbial activity, regardless of the microbes responsible for skeletal diagenesis. The term ‘bacterial bioerosion’ will be used to specifically describe evidence of bioerosion onset by endogenous microbes from the gut microbiota.

2.4 Microscopic-Computed Tomography

While histological assessments have traditionally been used to study microbial bioerosion (see Wedl, 1864; Hackett, 1981; Bell et al., 1996; Turner-Walker and Syversen, 2002; Jans, 2008; Turner-Walker, 2008; Szostek et al., 2011; White and Booth, 2014; Kontopoulos, 2019), micro-CT technology offers an alternative, non-destructive approach to assess these unique microstructures of osteological tissue and explore patterns of skeletal diagenesis (see Booth et al., 2016). Computed Tomography (CT) is a non-invasive, radiological imaging technology that can be used to orient two-dimensional (2D) radiographs (i.e., X-rays) in a volumetric context, creating three-dimensional (3D) images and models (Abel et al., 2012; Conlogue et al., 2020). Microscopic-Computed Tomography (micro-CT) is the application of CT technology at

the microscopic scale, representing object features measuring as small as a single micron (Conlogue et al., 2020). This technology can be applied to digitally view external and internal features of skeletal remains with immense clarity and to facilitate research into the microstructures of bone that cannot be visualized through macroscopic analyses alone.

2.4.1 X-ray Technology and the Principle of Attenuation

There are three fundamental mechanisms that directly influence the production and quality of micro-CT images: the X-ray tube, the collimator, and the photon detector (Abel et al, 2012; Garnett, 2020). The X-ray tube is the source where the X-ray current is created and from where the current is projected. At the one end of the tube is a filament; when heat is applied to the filament, electrons accelerate and are emitted from the filament (Buzug, 2008a). The electron beam projects through the X-ray tube and then hits an angled metal anode located at the opposite end of the X-ray tube, (Buzug, 2008a). The interaction with the anode converts the energy from unbound electrons to X-ray Bremsstrahlung energy, resulting in the development of X-ray photon radiation, which is then emitted through the object of interest onto the photon detector (Buzug, 2008a; Conlogue et al., 2020). Without the X-ray tube, there would be no source of radiation energy needed to create the 2D radiographs required to produce 3D CT images.

The collimator is a small opening comprised of highly attenuating material (i.e., lead) set external to the X-ray tube (Garnett, 2020). This mechanism shapes the radiation beam, which then directly influences the concentration of energy emitted through the object (Garnett, 2020). Because high energy concentrations typically result in

radiographs with less “noise,” (i.e., photons being represented on altered trajectories due to photon scattering), the collimator is an important component of the X-ray machine with consideration to the overall clarity of images captured. If the collimator facilitates the projection of high energy radiation, the radiographs will be taken at a higher quality, allowing for more precise analyses of micro-CT data (Buzug, 2008a; Bushong, 2013; Geva et al., 2018; Garnett, 2020).

As the photon beam passes through the object, photons are tracked by a photon detector that is set behind the object under analysis (Jiang et al., 2005; Buzug, 2008b; Abel et al., 2012; Conlogue et al., 2020; Garnett, 2020). The photon detector tracks the presence of photons as they hit the panel, which are then depicted on a single 2D radiograph (Jiang et al., 2005; Abel et al., 2012; Conlogue et al., 2020; Garnett, 2020). While the photon detector is instrumental in the development of radiographs, objects and features depicted on these radiographs are made visible due to the principle of differential attenuation (Conlogue et al., 2020).

Attenuation refers to the extent to which certain objects impede photons from continuing on their projected trajectory, and levels of attenuation are determined by the density, energy, and atomic number of the elements within the object (Buzug, 2008a; Geva et al., 2018; Christensen, 2019b; Garnett, 2020). Attenuation values of biological and non-biological materials have been studied extensively because object attenuation directly determines photon-object interactions, resulting in unique visualizations on radiographs (Buzug, 2008a; Geva et al., 2018).

2.4.2 Photon-Object Interaction and Bacterial Bioerosion

As the radiation beam is projected through an object, photons either interact with the medium or continue along their original trajectory (Buzug, 2008a; Geva et al., 2018). These interactions can result in three possible outcomes: 1) photons are completely absent from the radiograph, 2) photons are represented as they were originally trajected with the unchanged radiation concentration, or 3) photons are represented on their original trajectory with altered radiation concentrations (Buzug, 2008a; Bushong, 2013; Geva et al., 2018; Garnett, 2020).

When photons encounter highly attenuating objects (e.g., lead), their trajectory can be halted and they will not be able to emit through the medium or be represented on the radiograph (Buzug, 2008a; Hurrell, 2012; Conlogue et al., 2020). The absence of photons appears as distinguishable white voids that clearly outline the object. When photons do not encounter a medium and continue their trajectory towards the photon detector, black negative space is represented on the radiograph (Buzug, 2008a).

Photon beam energy and concentration may vary from their original value when photon-object interactions result in partial photon energy absorption (Buzug, 2008a; Geva et al., 2018). Photon energy can be absorbed within a medium resulting in photons with altered concentrations being represented on radiographs with varying grey scale values (Buzug, 2008a; Geva et al., 2018). For example, when examining an X-ray of a living individual, outlines and features of skeletal elements are brighter and more distinguished than organs, fatty tissue, and skin because osteological tissue has a higher attenuation value than soft tissues (Hurrell, 2012; Christensen et al., 2019b). No biological tissues maintain a high enough attenuation value to completely halt photon trajectory; therefore, all biological tissues are depicted in grey scale.

Because photon-object interactions can depict variations in object densities, radiographs allow for the visualization and analysis of different biological microstructures, such as vascular canals throughout cortical tissue (Buzug, 2008b; Geva et al., 2018). By assessing the color and shape of different features within skeletal tissue, it is possible to differentiate naturally occurring osteological tissue features, such as Haversian systems, from microbial tunneling. An understanding of differential attenuation and photon-object interactions is therefore fundamental in determining the presence or absence of bacterial bioerosion in bone.

Based on the endogenous model, micro-CT technology should provide evidence of bacterial bioerosion in skeletal remains of individuals who would have consumed food throughout their life, so long as the individual was buried with soft tissue intact; however, this is not always the case. There are instances where bacterial bioerosion is completely absent from the skeletal remains of individuals who would have undergone autolytic and putrefactive decomposition (Jans, 2008). In response to this, there has been increased interest regarding the presence or absence of bacterial bioerosion alongside additional taphonomic data to assess what external circumstances may hinder the autolytic and putrefactive processes that give rise to bacterial bioerosion (Jans, 2013; Booth, 2015; Booth, 2017; Eriksen et al., 2020).

2.5 External Influences Impacting the Development of Bacterial Bioerosion

Variation such as burial practices and the geochemical conditions of the burial environment are two significant factors that can influence the processes of autolytic and putrefactive decay. These conditions may in turn influence the development of bacterial bioerosion. For example, in a study conducted by Thomas Booth (2015) it was argued

that if individuals were not buried immediately after death additional factors such as insect scavenging and environmental exposure may have influenced the trajectory of soft tissue decomposition. This in turn would have influenced the likelihood of bacterial bioerosion development (see Booth, 2015).

The geochemical conditions of the soil (e.g., soil acidity and hydrology) in which an individual has been interred may also disrupt or halt the proliferation of bacteria during decomposition (Hedges, 2002; Turner-Walker, 2002; Szostek et al., 2011; Delannoy et al., 2018; Kendall et al., 2018; Kontopoulos et al., 2019). For example, the bacteria that reside within an adult's digestive tract thrive in highly acidic environments (i.e., environments with a pH range between 1 – 2) (Beasley et al., 2015); should a corpse be buried within neutral (pH range between 5.5 – 8.5) or alkaline soils (pH range between 7.5 – 11.5) the bacteria may not be able to thrive and the processes of soft tissue decomposition are slowed or arrested (Delannoy et al., 2018). Additionally, specific bacteria found in the gut microbiota will not survive in waterlogged environments (Hedges, 2002; Szostek et al., 2011), or in soil with constant fluctuations in moisture (i.e., repetitive wetting and drying cycles), as the flushing of environmental minerals through the biological tissues can disrupt typical microbial activity (Kendall et al., 2018; Kontopoulos et al., 2019).

This body of research has exemplified why certain individuals who should display evidence of bacterial bioerosion may not. Given that there are a variety of natural processes and human interventions that can influence the development of microbial bioerosion, it is important to examine contextual mortuary data in addition to the geologic and cultural context in which remains are recovered to fully understand the

process of skeletal diagenesis. While there are many factors that may contribute to the lack of bioerosion within a skeletal assemblage, certain research has demonstrated that the most consistent factor reducing the likelihood of bacterial bioerosion is age at death, specifically with consideration to fetuses and newborns (see White and Booth, 2015; Booth, 2015; Booth et al., 2016).

2.6 Non-Adults and the Development of Bacterial Bioerosion

2.6.1 Non-Adult Terminology

For the remainder of this thesis, the term "fetus" will refer to individuals undergoing prenatal development (<38 gestational weeks). In contrast, "newborn" will refer to individuals around the time around birth (38-40 gestational weeks), and "infant" will refer to those between 1-2 post-natal weeks to three years old (see Bogin, 1998).

2.6.2 Non-Adult Bone Structure and the Gut Sterility Hypothesis

The immature, woven bone of fetuses and newborns is less dense than that of adults and in a constant state of development, meaning that it is typically more porous, and there is a lower quantity of minerals (e.g., hydroxyapatite) incorporated into the collagen matrix (Guy et al., 2997; Goldman et al., 2009; Szostek et al., 2011; Kendall, 2018; Caruso, 2021). In order to adequately supply nutrients and blood to these developing skeletal tissues, woven bone has an intricate system of vascular canals that run throughout the bony matrix in addition to the forming Haversian systems (Goldman et al., 2009; Lewis, 2018). Therefore, the skeletal tissues of non-adults typically undergo significant skeletal decomposition after death (Szostek et al., 2011). However, there are many cases where microbial bioerosion is absent in these youngest demographic groups

(i.e., fetuses and newborns) (see Booth, 2015 and Booth et al., 2016). With consideration to the endogenous model of bacterial bioerosion, it was suggested that the lack of bacterial bioerosion in the newborn individuals was indicative of an underdeveloped gut microbiota at the time of death (see Booth, 2015; Booth et al., 2016).

When fetal or newborn skeletal remains do not display evidence of bacterial bioerosion it can be presumed that they did not live long enough to consume food and introduce food-specific bacteria into their digestive systems; therefore, their digestive tracts were sterile at the time of death (Jans, 2008; Booth, 2015; Booth et al., 2016). In contrast, when fetal or newborn skeletal remains display evidence of bacterial bioerosion it can be presumed that they lived long enough to engage in at least one feeding but still died shortly after birth (Jans, 2008; Booth, 2015; Booth et al., 2016). Identifying the presence or absence of bacterial bioerosion can therefore be used to recreate patterns in fetal mortality (e.g., stillborn vs. live birth) within skeletal assemblages.

2.7 Early Life Development of the Human Microbiome

The human microbiome is built up over time as humans interact with their environment, and the gut microbiota develops within the digestive tract primarily through the consumption of food (Benezra et al., 2012; Knight et al., 2017; Timmerman et al., 2017; Knoop et al., 2018). Some studies suggest that the development of gut microbiota begins during prenatal development (see Dunn et al., 2018, Ferretti et al., 2018). In contrast, other studies argue that the womb is relatively sterile, and the gut microbiota begin to flourish at the moment of birth, continuing through early life feeding events (see Knoop et al., 2018 and Kennedy et al., 2021).

While in utero, the transmission of bodily fluids through the placenta does facilitate the transmission of some endogenous bacterial strains from the expectant mother to the fetal body (Dunn et al., 2017; Ferretti et al., 2018; Knoop et al., 2018). Additionally, during vaginal birth the newborn will encounter fecal and vaginal bacteria that may also contribute to the development of the human microbiome (Dunn et al., 2017; Ferretti et al., 2018). However, studies have found that these bacteria are typically transient in nature, meaning that approximately 70% of the bacterial strains inherited during prenatal development and vaginal birth do not colonize successfully within the newborn gut and are replaced by other bacterial colonies within the first three days after birth (see Ferretti et al., 2018 and Kennedy et al., 2021).

It is suggested that the interactions newborns have with their external environments after birth are what prompt stable and consistent microbiome development (see Ferretti et al., 2018, Knoop et al., 2018 and Kennedy et al., 2021). For example, Ferretti and colleagues (2018) found that gut bacteria colonize more sustainably after the third day of life, likely due to events of feeding as well as additional environmental interactions. While these circumstances may vary, it can be assumed that the most significant developmental period for the gut microbiota begins during the first post-womb feeding and continues for the first few years of life (Gritz and Bhandari, 2015; Knight et al., 2017; Knoop et al., 2018).

Clinical research has explored how the mode of food consumption (e.g., breast feeding versus bottle feeding) influences the development of the human microbiome differently (see Timmerman et al., 2017). The results of these studies have shown that the bacteria within the digestive tract of breast-fed individuals is more individualistic –

or rather, unique to the woman who is conducting the breast feeding (Timmerman et al., 2017). In contrast, the bacteria within the digestive tract of bottle-fed individuals are more consistent in terms of the formula that is used, and the gut microbiota demonstrates less diversity (Timmerman et al., 2017). While it is clear that the mode of food consumption is significant in the early life development of the human microbiome, we cannot presume to apply these results of gut microbiota development to the 18th-19th century Halifax population studied for this thesis. This is because there is no supplementary data indicating how the individuals assessed for this study were fed during the early life. Additionally, because there are no data indicating the exact bacterial strains that prompt bacterial bioerosion development, it is not possible to determine if breast feeding versus bottle feeding would reduce the likelihood of these diagenetic microbes colonizing within the digestive tract during life.

The development of the gut microbiota is intersectional, influenced by many internal and external circumstances. While the specific conditions influencing the development of human microbiome of the individuals assessed will remain unknown, exploration into bacterial bioerosion in the remains of non-adult individuals – specifically fetal and newborn individuals – offers important contextual insights into the mother-infant nexus (Redfern and Gowland, 2011; Rutherford, 2012; Geronimus, 2013; Gowland and Halcrow, 2020; Thayer et al., 2020).

2.7.1 The Mother-Infant Nexus and Bacterial Bioerosion Analysis

The term ‘mother-infant nexus’ has been used to describe countless cultural and biological interactions between a mother and her newborn (Redfern and Gowland, 2011; Gowland and Halcrow, 2020; Agarwal, 2016). However, the specific biological bond

between an expectant mother and her developing fetus is a relatively new point of interest within anthropological research, as this relationship is significantly complex and influential on population health.

The wellbeing of an expectant mother is the single most influential factor shaping fetal development (see Rutherford and Tardif, 2009, and Rutherford, 2012). This is because when an expectant mother is exposed to stress (e.g., malnutrition, trauma and abuse, toxicants, etc.), placental growth and efficiency may be reduced (Rutherford, 2012). The placenta is the interface facilitating the transmission of blood, nutrients, and amino acids from the mother to the developing fetal body; therefore, reduced efficiency can negatively impact or offset trajectories of fetal development (Rutherford, 2012; Gluckman et al, 2016; Thayer et al., 2020). In cases where maternal health is compromised, the pregnancy may result in either prenatal death (i.e., stillbirth), or a predisposition to illness and disease for the fetus into adulthood (Hales and Barker, 1992; Rutherford and Tardif, 2009; Geronimus, 2013; Monk et al., 2013; Rutherford, 2012; Gluckman et al., 2016; Blake, 2018; Corley, 2021). Therefore, the assessment of fetal mortality patterns offers important insight into this specific biological bond and patterns of stress in these two demographic groups.

The analysis of bacterial bioerosion in fetal cortical tissue contributes directly to our understanding of the mother-infant nexus as its presence or absence in immature bone speaks to early life microbiome development which can be influenced by maternal health as well as living conditions at or around the time of birth. For example, a newborn individual with no evidence of bacterial bioerosion could be interpreted as evidence of poor maternal health where the individual was stillborn, or died very shortly after birth,

and was unable to engage in any feeding. This evidence of stillbirth or short-lived births may also suggest suboptimal living conditions immediately after birth, where prolonged food insecurities and maternal malnutrition may have influenced the mother's ability to breastfeed, stalling the development of the gut microbiome (Black et al., 2013; Valentine and Wagner, 2013; Corley, 2021). Therefore, analyses into bacterial bioerosion as it pertains to patterns of fetal and newborn mortality can supplement data regarding overall population health. With consideration to the skeletal assemblage assessed for this thesis, the data collected through the analysis of bacterial bioerosion could be used to better understand patterns of fetal mortality within the 18th – 19th century city of Halifax, Nova Scotia.

2.8 A Brief History of Halifax, Nova Scotia

The majority of Nova Scotia was declared under British rule in 1713; however, it was not until 1749 that Halifax, NS was established on unceded Mi'kmaq territory – known as Chebucto – due to the growing interest in developing a North Atlantic port to rival the French Fortress of Louisbourg on Cape Breton Island (Campbell, 1904; Griffiths, 1992; Whitfield, 2006). The establishment of Halifax began with the settlement of less than 2,000 individuals (Shimabuku and Hall, 1981), but waves of migration resulted in the displacement of countless Mi'kmaq and Wolastoqiyik communities, as well as many Acadian families in 1755 (Griffiths, 1992; Whitfield, 2006; Hanrahan, 2008).

The Mi'kmaq were the Indigenous peoples traditionally inhabiting vast regions of land from Quebec's Gaspe peninsula and Newfoundland to the southern coasts of Maine (Hanrahan, 2008). It is believed that the Mi'kmaq were the first people colonists

would have contacted during the earliest stages of settlement (Griffiths, 1992; Hanrahan, 2008). The Wolastoqiyik additionally inhabited regions throughout Nova Scotia, New Brunswick and Maine, but primarily remained in the southern regions of the St. John River due to the fishing resources (Patterson, 2009). These Indigenous communities were believed to live peacefully with the Acadians, who were the first colonists sent to settle what is now contemporarily known as Nova Scotia in 1604 through to the late 1680s by the French and English (Griffiths, 1992). It was not until the early 1700s that tensions between the French, English, and British regarding the settlement of the Atlantic coast saw the lasting destruction and displacement of the Indigenous communities throughout the region (Griffiths, 1992).

By 1816 Halifax's population was approximately 12,000, where an estimated 100 families of Acadian descent, approximately 300 Mi'kmaq, and an estimated 140 Wolastoqiyik remained due to their resistance to colonial attempts at displacement (Campbell, 1905; MacLean, 1907; Shimabuku and Hall, 1981; Whitfield, 2006). The additional residents were believed to be an array of European settlers, New England Loyalists and British colonialists, many of whom were believed to bring with them enslaved individuals of African descent (Campbell, 1905; MacLean, 1907; Shimabuku and Hall, 1981).

Even though the movement towards anti-slavery activism began in the New England colonies in the late 18th century, there were countless enslaved Indigenous and African individuals in the Atlantic world until slavery was officially abolished in the British Empire in 1834 (Whitfield, 2006; Whitehead, 2013). With promises to free anti-rebellion slaves from the British government, many enslaved individuals took part in the

American Revolutionary War in 1776 (Whitfield, 2006). After the cessation of the war in 1783, Nova Scotia saw an influx of nearly 30,000 Loyalists, disbanded soldiers, and African refugees, the majority of whom were previously enslaved (Campbell, 1904; Shimabuku and Hall, 1981; Whitfield, 2006).

Though Halifax was a significant trading port within the Maritimes, immense unrest throughout the region due to unceasing civil war and disputes between the Mi'kmaq and British settlers, growing conflict between the Congress of Colonies and the British Crown, and racial tensions regarding the freed slaves resulted in siege-like conditions throughout the 18th and 19th centuries (Fingard et al., 1999; Whitfield, 2006). Economic development did increase throughout the early 19th century; however, there was an uneven distribution of resources throughout the region resulting in prolonged periods of food insecurity (Fingard et al., 1999; Whitfield, 2006). Additionally, poor housing infrastructure alongside the transient military population and constant waves of immigration resulted in increased rates of disease (e.g., countless smallpox outbreaks and a cholera epidemic in 1834) (Shimabuku and Hall, 1981). The perilous living conditions resulted in the death of many individuals during this time period (Fingard et al., 1999; Whitfield, 2006).

2.8.1 The Methodist Church and Cemeteries of Halifax

There was a vast array of cemeteries within downtown Halifax between the mid-18th to mid-19th centuries. These included the cemeteries of the Halifax Methodist Church, the Poor House, St. Peter's Church, St. Paul's Church (also known as "The Old Burying Ground"), Fort Massey, and Holy Cross (Shimabuku and Hall, 1981; Cahill et al., 2008). Each cemetery generally served a specific parish or was selected based on an

individual's economic and/or political affiliations within society (Cahill et al., 2008; Shimabuku and Hall, 1981). Due to concerns of sanitation and cemeteries becoming over-crowded, all downtown Halifax cemeteries were closed in 1844, and all individuals, regardless of religious affiliation or social/political status, were interred at the Camp Hill Cemetery located approximately one kilometer northwest of the Halifax Methodist church.

According to historic records dating to the 18th and 19th centuries, the Halifax Methodist Church cemetery was primarily used to bury members of the congregation from 1793 to 1844 (see Davis MacIntyre & Associates Ltd, 2017a; 2017b; 2018). The congregation was noted as being comprised of middle-class Loyalist families, disbanded soldiers, and European immigrants (MacLean, 1907). However, individuals outside of the middle-class were also likely interred here. For example, historical records suggest William Black, the "Apostle of Methodism" and prominent member of the church is said to have been laid to rest at the Methodist burial ground (MacLean, 1907; Cahill et al., 2008, p 3). In contrast, the inconsistent mortuary patterns and high number of unmarked graves identified during excavation (see Davis MacIntyre & Associates Ltd, 2017a, 2017b, 2018) suggests more lower-class and impoverished individuals (Campbell, 1904; Fingard et al., 1999). However, there is a possibility that individuals exhumed during the 2016 excavation where originally interred at the Poor House cemetery, as it was located directly adjacent to the Methodist Church cemetery.

Methodism in the Atlantic region was supportive of the anti-slavery movement during the early 19th century and was believed to have welcomed to the congregation newly freed (but financially struggling) African refugees, Indigenous families, and

European immigrants unable to find work (Whitehead, 2013). While historical documents are exceptionally valuable in the analyses of burial records and data regarding interment, they are incomplete and therefore cannot represent the entire population of individuals interred within this cemetery before its closure in 1844. However, based on the records that do exist, it appears that this cemetery may have been the final resting place for a variety of individuals from this 18th century British colony.

2.9 Conclusion

This chapter reviewed the relevant literature related to this research including skeletal composition and structure, an overview of microbial bioerosion research and how it can be visualized, and the significance of the development of the human microbiome as it relates to skeletal diagenesis. A brief introduction to the city of Halifax, NS was provided, as well as a discussion on some of the cemeteries established in the downtown area. The information outlined in this chapter will contextually contribute to the interpretation of the data collected throughout this research, and more broadly, continued bioerosion research in archaeological skeletal collections.

CHAPTER 3 – Materials and Methods

3.1 Introduction

This chapter will begin by reviewing the permissions granted to assess the Halifax Methodist Church skeletal collection, followed by the methods used to estimate skeletal age of each individual assessed for this research. Second, the steps and standards implemented during microscopic Computed Tomography (micro-CT) image capturing, rendering, and analysis will be outlined. Finally, an overview of the metric analyses and developmental characteristics assessed to determine the presence or absence of bacterial bioerosion will be provided.

3.2 Permissions and Access to the Skeletal Collection

Permission to conduct analysis on the Halifax Methodist Church skeletal assemblage was granted to Dr. Amy Scott and the University of New Brunswick via a Memorandum of Understanding with the Presbyterian Church of St. David (current curators of the skeletal collection) in Halifax, NS. All macroscopic skeletal analyses were completed in the Presbyterian Church of St. David crypt where the collection is currently stored. The selected non-adult skeletal remains chosen for micro-CT imaging were temporarily transported to the Museum of Ontario Archaeology in London, ON where they were scanned under the supervision of Dr. Andrew Nelson.

During image capture all data were temporarily stored on two computer systems at the Museum of Ontario Archaeology. Once scanning was complete, all radiographs were transferred to an external hard drive and deleted from the museum computers. During data collection, no other students or staff were permitted to access these

computers or the external hard drive. After image capture, all skeletal remains were returned to the Presbyterian Church of St. David crypt. All image rendering was completed remotely at the University of New Brunswick with no images saved to any physical computers or digital platforms. The hard drive with all skeletal CT images will be stored in perpetuity in the Bioarchaeology Research and Teaching (BART) laboratory at the University of New Brunswick under the supervision of Dr. Amy Scott. Throughout data collection, all precautions were taken to minimize the destruction of the remains and ensure ethical handling and treatment.

3.3 The Halifax Methodist Church Skeletal Collection

3.3.1 The Halifax Methodist Church Cemetery

The skeletal remains to be assessed for this research were recovered during a 2016 archaeological excavation of the Halifax Methodist Church by Davis McEntyre Archaeological Associates of Halifax, NS. Having been renamed, the now Presbyterian Church of St. David requested that the archaeological consulting firm conduct site mitigation and recover burials on the church land before the demolition of the church hall which was located over the historic Methodist Church cemetery. Currently curated at the Presbyterian Church of St. David in Halifax, NS, these skeletal remains represent those from the late 18th to early 19th century Methodist Church congregation. The burials in this cemetery consisted of single coffin burials, multiple coffin burials, and small mass graves (i.e., more than one interment per grave shaft) (Davis MacIntyre & Associates Ltd, 2017a, 2017b, 2018). Over 200 individuals of various ages were recovered and returned to the stewardship of the Presbyterian Church of St. David and currently reside in the church crypt.

3.3.2 The Population Sample

Unfortunately, there was an inconsistent labelling strategy applied to the skeletal collection during the 2016 Davis MacIntyre & Associates excavation; therefore, for simplicity and clarity each individual has been relabelled using a letter designation (see Table 2). These letter designations will be used throughout the remainder of the thesis.

Table 2: Renamed Halifax Methodist Church skeletal samples analyzed for this thesis

Original Sample Name	New Sample Name
Individual 47	Individual A
Articulated 4-5-6	Individual B
Articulated/ Individual 55	Individual C
Individual 52	Individual D
Individual 7	Individual E
Individual 51	Individual F
Individual 90	Individual G

Age assessment was completed using metric and/or morphological analysis depending on the degree of skeletal preservation. Metric analysis to estimate age included the measurement of long bones (see Maresh, 1970; Fazekas and Kosa, 1978; Scheuer et al., 2010), the basilar part of the occipital bone (see Scheuer and MacLaughlin-Black, 1994; and Scheuer et al., 2010), and the pubis (see Fazekas and Kosa, 1978; and Scheuer et al., 2010). Morphological analysis to estimate age included the examination of tooth mineralization and dental eruption patterns (see AlQahtani et al., 2010; Christensen et al., 2019c).

3.4 Macroscopic Analysis of Remains

Because bacterial bioerosion primarily develops throughout the cortical tissue, all bone samples selected for micro-CT analysis were chosen based on osteological preservation. Additionally, a qualitative macroscopic assessment was conducted to assess the quality of the cortical bone preservation, or rather, determine the Macroscopic Preservation Index (MPI). This assessment was based off the method proposed by Galligani and colleagues (2019), with modifications to include external cortical porosity and exclude values assessed through histological assessments (i.e., Oxford Histological Index).

Each of the cortical bone preservation features (i.e., tiled cracking, surface corrosion, surface porosity, fractures/cracks, loss of tensile strength) were assessed on a scale of 0-1. For tiled cracking, surface corrosion, and surface porosity the following criteria and associated scores were used: (0) 60-100% of the bone was affected by the specific characteristic; (0.5) 25-60% of the bone was affected; and (1) 0-25% of the bone was affected. For fractures and cracks, the following criteria and associated scores were used: (0) more than two major cracks were identified on the cortical surface; (0.5) one or two cracks were identified on the cortical surface; and (1) no cracks were identified on the cortical surface. For determining tensile strength, the following criteria and associated scores were used: (0) the bone was extremely fragile and was at risk of fracturing when touched; (0.5) the bone was somewhat fragile with some give when touched; and (1) the bone was extremely rigid with no give when touched. Using this scoring system, an MPI sum score of 5 meant excellent cortical preservation, whereas an MPI sum score of 0 meant extremely poor cortical preservation.

The MPI assessment was completed prior to micro-CT image capture for each skeletal element but did not influence the sample selection, as cortical preservation was relatively consistent across the skeleton for each individual. Rather, this MPI assessment was conducted to determine (1) if cortical preservation as it relates to the MPI assessment influenced the ability to visualize internal microstructures of bone, and (2) if cortical preservation influenced patterns of microbial tunnel development within the cortical tissue.

3.5 Microscopic-Computed Tomography Image Capture

3.5.1 Preliminary Nikon XT 225 ST Setup

Micro-CT image capture took place at the Museum of Ontario Archaeology in London, ON with a Nikon XT 225 ST Micro-CT machine. Before each scanning session the Nikon XT was put through an automatic conditioning (auto-conditioning) procedure to ensure the system settings were stable prior to image capture. After the auto-conditioning was complete, shadow correction adjustments were programmed. Shadow correction settings include the x-ray tube voltage (measured in kilovolts (kV)), the current exposure time (where the current is measured in microampères (µA)), and the power of the x-ray current (measured in watts (W)) (see Table 16: Appendix A). The x-ray current exposure time and energy of the x-ray current were adjusted so that the overall micro-CT exposure settings ranged between a value of 10,000 - 60,000 to ensure micro-CT image clarity. Once the shadow correction adjustments were made, multiple scans were run. However, whenever the Nikon XT had to be turned off or reset, these two set-up procedures were completed again before any images were captured.

3.5.2 Spatial Resolution and Projection Settings

Once the shadow correction settings were programmed, the bone samples were mounted within the Nikon XT on the turntable, and the image spatial resolution was determined. Spatial resolution is the smallest quantifiable distance required to distinguish different structural components from one another. When producing a single 2D radiograph, spatial resolution is represented as a 2D value, and can be quantified to scale (i.e., when spatial resolution is 2.5 µm, each visualized pixel represents a 2.5 µm x 2.5 µm section of biological tissue) (Abel et al., 2012; Conlogue et al., 2020). When producing micro-CT images, spatial resolution must be represented as a 3D value (i.e., volumetric pixels, or voxels, where when spatial resolution is 2.5 µm, each visualized pixel representsa a 2.5 µm x 2.5 µm x 2.5 µm section of biological tissue) because these images are assessed in 3D contexts during image rendering (Abel et al., 2012; Conlogue et al., 2020). For each scan, image spatial resolution (i.e., voxel size) was set to the smallest possible value, contingent on the size of the bone sample, to increase microstructure clarity (Conlogue et al., 2020).

3.5.3 Projection Settings

Where the projection refers to the orientation of each individual radiograph, a frame refers to each captured radiograph. With this, there are two different methods that can be applied to micro-CT image capture: the short scan method and the long scan method. The majority of the micro-CT images (n=21, 80.8%) were created through short scan image capture, where one frame was captured for 3,141 different projections. The remaining micro-CT images (n=5, 19.2%) were created through long scan image capture, where eight frames were captured for 1,571 different projections. Long scan

image capture requires a longer scan time (see Table 16: Appendix A) but facilitates the production of micro-CT images with minimal visual ring artifacts. Because of time and funding constraints, not all micro-CT images could be captured using the long scan method, therefore only the femora scans of Individual E and Individual G were captured in this way (see Table 16: Appendix A).

3.5.4 Converting Radiographs to Volumetric Data

Once all the radiographs for each bone sample were captured, they were stored as a collective file, described as a TIFF stack, which were then uploaded to the CT Pro computer software. This software was first used to conduct image reconfiguration. This step of data collection allows for the selection of optimal settings to organize the radiographs from each scan with one another to increase image clarity, as well as reduce micro-CT "image noise." Once the optimal settings were chosen, the CT Pro software was used to transform the 2D data into 3D data through volume editing.

The CT Pro volume editing produced two distinct data files for each element scanned, volumetric files (vol files) and volume group information files (vgi files). The combination of both file types allowed for the data to be imported into the Dragonfly 2022.3 software and rendered appropriately within a 3D context.

3.6 Microscopic-Computed Tomography Image Rendering

3.6.1 Windowing and Leveling

Once the data were uploaded to the Dragonfly 2022.3 software, windowing and leveling settings were adjusted. These settings allow for the contrast of density variation within a single object where more dense regions are lighter in coloration, less dense

regions are darker grey in coloration, and microbial tunnels or canals through the osteological tissue are black in coloration. While windowing settings of 200 and leveling settings of 1,800 are optimal for visualizing the microstructures of osteological tissue, these values were adjusted for each scan as variation in image capture settings may influence osteological microstructure visualizations (see Table 17: Appendix A).

3.6.2 Creating a Region of Interest

Bacterial bioerosion associated with the accumulation of endogenous gut bacteria (i.e., non-Wedl microbial tunnels, specifically linear-longitudinal, lamellate, and budded) typically develop with a diameter size ranging between 5 to 60 microns (see Table 1). Therefore, a thickness mesh was applied to each sample to ensure microbial tunnels smaller than 5 microns were removed from visualization, increasing clarity on the larger microbial tunnels of interest.

3.7 Microscopic Cortical Bone Analysis

3.7.1 Metric Analysis: Range of Microbial Tunnel Diameter

The first step in determining the presence or absence of bacterial bioerosion was to identify the range in microbial tunnel diameter size to ensure the microbial tunnels that developed throughout the cortical tissue since death were due to endogenous gut bacteria (see Table 1). This additionally allowed for the assessment of patterns of microbial tunnel diameter within each skeletal element and across the skeleton. Two measurement strategies were implemented to determine the most efficient method to metrically assess microbial tunnels: the systematic sample method and the random

sample method. The methods and results of this preliminary analysis are presented below.

Both methods were applied to the scan of femur midshaft from Individual F, as this scan was exceptionally clear with skeletal landmarks (i.e., the nutrient foramen) present to facilitate accurate bone orientation during analysis. During the systematic assessment, once anatomical orientation was determined, the femoral scan was divided into quadrants representing the anterior, posterior, medial, and lateral regions of the bone (see Figure 1). Multiple square sub-quadrant sampling regions, measuring approximately one millimetre in width and length, were then aligned through the center of each quadrant (see Figures 1 and 2). The first sample region for each quadrant was set at the sub-periosteal surface and the final sample region for each quadrant was set at the sub-endosteal surface, adjacent to the medullary cavity. Once the sub-quadrant sample regions were established, up to ten microbial tunnels with relatively delineated edges inside each sample region were chosen and measured with the ruler annotation tool in the Dragonfly 2022.3 program to determine microbial tunnel diameter (see Figure 2). All raw data is provided in Table 18 of Appendix A. The benefit of this method was an increase in the data collected which provided a more precise representation of average microbial tunnel diameter than the random sample method described below.

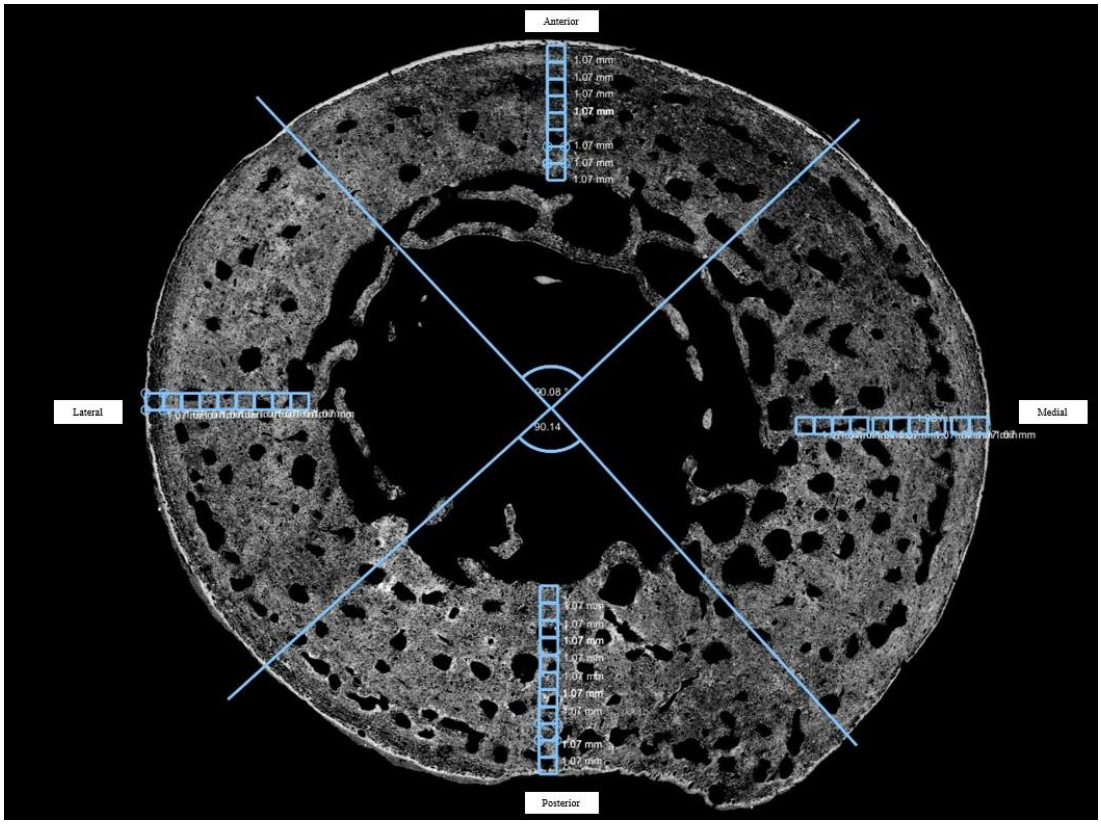

Figure 1: The depicted image is a single transverse cross section of the femur midshaft from Individual F examined during the systematic sample method. The blue lines indicate the distinction between anatomical quadrants of bone, whereas the blue squares indicate the sub-quadrant sample regions throughout each quadrant of bone.

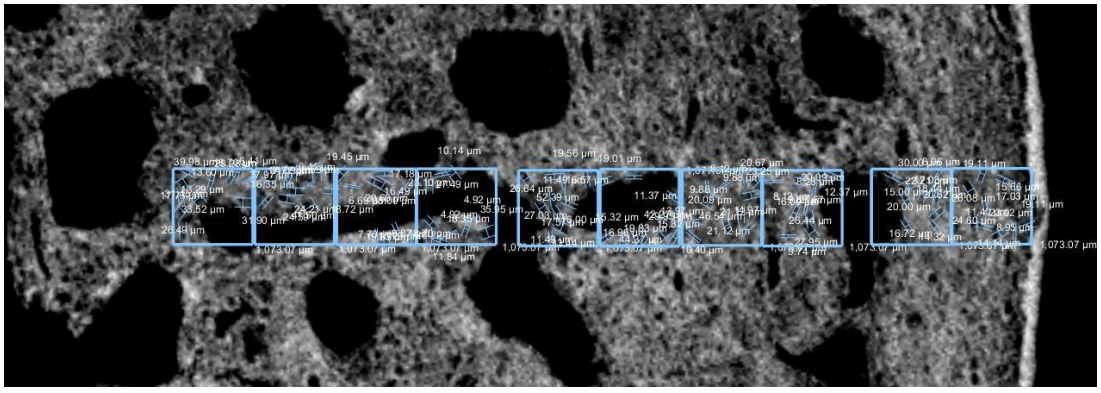

Figure 2: This image is a single transverse cross-section of medial region of the femur midshaft from Individual F examined during the systematic sample method. All individual microbial tunnel measurements within each sub-quadrant sample region can be visualized.

During the random sample method, twenty microbial tunnels of various sizes were selected and measured with the ruler annotation tool in the Dragonfly 2022.3

program to determine a more general range of microbial tunnel diameter across the cortical tissue. These twenty samples were selected at random across all four quadrants of the bone, with approximately five microbial tunnels sampled within each quadrant (see Table 19: Appendix A). While this method provided a lower quantity of data, it was beneficial in terms of efficiency when calculating average microbial tunnel diameter.

A statistical analysis was conducted to determine if the two methods produced comparable microbial tunnel diameter data. First, the results from the systematic assessment were analyzed. The mean microbial tunnel diameter within each 1mm x 1mm sub-quadrant sample region within each region of bone were compared to one another (e.g., sub-quadrants 1-8 within the anterior quadrant of bone) to determine whether there was a statistically significant difference in mean microbial tunnel diameter from sub-quadrant to sub-quadrant within the specific quadrants. This was analyzed using an independent sample t-test within the IBM SPSS Statistics 28.0 software. Following this, the mean diameter of all microbial tunnels sampled within a specific quadrant of bone were compared to all other quadrants to determine whether there was a statistically significant difference in mean microbial tunnel diameter across the four specific quadrants. An independent samples t-test was also used for this analysis. Finally, an independent sample t-test was used to compare the results of the mean microbial tunnel diameter for each quadrant of bone in the systematic sample method to the mean microbial tunnel diameter collected in the random sample method.

When comparing the mean microbial tunnel diameter from each of the sub-quadrant sample regions collected during the systematic sample method, only four of one hundred and fifty-one comparisons (2.6%) produced statistically significant results

(see Table 20, 21, 22 and 23 in Appendix A). Using the systemic sampling method, the mean microbial tunnel diameter for Individual F in the anterior, medial, posterior, and lateral quadrants was 19.48 µm, 19.75 µm, 21.62 µm, and 20.95 µm, respectively. When statistically comparing these values to one another, there were no statistically significant differences (Table 3). These results suggest that microbial tunnel diameter is relatively consistent across the various quadrants of bone. When using the random sample method, the mean microbial tunnel diameter was 28.88 and was not significantly different from the mean diameter values in any of the four quadrants captured in the systemic method of analysis (see Table 4).

Table 3: Statistical analysis of the systematic diameter assessment

Quadrant Comparisons	t	df	p
Anterior - Medial	-0.191	174	0.849
Anterior - Posterior	-0.97	177	0.333
Anterior - Lateral	-1.258	149.891	0.21
Medial - Posterior	-0.828	201	0.409
Medial - Lateral	-1.13	184	0.26
Posterior - Lateral	-0.383	187	0.702

Table 4: Statistical analysis of the systematic and random sample method

Pore Data Comparisons	t	df	p
RS - SS Anterior	-1.949	20.691	0.065
RS - SS Medial	-1.895	20.627	0.072
RS - SS Posterior	-1.637	21.033	0.116
RS - SS Lateral	-1.478	22.346	0.153
RS: Random Sample Data - SS: Systematic Sample Data			

These results suggest that both methods produce similar mean microbial tunnel diameter data. The systematic method was thorough and provided a vast amount of data

within each quadrant of bone; however, considering these preliminary results, all remaining microbial tunnel diameter data were calculated using the more efficient random sample method.

3.7.2 Morphological Analysis: Distribution of Microbial Tunnels

The assessment of where microbial tunnels develop across each skeletal element may be an important factor in determining whether the microbial tunnels are the result of environmental microbes or endogenous gut bacteria. For example, as discussed by Hackett (1981), the branch-like microbial tunnels brought on by environmental microbes primarily form at the periosteal surface and extend from the most external surface of the cortical tissue towards the center of the cortical tissue. Therefore, if microbial tunnels formed at the most external surface of bone, they are likely the result of environmental microbes. In contrast, if microbial tunnels are developing below the periosteal surface, throughout the center of the cortical tissue, near the endosteal surface (i.e., the medullary cavity), or evenly throughout the cortical bone, they are likely the result of endogenous microbes (see Figure 3) (Bell et al., 1996; Bronnimann et al., 2018). Additionally, as natural openings in the cortical surface, the nutrient foramina are likely specific locations where endogenous bacteria could easily infiltrate into the surrounding tissue during the early putrefactive stages of decomposition. Therefore, the general location and distribution of microbial tunnel formation in association to the nutrient foramina was an important source of data considered in this study.

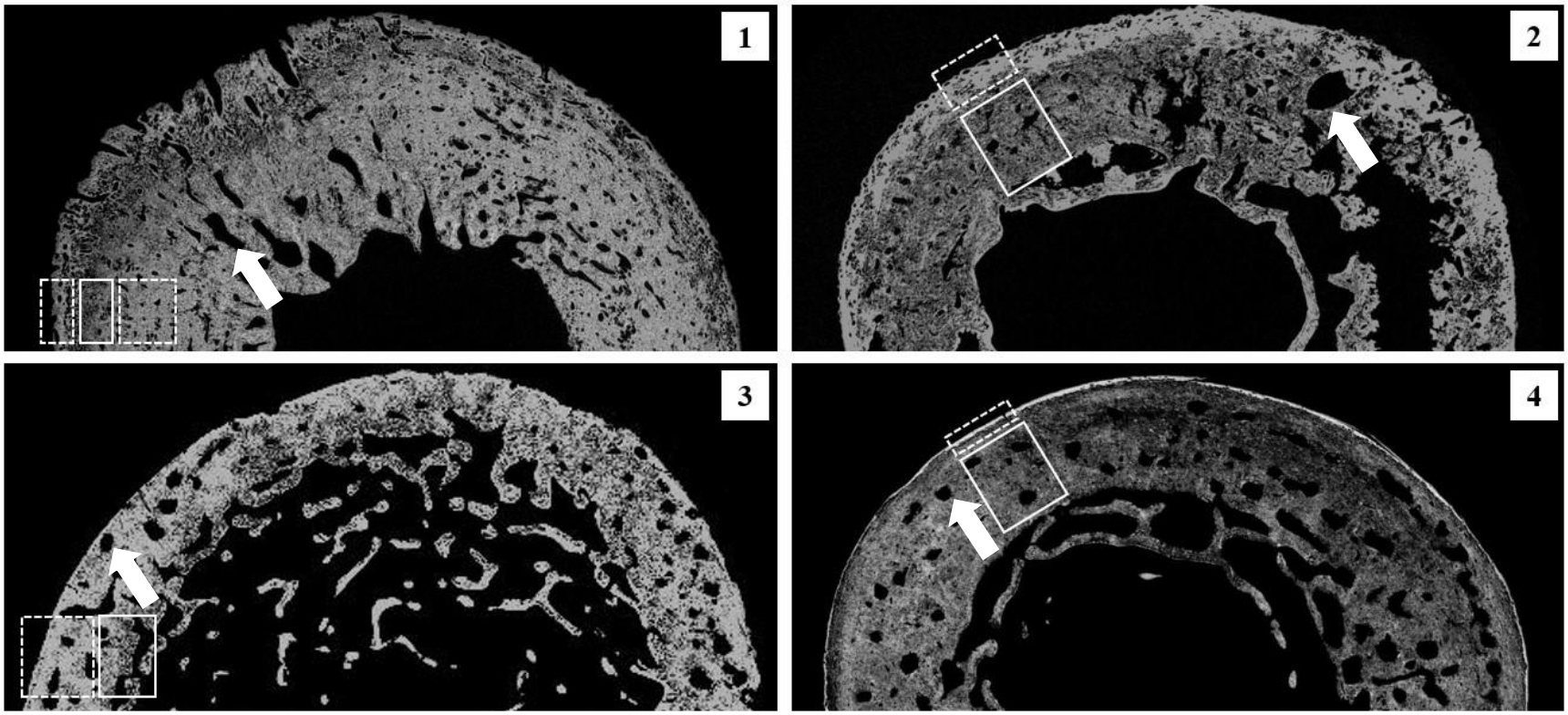

Figure 3: This image represents four single transverse cross section scans of the femora from three individuals. The white arrows are indicating naturally occurring vascular canals, not to be confused with microbial tunneling. The white line boxes are highlighting the region of bone with decreased density due to increased microbial tunnel formation, whereas the white dotted-line boxes are highlighting the region of bone with greater density due to decreased microbial tunnel formation. All depicted scans would be scored as 3 on the sub-periosteal ridge distinction scale. (1) The femur scan from Individual C displays microbial tunnels primarily located below the periosteal surface but did not extend to the very exterior surface of bone, resulting in cortical tissue with greater density along the external surface of bone; (2) the femur scan from Individual G displays microbial tunnels primarily located throughout the center of the cortical tissue as well as the endosteal surface; (3) the distal femur scan from Individual F displays microbial tunnels primarily located near the endosteal surface; (4) the midshaft femur scan of Individual F displays microbial tunnels that are distributed evenly throughout the cortical tissue.

Microbial tunnel development was assessed by examining the colour differentiation between microbial tunnels (i.e., black) and the surrounding cortical tissues (i.e., shades of grey), where it was then possible to identify microbial tunnel and cluster distribution throughout the cortical tissue (see Figure 3).

3.7.3 Morphological Analysis: Cluster Formation

Sasso and colleagues (2014) argue that few microbial tunnels with small diameter sizes (5-15 microns) are indicative of isolated microbial attacks, whereas an increase in microbial tunnels with larger diameter sizes (>100 microns) indicate "superimposed bacterial colonies" (p. 37). Though there was no clear discussion determining the significance of microbial tunnels with diameter size ranging between 16 and 99 microns, this claim did inspire the inclusion of cluster analysis in this study in an attempt to examine bacterial load and bacterial bioerosion development. Where a cluster represents a unique concentration of microbial tunnels which can be differentiated from regions of bone with consistent density, cluster formation was visually assessed as either present or absent (see Figure 4 and 5).

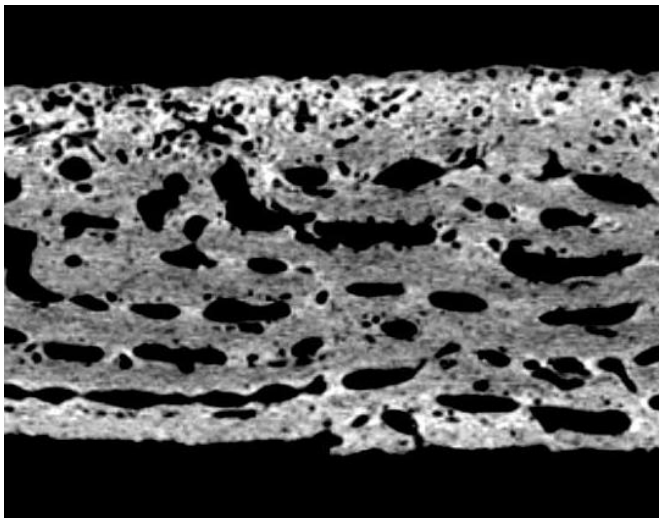

Figure 4: The depicted image is a single transverse cross section, demonstrating variation in cortical density throughout the center of the tissue (visualized as the darker grey region of bone), but there is no clear evidence of cluster formation (cranial fragment scan from Individual C).

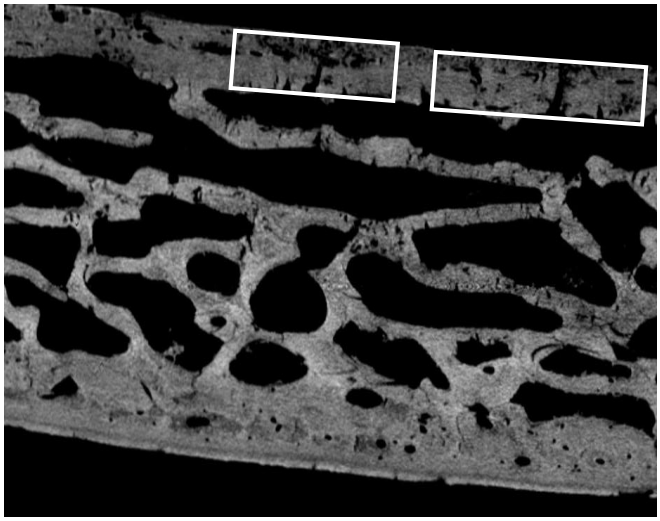

Figure 5: The depicted image is a single transverse cross section, where the white line boxes are highlighting regions of bone with variations in cortical density due to distinct concentrations of microbial tunnels (i.e., clusters) located through the center of bone and near the periosteal surface (cranial fragment scan from Individual F).

3.7.4 Morphological Analysis: Sub-Periosteal Ridge Distinction

Typically, as microbial tunnels brought on by endogenous gut bacteria develop below the periosteal surface a unique ridge of concentrated cortical tissue can be identified at the periosteal surface. Therefore, by assessing the formation of microbial tunnels alongside the density of the periosteal surface of cortical bone (i.e., a clear sub-periosteal ridge) it is possible to exclude environmental microbes as the causative agent of the microbial tunnel development (see Figure 6).

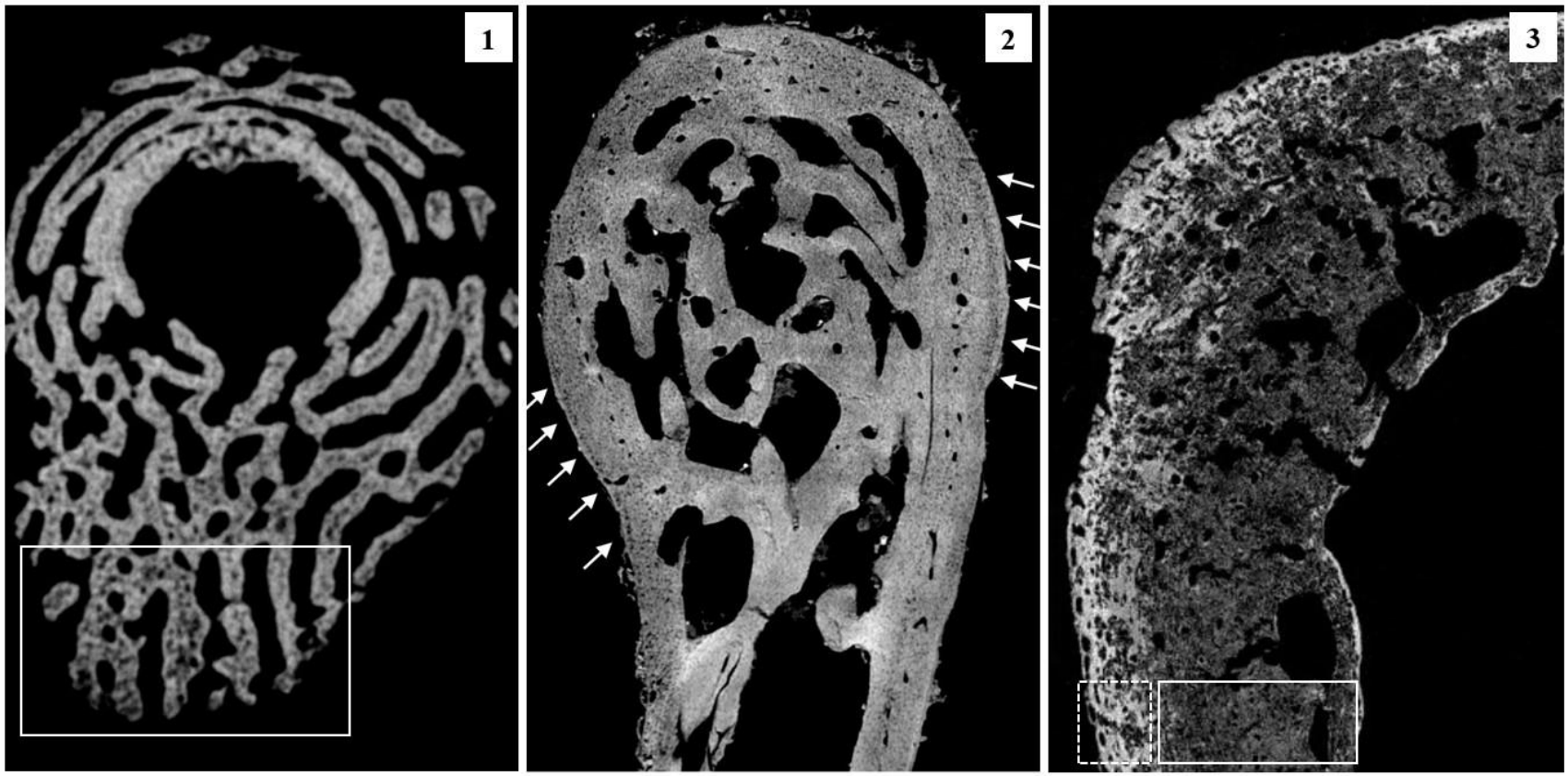

Figure 6: This image represents three single transverse cross section scans from three individuals. The white line boxes are highlighting the regions of bone with decreased density due to increased microbial tunnel formation, whereas the white dotted-line box is highlighting the region of bone with greater density due to decreased microbial tunnel formation. (1) Due to the concentration of microbial tunnels developing at the periosteal surface, there was no identifiable sub-periosteal ridge. This scan was scored a value of 0 during sub-periosteal ridge distinction assessment (long bone scan from Individual A); (2) the white arrows are indicating the surface of bone demonstrating ridge distinction due to the subtle but consistent formation of microbial tunnels below the external surface of cortical tissue. This scan was scored a value of 2 during sub-periosteal ridge distinction assessment (neural arch scan from Individual D); (3) consistent microbial tunnels through the center of the cortical tissue resulted in greater density at the periosteal surface. This scan was scored a value of 3 during sub-periosteal ridge distinction assessment (femur midshaft scan from Individual G).

Sub-periosteal ridge distinction was assessed on a scale of 0-3 and scored using the following criteria: (0) no external ridge distinction was identified; (1) external ridge distinction was identified across 1 - 25% of the periosteal surface; (2) external ridge distinction was identified across 25 - 60 % of the periosteal surface; and (3) external ridge distinction was identified across 60 - 100% of the periosteal surface. Given this system of analysis, a score of 0 would indicate no external ridge development and consistent density throughout the cortical tissue, or porosity extending across the entire external surface of the bone. In contrast, a score of 3 would indicate a clear and distinct external ridge, with increased bone density concentrated along the external surface of the bone (see Figure 6).

3.8 Intraobserver Error

3.8.1 Metric Analysis

To ensure that the metric measurements taken throughout this study produced accurate and consistent results, an intraobserver analysis was conducted. Five specific microbial tunnels were marked on the transverse cross section of ten different CT scans. The microbial tunnels were then measured with the Dragonfly 2022.3 ruler annotation tool and recorded. After recording the measurements, the program was closed for thirty days. After the thirty days, the same microbial tunnels highlighted were remeasured. Using an independent sample t-test in the IBM SPSS Statistics 28.0 software, the diameter measurements from the first and second measures were statistically compared. There were no significant differences between the first and second measurements of microbial tunnel diameter ($t = 0.107$; $df = 98$; p value $= 0.915$). These results confirm that diameter measurements were accurate moving forward with analysis.

3.8.2 Morphometric Analysis

Intraobserver error was also calculated for the assessed morphometric characteristics associated with bacterial bioerosion. Each morphometric trait for every micro-CT image was analyzed and recorded on November 14, 2021. After recording these assessments, the program was closed for sixty-five days. The increased time between the first and second round of scoring the morphometric traits was due to the fact that the assessments were conducted on recorded images, and the Dragonfly 2022.3 program and annotation tools were not needed. Therefore, these analyses were not contingent on program accessibility. After the sixty-five days, all micro-CT images were re-evaluated. The results from both assessments were compared using the kappa statistic (κ_w) assessment to calculate the precision between the first and second rounds of morphological assessments. The kappa statistic value is meant to account for the variation in multiple rounds of subjective observation with consideration to chance, where 1.000 represents perfect agreement and 0.000 represents agreement due to chance (see Table 5) (Viera and Garrett, 2005).

Table 5: Landis and Koch (1977) interpretation of the Kappa statistic

Kappa Statistic	Strength of Agreement
<0.00	Poor
0.00-0.20	Slight
0.21-0.40	Fair
0.41-0.60	Moderate
0.61-0.80	Substantial
0.81-1.00	Almost Perfect

When comparing the first and second round of morphological evaluations, four of the five assessments produced almost perfect agreement (Table 6). However, the

microbial tunnel distribution assessment near the endosteal surface produced only a moderate rate of agreement. This result is likely due to the nonuniform nature of the trabecular bone near the endosteal surface and the difficultly associated with identifying clearly delineated tunnels in this region.

Table 6: Kappa statistic values for morphological trait assessments

Pore Distribution	κ_w	Standard Error	Confidence Interval (95%)
Endosteal Analysis	0.463	0.305	0.322-0.604
Central Analysis	0.831	0.163	0.696-0.966
Periosteal Analysis	1	0	N/A
Even Distribution Analysis	0.891	0.106	0.797-0.985
Cluster Formation	1	0	N/A
Ridge Distinction*	0.96	0.039	0.884-1.037

* The assessment comparison of the sub-periosteal ridge distinction was made using a weighted kappa statistic analysis rather than a standard kappa statistic analysis due to the ranked nature of the categorical variables

3.9 Conclusion

This chapter provided background information regarding the skeletal collection assessed for this research and the context of its excavation. Additionally, all methods used to conduct both the micro-CT image capture and rendering were outlined. A brief overview of each bioerosion characteristic was discussed to demonstrate the reason why it was included in this analysis. Preliminary statistical results and intraobserver error data were also provided to ensure accurate methods were used in this analysis and subsequent interpretation of the data.

CHAPTER 4 – Results

4.1 Introduction

This chapter will present data generated from this research. First, there will be a review of the study sample and estimated age range for each individual followed by a review of the state of cortical preservation of the skeletal elements assessed. The results of the metric and morphological cortical tissue microstructure analyses will then be reviewed which were used to determine the presence or absence of bacterial bioerosion.

The age of the seven individuals assessed in this study ranged between fourteen prenatal weeks of gestational development to two and a half years of age (see Table 7). For this research nineteen skeletal elements were scanned and analyzed (see Table 7). Four skeletal elements (the femur of Individual E, the humerus and femur of Individual F, and the femur of Individual G) were scanned multiple times to capture different regions of cortical tissue. Therefore, in total twenty-six micro-CT scans were captured.

Table 7: Age range and scanned skeletal elements for the assessed individuals

Individual	Estimated Age	Element Scanned
Individual A	14-16 prenatal weeks	Longbone
Individual B	38-40 prenatal weeks	Rib One (Inferior)
		Rib Two (Superior)
		Tibia Midshaft
Individual C	38-40 prenatal weeks	Cranial Fragment
		Ilium
		Femur Midshaft
Individual D	38-40 prenatal weeks	Cranial Fragment
		Neural Arch
Individual E	10.5 months of age	Cranial Fragment
		Neural Arch
		Femur Midshaft (Superior Region)
		Femur Midshaft (Inferior Region)
Individual F	1-2 years of age	Cranial Fragment
		Rib
		Proximal Humerus
		Humerus Midshaft
		Distal Humerus
		Ilium
		Proximal Femur
		Femur Midshaft
		Distal Femur
Individual G	2.5 years of age	Cranial Fragment
		Proximal Femur
		Femur Midshaft
		Distal Femur

4.2 Macroscopic Preservation Index

The Macroscopic Preservation Index (MPI) scoring system adopted and modified from Galligani and colleagues (2019) ranges between an MPI sum score of 5, meaning excellent cortical preservation, versus an MPI sum score of 0, meaning extremely poor cortical preservation. All raw data is presented in Table 8. The average MPI score for the skeletal elements assessed in this research was 3.5. As shown in Table 9, 57.1% of

individuals (n=4) had a sum MPI score of ≥ 3.5, meaning that over half of the skeletal elements assessed had very good to excellent cortical preservation. The macroscopic feature most prominent across skeletal elements was tiled cracking, whereas loss of tensile strength was least prominent.

Table 8: Macroscopic Preservation Index assessment

Individual	Estimated Age	Element Scanned	Macroscopic Assessment: Cortical Bone Preservation					
			Tiled Cracking	Surface Corosion	Surface Porosity	Fractures/ Cracks	Loss of Tensile Strength	Macroscopic Preservation Index
Individual A	14-16 prenatal weeks	Longbone	0.5	1	0	1	0.5	3
Individual B	38-40 prenatal weeks	Rib (superior thorax)	0.5	0.5	0.5	0.5	1	3
		Rib (inferior thorax)	0.5	0.5	0.5	0.5	1	3
		Tibia	0.5	0.5	0.5	0	0	1.5
Individual C	38-40 prenatal weeks	Cranial fragment	0.5	0.5	1	1	1	4
		Ilium	0.5	0.5	0	1	1	3
		Femur	0.5	0.5	0.5	1	1	3.5
Individual D	38-40 prenatal weeks	Cranial fragment	1	0.5	1	0.5	1	4
		Neural arch	1	1	1	0.5	1	4.5
Individual E	10.5 months of age	Cranial fragment	0.5	0.5	1	0.5	1	3.5
		Neural arch	1	0.5	1	0.5	1	4
		Femur	0.5	0	0.5	0.5	0.5	2
Individual F	1-2 years of age	Cranial fragment	0.5	1	1	0.5	1	4
		Humerus	0.5	1	0.5	1	1	4
		Rib	0.5	1	0.5	1	1	4
		Ilium	0.5	1	0.5	1	1	4
		Femur	0.5	0.5	1	1	1	4
Individual G	2.5 years of age	Cranial fragment	0.5	0.5	1	1	1	4
		Femur	0.5	1	0.5	0.5	1	3.5

Table 9: Individual Macroscopic Preservation Index data

Individual	Number of Bone Samples	Average MPI Score
A	1	3
B	3	2.5
C	3	3.5
D	2	4.3
E	3	3.2
F	5	4
G	2	3.8

4.3 Microscopic Cortical Bone Analysis

4.3.1 Metric Analysis: Microbial Tunnel Diameter

Microbial tunneling was identified in twenty-two of the twenty-six micro-CT scans (84.6%) (see Table 10). The cranial fragment scan of Individual D and the ilium scan of Individual F were inconclusive due to suboptimal scanning conditions and could not be assessed for traces of bacterial bioerosion. The range in microbial tunnel diameter was a primary consideration for this research to identify patterns of bacterial bioerosion across the skeleton. However, through the analysis of the microbial tunnel mean in conjunction with the median, a more precise representation of microbial tunnels extending throughout the cortical tissue can be illustrated (see Figure 7). The mean value represents the average microbial tunnel diameter with consideration to all data from each scan. In contrast, the median value represents the central microbial tunnel value with consideration to all data from each scan.

Table 10: Microbial tunnel prevalence and diameter measurement data

Individual	Estimated Age	Scan Number	Element Scanned	Microbial tunnels (P/A)	Diameter Range (µm)	Diameter Mean (µm)	Diameter Median (µm)
Individual A	14-16 prenatal weeks	1	Longbone	Present	5.16-13.72	8.79	8.38
Individual B	38-40 prenatal weeks	2	Rib One (Inferior)	Present	11.36-35.67	19.27	17.93
		3	Rib Two (Superior)	Present	12.44-41.68	20.45	17.99
		4	Tibia Midshaft	Present	6.15-29.63	13.98	11.26
Individual C	38-40 prenatal weeks	5	Cranial Fragment	Present	10.35-37.84	19.99	18.49
		6	Ilium	Present	7.53-51.64	31.99	34.43
		7	Femur Midshaft	Present	6.34-43.91	27.21	28.56
Individual D	38-40 prenatal weeks	8	Cranial Fragment	Inconclusive	-	-	-
		9	Neural Arch	Present	6.74-24.62	23.52	20.54
Individual E	10.5 months of age	10	Cranial Fragment	Absent	-	-	-
		11	Neural Arch	Present	10.98-24.32	16.62	15.81
		12	Femur Midshaft (Superior Region)	Present	7.71-17.24	10.72	9.63
		13	Femur Midshaft (Inferior Region)	Present	8.24-21.14	14.58	14.92
Individual F	1-2 years of age	14	Cranial Fragment	Present	16.88-48.98	26.25	21.95
		15	Rib	Present	11.44-56.77	32.05	30.21
		16	Proximal Humerus	Present	7.11-58.30	32.38	30.21
		17	Humerus Midshaft	Present	16.23-52.81	30.05	27.74
		18	Distal Humerus	Present	15.74-55.31	30.35	27.99
		19	Ilium	Inconclusive	-	-	-
		20	Proximal Femur	Present	8.56-49.88	26.75	25.84
		21	Femur Midshaft	Present	6.66-85.11	32.8	25.32
		22	Distal Femur	Present	10.17-47.24	28.15	27.04
Individual G	2.5 years of age	23	Cranial Fragment	Absent	-	-	-
		24	Proximal Femur	Present	11.32-116.04	48.14	36.51
		25	Femur Midshaft	Present	12.47-72.99	36.6	31.43
		26	Distal Femur	Present	11.48-92.58	41.79	40.23

The dash symbols (-) are indicating that microbial tunnels were unobservable, whether due to an absence of microbial tunnels or inconclusive results

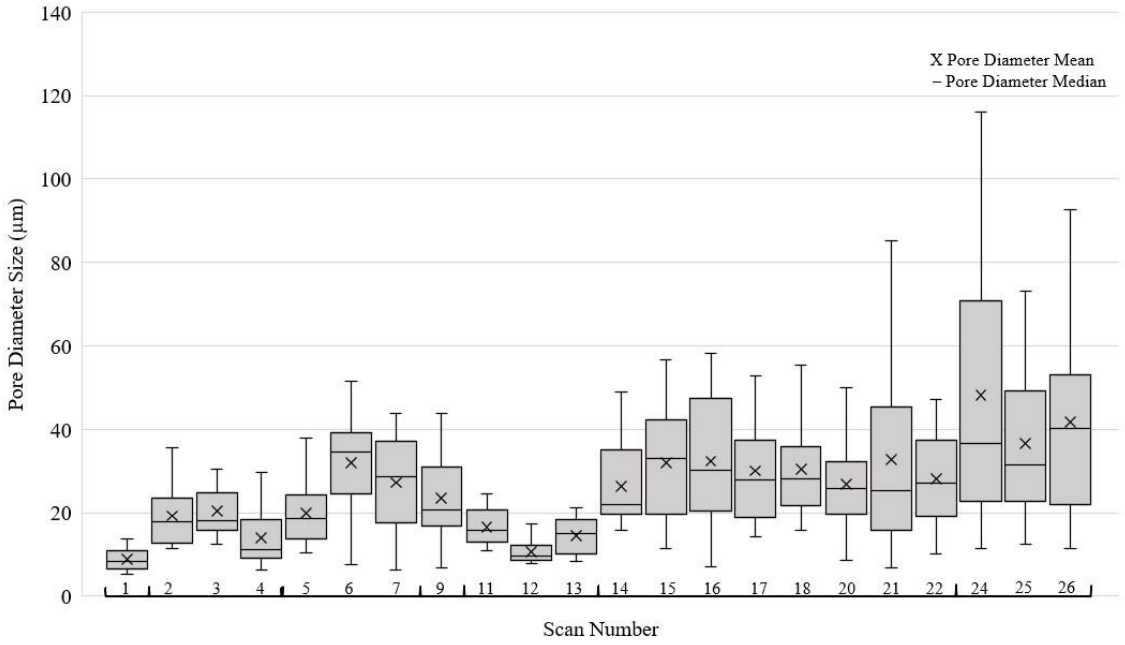

Figure 7: This boxplot graph depicts the metric microbial tunnel diameter data. The scan number provided along the x-axis corresponds with Table 10, representing each micro-CT scan that display microbial tunneling.

When comparing all microbial tunnel diameters, 50% of scans displaying microbial tunnels (n=11) show positively skewed data, where the diameter mean and median were closer to the lower quartile with consideration to the metric data boxplot (see Figure 7). This demonstrates that the majority of measured microbial tunnels per scan have diameters smaller than the midpoint of the diameter range. Additionally, in eighteen of the twenty-two scans (81.8%) which display deteriorating pores, the diameter mean was larger than the diameter median. This demonstrates that the majority of measured microbial tunnels per scan have diameters larger than the central diameter value.

The microbial tunnels with the smallest diameter were from the long bone of Individual A, the youngest individual assessed for this study (see Table 10). In contrast,

the microbial tunnels with the largest diameter were from the femur of Individual G, the oldest individual assessed for this study (see Table 10).

The bone fragments scanned from the same type of skeletal elements (e.g., both neural arches, both cranial fragments, and all three ribs) display microbial tunnels with similar diameter sizes to one another, regardless of age discrepancies (see Table 10). However, when comparing the microbial tunnel diameters of the multiple femora scans from different individuals, the diameter range typically increased in the older individuals, with the exception of Individual E (see Figure 8).

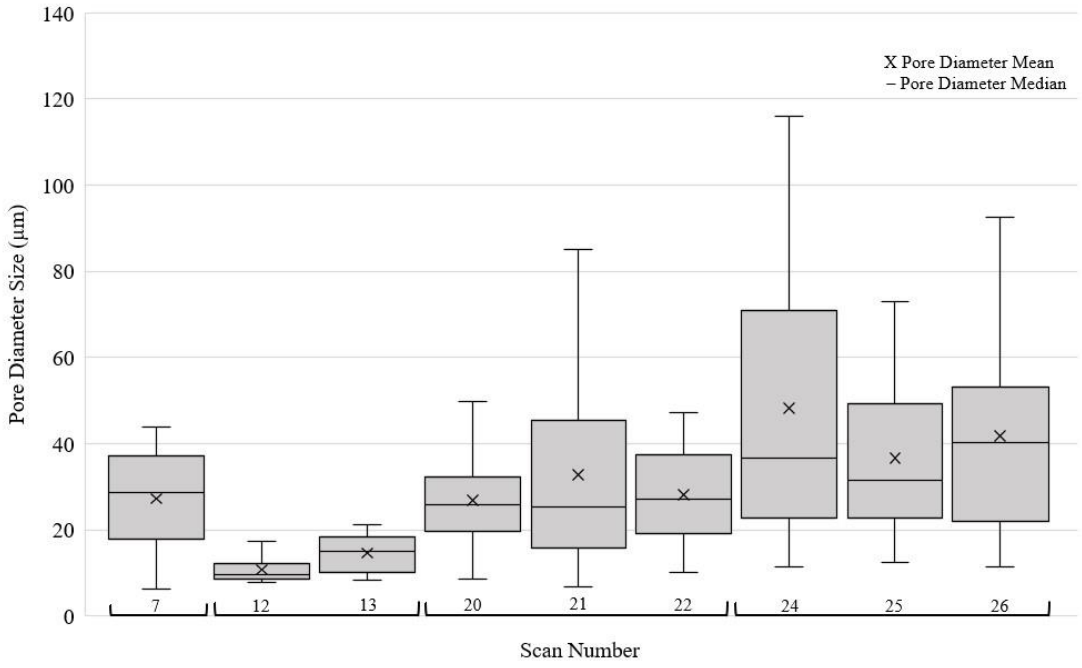

Figure 8: This boxplot depicts the metric microbial tunnel diameter data from all femora scanned for this thesis. The scan number provided along the x-axis corresponds with Table 10, representing each micro-CT femur scan that display microbial tunneling.

4.3.2 Morphological Analysis: Distribution of Microbial Tunnels

The first morphological assessment conducted was the analysis of the distribution of microbial tunnels (see Figure 3). Of the twenty-two viable scans where

microbial tunnels were identified, the majority of the scans (n=16; 72.7%) display microbial tunnels extending evenly throughout the cortical tissue. In contrast, microbial tunnel development near the periosteal surface, throughout the center of the cortical tissue, and near the endosteal surface were identified less commonly. All raw data is presented in Table 11.

Table 11: Distribution of microbial tunnels assessment

Individual	Estimated Age	Element Scanned	Deteriorating Pores (P/A)	Location of Microbial Tunnels Distribution			
				Periosteal	Center of Cortical Tissue	Endosteal	Throughout Cortical Tissue
Individual A	14-16 prenatal weeks	Longbone	Present	X	X		
Individual B	38-40 prenatal weeks	Rib One (Inferior)	Present				X
		Rib Two (Superior)	Present				X
		Tibia Midshaft	Present				X
Individual C	38-40 prenatal weeks	Cranial Fragment	Present				X
		Ilium	Present				X
		Femur Midshaft	Present	X			
Individual D	38-40 prenatal weeks	Cranial Fragment	Inconclusive	-	-	-	-
		Neural Arch	Present				X
Individual E	10.5 months of age	Cranial Fragment	Absent	-	-	-	-
		Neural Arch	Present				X
		Femur Midshaft (Superior Region)	Present		X		
		Femur Midshaft (Inferior Region)	Present				X
Individual F	1-2 years of age	Cranial Fragment	Present	X			
		Rib	Present				X
		Proximal Humerus	Present				X
		Humerus Midshaft	Present				X
		Distal Humerus	Present				X
		Ilium	Inconclusive	-	-	-	-
		Proximal Femur	Present				X
		Femur Midshaft	Present				X
		Distal Femur	Present			X	
Individual G	2.5 years of age	Cranial Fragment	Absent	-	-	-	-
		Proximal Femur	Present				X
		Femur Midshaft	Present				X
		Distal Femur	Present		X		

The dash symbols (-) are indicating that microbial tunnels were unobservable, whether due to an absence of microbial tunnels or inconclusive results

The specific location of microbial tunnel distribution is not a consistent morphological characteristic for specific bones. While most of the same types of skeletal elements from different individuals display microbial tunnel distribution extending evenly across the cortical tissue (e.g., ribs and neural arches), the scanned cranial fragments and femoral shafts from different individuals did not show similar patterns of microbial tunnel distribution (see Table 11). The cranial fragment of Individual F displays microbial tunnels throughout the center of cortical tissue and near the periosteal surface, whereas the cranial fragment of Individual C displays microbial tunnels extending evenly throughout the cortical tissue. Of the nine femora scanned, one femur (11.1%) displays microbial tunnels extending near the periosteal surface; two femora (22.2%) display microbial tunnels extending throughout the center of the cortical tissue; one femur (11.1%) displays microbial tunnels extending near the endosteal surface; and five femora (55.5%) display microbial tunnels extending evenly throughout the cortical tissue.

While assessing microbial tunnel development with consideration to the location of the nutrient foramen, the long bone scan of Individual A, the femora scans of Individual C and F, and the humeral scans of Individual F displayed the most conclusive results. In these scans, an increased concentration of microbial tunnels were identified around the region of the nutrient foramen.

In general, the younger individuals typically display lower concentrations of microbial tunnel development extending across a smaller area of cortical tissue (see Figure 9). In contrast, the older individuals display higher concentrations of microbial tunnel development extending across a larger area of cortical tissue (see Figure 10).

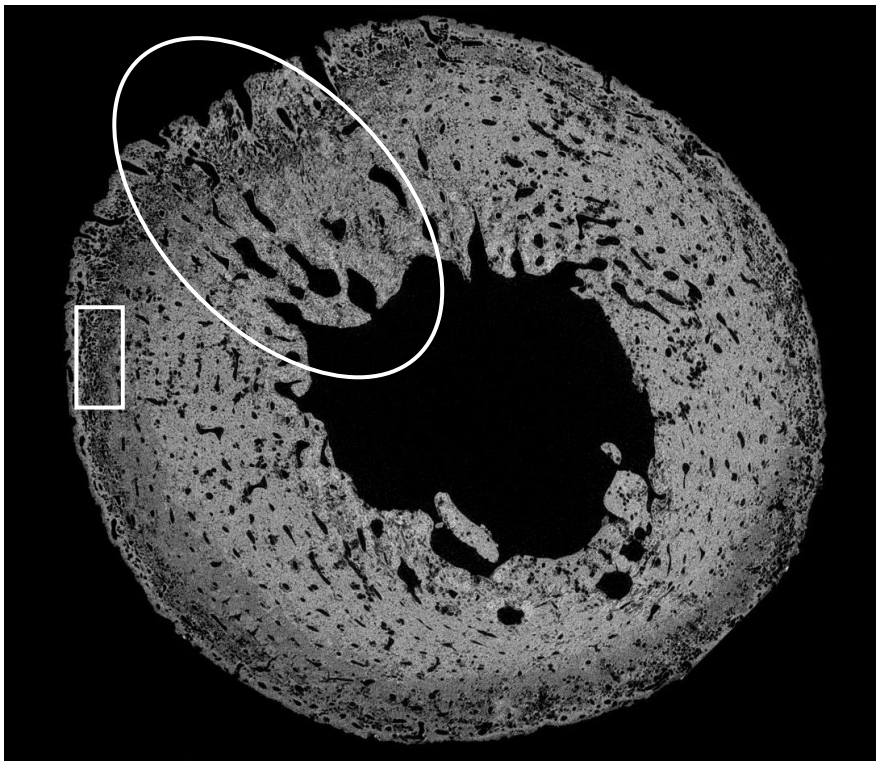

Figure 9: This image is a single transverse cross-section of the femur midshaft from Individual C (between the 38th and 40th week of gestational development at the time of death). The white line box is highlighting the region of bone with an increased concentration of microbial tunnels below the periosteal surface of the cortical tissue. The white oval is indicating the region where the nutrient foramen is beginning to take form.

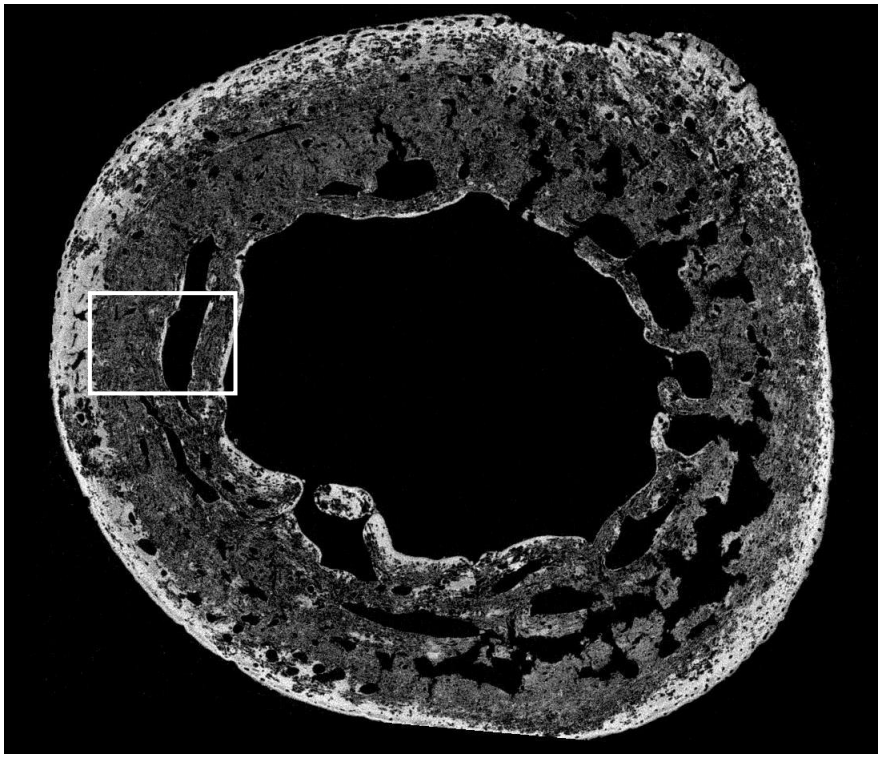

Figure 10: This image is a single transverse cross-section of the femur midshaft from Individual G (approximately two and a half years old at the time of death). The white line box is highlighting the region of bone with an increased concentration of microbial tunnels developing throughout the center of the cortical tissue around naturally occurring vascular canals.

4.3.3 Morphological Analysis: Cluster Formation

Cluster formation was scored as either present or absent, and of the twenty-two bone scans that display microbial tunnels, seventeen (77.3%) display clusters of microbial tunnels (see Table 12). It has been argued that microbial tunnel cluster formation can be assessed to better understand bacterial load and infiltration of endogenous gut bacteria into the cortical tissue (see Sasso et al., 2014). However, the results of this study did not support this theory. There was seemingly no correlation between the amount of specific cluster formations identified within a single scan and the age of the individual. Additionally, cluster formation did not occur consistently across the skeleton as not all individuals display cluster formation in all sampled skeletal elements (see Table 12).

Table 12: Cluster formation assessment

Individual	Estimated Age	Element Scanned	Microbial tunnels (P/A)	Cluster Formation (P/A)
Individual A	14-16 prenatal weeks	Longbone	Present	Present
Individual B	38-40 prenatal weeks	Rib One (Inferior)	Present	Present
		Rib Two (Superior)	Present	Present
		Tibia Midshaft	Present	Absent
Individual C	38-40 prenatal weeks	Cranial Fragment	Present	Absent
		Ilium	Present	Present
		Femur Midshaft	Present	Present
Individual D	38-40 prenatal weeks	Cranial Fragment	Inconclusive	-
		Neural Arch	Present	Present
Individual E	10.5 months of age	Cranial Fragment	Absent	-
		Neural Arch	Present	Absent
		Femur Midshaft (Superior Region)	Present	Absent
		Femur Midshaft (Inferior Region)	Present	Absent
Individual F	1-2 years of age	Cranial Fragment	Present	Present
		Rib	Present	Present
		Proximal Humerus	Present	Present
		Humerus Midshaft	Present	Present
		Distal Humerus	Present	Present
		Ilium	Inconclusive	-
		Proximal Femur	Present	Present
		Femur Midshaft	Present	Present
		Distal Femur	Present	Present
Individual G	2.5 years of age	Cranial Fragment	Absent	-
		Proximal Femur	Present	Present
		Femur Midshaft	Present	Present
		Distal Femur	Present	Present

The dash symbols (-) are indicating that microbial tunnels were unobservable, whether due to an absence of microbial tunnels or inconclusive results

4.3.4 Morphological Analysis: Sub-Periosteal Ridge Distinction

Sub-periosteal ridge distinction was scored on a scale of 0-3 where 0 indicates no ridge distinction development and 3 indicates complete ridge distinction across 60-100% of the external bone surface. All raw data is presented in Table 13. Of the twenty-two bone scans which display traces of microbial tunnels throughout the cortical tissue, over half of the scans (n=12; 54.5%) display evidence of complete sub-periosteal ridge

distinction (see Table 14). Complete sub-periosteal ridge distinction was identified more commonly in older individuals and irregularly in younger individuals (see Table 13).

Table 13: Sub-periosteal ridge distinction assessment

Individual	Estimated Age	Element Scanned	Microbial Tunnels (P/A)	Sub-Periosteal Ridge Distinction Score (0-3)
Individual A	14-16 prenatal weeks	Longbone	Present	0
Individual B	38-40 prenatal weeks	Rib One (Inferior)	Present	3
		Rib Two (Superior)	Present	0
		Tibia Midshaft	Present	3
Individual C	38-40 prenatal weeks	Cranial Fragment	Present	2
		Ilium	Present	2
		Femur Midshaft	Present	3
Individual D	38-40 prenatal weeks	Cranial Fragment	Inconclusive	-
		Neural Arch	Present	1
Individual E	10.5 months of age	Cranial Fragment	Absent	-
		Neural Arch	Present	0
		Femur Midshaft (Superior Region)	Present	1
		Femur Midshaft (Inferior Region)	Present	1
Individual F	1-2 years of age	Cranial Fragment	Present	2
		Rib	Present	3
		Proximal Humerus	Present	3
		Humerus Midshaft	Present	3
		Distal Humerus	Present	3
		Ilium	Inconclusive	-
		Proximal Femur	Present	3
		Femur Midshaft	Present	3
		Distal Femur	Present	1
Individual G	2.5 years of age	Cranial Fragment	Absent	-
		Proximal Femur	Present	3
		Femur Midshaft	Present	3
		Distal Femur	Present	3

The dash symbols (-) are indicating that microbial tunnels were unobservable, whether due to an absence of microbial tunnels or inconclusive results

Table 14: Sub-periosteal ridge distinction sample data

Sub-Periosteal Ridge Distinction Scores	Number of Scans Assessed	Percentage of Total
0	3	13.6%
1	4	18.2%
2	3	13.6%
3	12	54.5%
Total	22	100%

Sub-periosteal ridge distinction did not develop consistently across the skeleton, as multiple skeletal elements from the same individual were scored differently. Additionally, sub-periosteal ridge distinction did not develop consistently within individual skeletal elements as the proximal, midshaft, and distal regions of the femur for Individual F were not scored the same (see Table 13).

4.4 Individual Assessments

4.4.1 Individual A

Due to the developmental age, one unidentifiable long bone (likely femur, tibia, or humerus) from Individual A was scanned for this thesis. Based on long bone length, it was determined Individual A was between 14 and 16 weeks of gestational development at the time of death (see Fazekas and Kosa, 1978). The MPI score for the scanned long bone was 3 (see Table 8). Microbial tunnels were identified in the long bone with diameters ranging between 5.16 and 13.72 micrometers (μm) (see Table 10).

The microbial tunnels and clusters developed at the periosteal surface rather than below the periosteal surface, resulting in no sub-periosteal ridge distinction (see Figure 10). Due to the location and morphology of the microbial tunnel development it was determined the scanned skeletal remains from Individual A do not display evidence of bacterial bioerosion.

4.4.2 Individual B

Two different ribs and one tibia from Individual B were scanned for this thesis. Individual B was between 38 and 40 weeks of gestational development at the time of death. The MPI score for the scanned skeletal elements ranged between 1.5 and 3 (see

Table 8). Microbial tunnels were identified in all three scans. The one rib had microbial tunnels ranging between 12.44 and 41.68 µm in diameter. The other rib had microbial tunnels ranging between 11.36 and 35.67 µm in diameter. The tibia midshaft had microbial tunnels ranging between 6.15 and 29.63 µm in diameter (see Table 10).

Microbial tunnels were identified in all three skeletal elements and clusters were present in both rib scans (see Table 12). There was greater density at the periosteal surface of the one rib and tibia scanned, both were scored as 3 on the sub-periosteal ridge distinction scale (see Table 13). However, it was determined that scanned skeletal remains from Individual B do not display evidence of bacterial bioerosion.

4.4.3 Individual C

One cranial fragment, ilium, and femur from Individual C were scanned for this thesis. Individual C was between 38 and 40 weeks of gestational development at the time of death. The MPI score for the scanned skeletal elements ranged between 3 and 4 (see Table 8). Microbial tunnels were identified in all three scans. The cranial fragment had microbial tunnels ranging between 10.35 and 37.84 µm in diameter. The ilium had microbial tunnels ranging between 7.53 and 51.64 µm in diameter. The femur midshaft had microbial tunnels ranging between 6.34 and 43.91 µm in diameter (see Table 10).

Cluster formation was not present in the cranial fragment but was present in the ilium and femoral scans (see Table 12). There was greater density at the periosteal surface in all three scans, with scores ranging between 2 and 3 on the sub-periosteal ridge distinction scale (see Table 13). It was determined that all three skeletal elements scanned from Individual C do display evidence of bacterial bioerosion.

4.4.4 Individual D

One cranial fragment and neural arch from Individual D were scanned for this thesis. Individual D was between 38 and 40 weeks of gestational development at the time of death. The MPI score for the scanned skeletal elements ranged between 3 and 4 (see Table 8). The cranial fragment had inconclusive results due to scanning limitations and was therefore omitted from further analysis. Microbial tunnels were identified in the neural arch ranging in diameter from 6.74 to 24.62 µm (see Table 10).

Cluster formation was present in the neural arch. There was greater density at the periosteal surface and was scored as 1 on the sub-periosteal ridge distinction scale (see Table 13). It was determined that the scanned neural arch from Individual D does display evidence of bacterial bioerosion.

4.4.5 Individual E

One cranial fragment, neural arch, and femur from Individual E were scanned for this thesis. Individual E was approximately ten and a half months old at the time of death. The MPI score for the scanned skeletal elements ranged between 2 and 4 (see Table 8). Microbial tunnels were not identified in the cranial fragment but were identified in the neural arch and femoral scans. The neural arch had microbial tunnels ranging between 10.98 and 24.32 µm in diameter. The midshaft of the femur was scanned in two separate locations, with the microbial tunnels in the proximal region ranging between 7.71 and 17.24 µm in diameter and microbial tunnels in the distal region ranging between 8.24 and 21.14 µm in diameter (see Table 10).

Cluster formation was not identified in any of the scanned skeletal elements (see Table 12). Greater density at the periosteal surface was only identified in the femoral scans, with both regions scored as 1 on the sub-periosteal ridge distinction scale (see Table 13). It was determined that the cranial fragment and neural arch do not display evidence of bacterial bioerosion, but the femur does display evidence of bacterial bioerosion.

4.4.6 Individual F

One cranial fragment, rib, humerus, ilium, and femur from Individual F were scanned for this thesis. Individual F was between one and two years old at the time of death. The MPI score for all the scanned skeletal elements was 4 (see Table 8). The ilium produced inconclusive results due to scanning limitations and was therefore omitted from further analysis. The cranial fragment had microbial tunnels ranging between 16.88 and 48.98 µm in diameter. The rib had microbial tunnels ranging between 11.44 and 56.77 µm in diameter. The humerus was scanned in three separate locations, with the microbial tunnels in the proximal region ranging between 7.11 and 58.3 µm in diameter, the midshaft ranging between 16.23 and 52.81 µm in diameter, and the distal region ranging between 15.74 and 55.31 µm in diameter (see Table 10). The femur was also scanned in three separate locations, with the microbial tunnels in the proximal region ranging between 8.56 and 49.88 µm in diameter, the midshaft ranging between 6.66 and 85.11 µm in diameter, and the distal region between 10.17 and 47.24 µm in diameter (see Table 10).

Cluster formation was identified in all scanned skeletal elements (see Table 12). Greater density at the periosteal surface was identified in all scanned skeletal elements,

with scores ranging between 1 and 3 on the sub-periosteal ridge distinction scale (see Table 13). It was determined that all skeletal elements display evidence of bacterial bioerosion.

4.4.7 Individual G

One cranial fragment and femur from Individual G were scanned for this thesis. Individual G was approximately two and a half years old at the time of death. The MPI score for the scanned skeletal elements ranged between 3.5 and 4 (see Table 8). Microbial tunnels were not identified in the cranial fragment but were identified in the femur scans. The femur was scanned in three separate locations, with the microbial tunnels in the proximal region ranging between 11.32 and 116.04 µm in diameter, the midshaft ranging between 12.47 and 72.99 µm in diameter, and the distal region ranging between 11.48 and 92.58 µm in diameter (see Table 10).

Cluster formation was identified in all three regions of the femur (see Table 12). Greater density at the periosteal surface was identified in all three regions of the femur with each scored as 3 on the sub-periosteal ridge distinction scale (see Table 13). It was determined that the cranial fragment does not display evidence of bacterial bioerosion, but the femur does display evidence of bacterial bioerosion.

4.5 Conclusion

Of the nineteen skeletal elements scanned, the MPI scores for all remains ranged between 1.5 and 4.5. Variations in MPI scores did not influence the ability to scan and assess osteological microstructures. Microbial tunnels were identified in twenty-two of the twenty-six scans. Typically, mean microbial tunnel diameter remained similar

between specific bones, except in the case of the femur where microbial tunnel diameter increased in older individuals. Cluster formation and microbial tunnel distribution did not seem to develop consistently in terms of scan analyses. However, the microbial tunnel distribution data alongside the results of sub-periosteal ridge distinction were useful when differentiating whether microbial tunnels were the result of endogenous gut bacteria or environmental microbes. With consideration to the metric and morphological analyses of the scans with evidence of microbial tunnels (n=22), seventeen (77.3%) were identified as specifically having bacterial bioerosion present, affecting five of the seven individuals assessed (see Table 15).

Table 15: Summary of scans and individuals (highlighted) affected by bacterial bioerosion

Individual	Element Scanned	Estimated Age	Deteriorating Pores (P/A)	Bacterial Bioerosion (P/A)
Individual A	Longbone	14-16 prenatal weeks	Present	Absent
Individual B	Rib One (Inferior)	38-40 prenatal weeks	Present	Absent
	Rib Two (Superior)		Present	Absent
	Tibia Midshaft		Present	Absent
Individual C	Cranial Fragment	38-40 prenatal weeks	Present	Present
	Ilium		Present	Present
	Femur Midshaft		Present	Present
Individual D	Cranial Fragment	38-40 prenatal weeks	Inconclusive	-
	Neural Arch		Present	Present
Individual E	Cranial Fragment	10.5 months of age	Absent	Absent
	Neural Arch		Present	Absent
	Femur Midshaft (Superior Region)		Present	Present
	Femur Midshaft (Inferior Region)		Present	Present
Individual F	Cranial Fragment	1-2 years of age	Present	Present
	Rib		Present	Present
	Proximal Humerus		Present	Present
	Humerus Midshaft		Present	Present
	Distal Humerus		Present	Present
	Ilium		Inconclusive	-
	Proximal Femur		Present	Present
	Femur Midshaft		Present	Present
	Distal Femur		Present	Present
Individual G	Cranial Fragment	2.5 years of age	Absent	Absent
	Proximal Femur		Present	Present
	Femur Midshaft		Present	Present
	Distal Femur		Present	Present

The dash symbols (-) are indicating that microbial tunnels were unobservable, whether due to an absence of microbial tunnels or inconclusive results

CHAPTER 5 – Discussion

5.1 Introduction

This chapter will discuss and interpret the data collected for this thesis, beginning with how osteological preservation can influence bacterial bioerosion development. The metric and morphological data will also be discussed with an overview of how bacterial bioerosion can affect the entire skeleton. The results of this analysis as it pertains to each individual will also be discussed. This chapter concludes with a review of the metric, morphological, and imaging limitations of this study.

5.2 Bacterial Bioerosion as it Relates to Macroscopic Preservation Index

As discussed in section 3.4, the Macroscopic Preservation Index (MPI) assessment was conducted to determine if cortical preservation (as it relates to the MPI assessment) influenced the ability to visualize internal microstructures of bone, and if cortical preservation influenced patterns of microbial tunnel development within the cortical tissue. It was assumed that the rate of macroscopic bone deterioration would impact, at least to some extent, the ability to assess microbial tunneling. Interestingly, skeletal MPI did not have a significant impact on the ability to visualize and assess microstructures of the cortical tissue, as the micro-CT image quality was not affected by overall cortical preservation.

When the results of the MPI assessment were analyzed with consideration to microbial tunnel development, the two skeletal elements with the lowest MPI score – the tibia from Individual B and the femur from Individual E – had microbial tunnels with smaller than expected diameters (see Table 8 and Table 10). In contrast, the other

scanned skeletal elements from Individual B and Individual E that had higher MPI scores display microbial tunnels with more typical diameters (see Table 8 and Table 10).

Though the trajectory of skeletal diagenesis is relatively predictable, skeletal decomposition can vary depending on the interactions between the physical body and the burial environment (Hedges, 2002; Kendall, 2018; Kontopoulos, 2019). While the conditions of the burial environment (i.e., soil acidity and hydrology) for the individuals assessed in this thesis remain undetermined, the trend of reduced microbial tunnel diameter in association with low MPI values does support the argument that the burial environment influences cortical preservation, which in turn may impact the development bacterial bioerosion. This interpretation is unsurprising as previous research (see Turner-Walker, 2008; Booth, 2015; Kendall et al., 2018; Christensen et al., 2019a) and more recent work by Turner-Walker and colleagues (2019) highlight that some environmental microbes (e.g., certain strains of fungus and moss) can influence cortical preservation alongside the typical trajectory of skeletal diagenesis due to the leaching of certain metabolites and acids. These interactions can prompt skeletal decalcification, resulting in poor cortical preservation (i.e., "crumbly texture" of the cortical bone) as well as irregular porosity throughout the cortical tissue (Turner-Walker, 2019, p. 35). This is not to say that these types of environmental microbes influenced the osteological diagenesis of Individual B and Individual E, but it does demonstrate that there are a variety of environmental conditions that can impact the state of cortical preservation, and the formation of microbial bioerosion therein. With this, it is recommended that skeletal elements selected for bacterial bioerosion analyses should be chosen with consideration to cortical preservation. Evidence of bacterial bioerosion was confidently identified in

the skeletal elements with an MPI score of 2 or higher. Based on these findings, bones studied for this type of diagenetic research should maintain an MPI score of no less than 2.

5.3 Metric Analyses: Microbial Tunnel Assessments

5.3.1 Microbial Tunnel Diameter Range

For this research, the range of microbial tunnel diameter was assessed to ensure the microbial tunnels that developed throughout the cortical tissue since death were due to endogenous gut bacteria (see Table 1), as well as to explore bacterial bioerosion development across the skeleton. Upon analysis of the data, it was determined that metric analyses cannot be used independently from tunnel morphology to determine whether the microbial tunnels are strictly the result of endogenous bacteria. This is because individual microbial tunnels could not be differentiated from one another, and it was not possible to determine if larger microbial tunnels were the result of one large microbial tunnel taking form, or the amalgamation of multiple smaller microbial tunnels. Further micro-CT image rendering methods such as the isolation of microbial tunnels as specific Regions of Interest could allow for a more thorough assessment of tunnel morphology (see Caruso et al., 2021), and possibly help in the determination of what specific forms of bioerosion are present. Unfortunately, these additional steps were outside the scope of this thesis and were not completed.

While the metric analysis of microbial tunnels was not necessary for identifying specific forms of bioerosion, microbial tunnel diameter was useful in the assessment of

bacterial bioerosion development with consideration to specific factors such as age and specific skeletal elements (see section 4.3.1).

5.3.2 Bacterial Bioerosion and Age

Assessing bacterial bioerosion based on the range of microbial tunnel diameter can be useful when interpreting contextual information such as bacterial load. As older individuals would have had more interactions with their environment through the consumption of food, they would theoretically have more bacteria within their digestive tract at the time of death. Therefore, it was expected that a higher quantity of microbial tunnels developing with larger diameters – whether the result of one microbial tunnel or the amalgamation of multiple microbial tunnels – would be present in the cortical tissue of older individuals due to proliferating bacterial colonies (Sasso et al., 2014). In contrast, as younger individuals would have had less opportunity to interact with their environment through the consumption of food, they would theoretically have fewer bacteria within their digestive tract at the time of death. Therefore, it was expected that fewer microbial tunnels with smaller diameters would be present.

Femoral data were used for this analysis as the femur was available for analysis in over half of the individuals assessed (n=4; 57.1%) and many of these femora were scanned multiple times (see Table 10). As expected, older individuals typically display more microbial tunnels with larger diameters in comparison to younger individuals (see Table 10). However, other considerations beyond the range of microbial tunnel diameter must be made. First, as discussed in section 4.3.1, the entire diameter dataset should be analyzed while interpreting contextual information such as microbial attack and bacterial load. This is because the mean and median values of microbial tunnel diameter offer a

more precise representation of the size of microbial tunnels that have formed within the cortical tissue. Second, variations in expected microbial tunnel diameter (e.g., the reduced microbial tunnel diameter in the tibia of Individual E) may be reflective of other factors influencing bacterial bioerosion development, such as environmental conditions which could impact biological decomposition. In conclusion, the microbial tunnel diameter of bacterial bioerosion within the femur seems to be correlated with age, as older individuals typically had more microbial tunnels with larger diameters.

5.3.3 Bacterial Bioerosion and Specific Skeletal Elements

Other than in the femur, microbial tunnel diameter remained similar across other skeletal elements regardless of age. For example, in the cranial fragments displaying bacterial bioerosion from Individuals C and F the microbial tunnel diameter remained relatively consistent, despite there being an approximated year and a half age difference between these two individuals (see Table 10 and Figure 7). This pattern seems to apply to all microbial tunneling, not just bacterial bioerosion. For example, the microbial tunnels identified in the neural arch from Individual D were likely the result of bacterial bioerosion, whereas the microbial tunnels observed in the neural arch from Individual E were not, yet microbial tunnel diameter remained consistent between these two individuals (see Table 10). Similarly, though the microbial tunnels identified in the ribs from Individual B were not believed to be the result of bacterial bioerosion, whereas the rib of Individual F did have bacterial bioerosion present, they both had microbial tunnels with similar diameters (see Table 10).

These observed patterns in microbial tunnel diameter are likely due to the fact that the cortical thickness of the femur changes drastically within the first few years of

life (see Gosman et al., 2013), whereas the cortical thickness of other skeletal elements such as cranial fragments, neural arches, and ribs do not see as drastic a size variation over time and remain relatively consistent. With consideration to this pattern of microbial bioerosion as it relates to cortical thickness, it is possible that the rate of bioerosion is contingent on the quantity of cortical tissue that can be infiltrated by bacteria, and the amount of collagen fibrils therein which can be resorbed by endogenous or environmental microbes.

5.4 Morphological Analyses: Distribution of Microbial Tunnels

The distribution of microbial tunnels was analyzed in an attempt to better understand the development of bacterial bioerosion within cortical tissue The distribution and location of these microbial tunnels was not consistent within or between skeletal elements (see Table 11); however, the assessments of microbial tunnel development in relation to the external surface of bone were useful in determining the presence or absence of bacterial bioerosion. For example, if microbial tunnels were primarily formed at the periosteal surface, extending from the most external surface of cortical tissue, it was assumed that the microbial tunnels were the result of environmental microbes. Arguably then, when exploring bacterial bioerosion it is necessary to consider the distribution of these microbial tunnels as they relate to the internal and external surfaces of bone.

5.4.1 Distribution of Microbial Tunnels and the Nutrient Foramen

When assessing the distribution of microbial tunnels with consideration to the nutrient foramen, the long bone scan of Individual A, the femoral scans of Individual C

and F, and the humeral scans of Individual F displayed the clearest results. This is because the primary nutrient foramen of long bones form on the diaphysis and are therefore, easily identifiable while assessing the cortical tissue of the long bone shafts. Regardless of where the microbial tunnels formed in the cortical tissue (i.e., below the periosteal surface, throughout the center of the cortical tissue, near the endosteal surface, or evenly throughout the cortical tissue), there seemed to be increased microbial tunneling extending across a larger cross-sectional area near the long bone midshafts where the nutrient foramen typically develops (see Figure 11 and Figure 12).

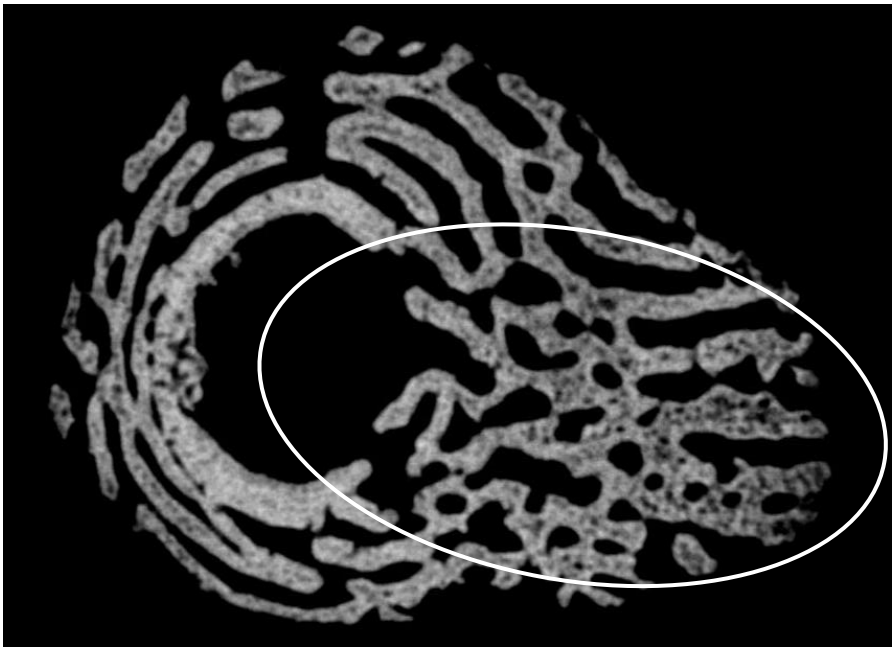

Figure 11: This image is a single transverse cross-section of the long bone midshaft from Individual A (between the 14th and 16th week of gestational development at the time of death). The white oval is indicating the region of bone where the primary nutrient foramen is located. Increased concentration of microbial tunnels can be identified within this region of interest in comparison to the opposing regions of bone where fewer microbial tunnels have developed.

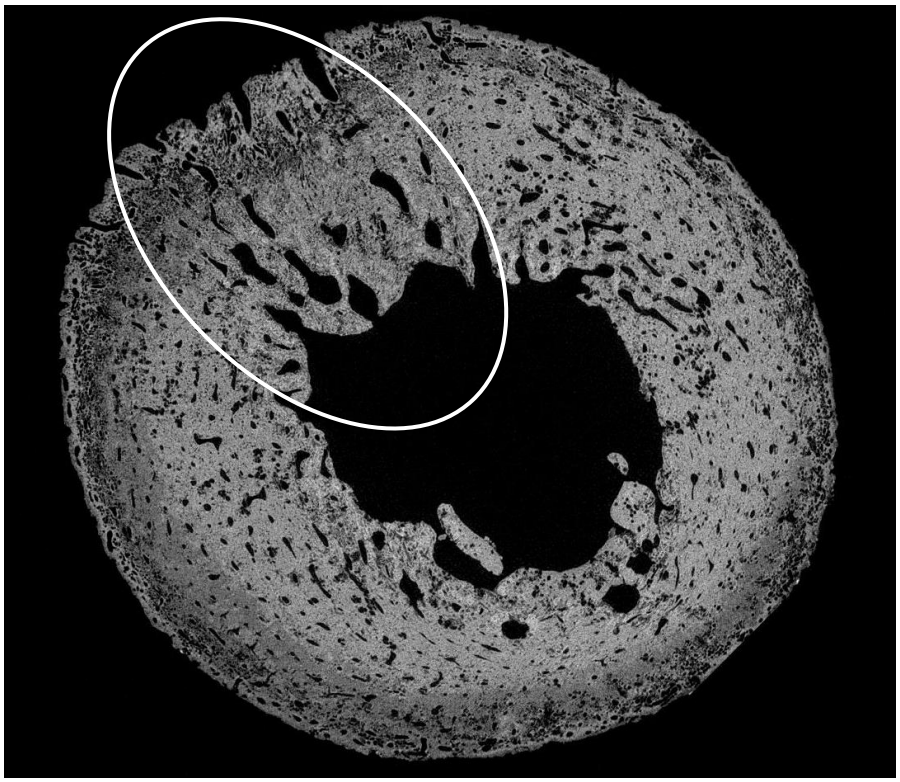

Figure 12: This image is a single transverse cross-section of the femur midshaft from Individual C (between the 38th and 40th week of gestational development at the time of death). The white oval is indicating the region of bone where the primary nutrient foramen is located. An increased concentration of microbial tunnels can be identified extending further into the center of the cortical tissue (highlighted by the white circle) near the region of interest in comparison to the opposing regions of bone where fewer microbial tunnels have developed and are located more closely to the periosteal surface.

As a pathway that connects the circulatory and skeletal systems, it was hypothesized that an increased number of microbial tunnels around the nutrient foramen may indicate endogenous diagenesis. This is because the movement of gut bacteria through the remaining circulatory system during decomposition would not necessarily facilitate contact between the external surface of bone at random, rather it would promote the infiltration into the Haversian system and medullary cavity. In contrast, rather than entering the cortical tissue directly through the nutrient foramen, skeletal diagenesis due to environmental microbes would depend on skeletonization. In these instances, upon making contact with the external surface of bone, microbes would begin

decomposing the external cells of the cortical tissue and would extend toward the central cortical tissue. However, when examining the long bone of Individual A this expected pattern was not observed. Because microbial tunnels identified in the long bone scan of Individual A were developing along the periosteal surface rather than the endosteal surface, and no sub-periosteal ridge was identified, it was determined that the microbial tunnels identified in this scan were the result of environmental microbes, despite the increased concentration of microbial tunneling at the site of the nutrient foramen.

The bond between the mineral (hydroxyapatite) and collagen of bone is not easily deconstructed by microbial enzymes (Kendall et al., 2018; Turner-Walker, 2019). Therefore, the collagen resorption prompted by microbes is more successful when microbes can infiltrate the naturally occurring pore structures in bone (e.g., the Haversian system and vascular canals) and can deconstruct the cells around osteological lacunae rather than on the dense external surface of the cortical tissue (Kendall et al., 2018; Turner-Walker, 2019). With consideration to the patterns of microbial tunnel formation identified in the long bone of Individual A, it can be argued that this process of osteological diagenesis applies to both endogenous gut bacteria and environmental microbes – both of which are more likely to initiate microbial bioerosion when infiltrating the cortical tissue through the nutrient foramen than making contact with the external cortical surface.

Assessing the region of bone that includes the nutrient foramen can be helpful in orientating the bone in anatomical position and interpreting microbial tunneling in association to the internal medullary cavity and the external surface of bone. However, microbial tunnel development in proximity to the nutrient foramen is not direct evidence

of bacterial bioerosion as any microbes, endogenous or environmental, could successfully prompt skeletal diagenesis at this naturally porous site.

5.4.2 Distribution of Microbial Tunnels and Age

Based on immature bone structure (see section 2.6.2), it was expected that traces of bacterial bioerosion would develop throughout the cortical tissue of younger individuals where their skeletal tissues are more susceptible to the effects of bioerosion and collagen resorption. However, this expected pattern was not observed in this dataset. Younger individuals generally display bacterial bioerosion across a smaller spatial area of cortical tissue in comparison to older individuals (see Figure 13 and Figure 14). Arguably then, the distribution of microbial tunnels relates more to bacterial load within the digestive tract at the time of death, rather than the maturation of the surrounding osteological tissue. Therefore, a reduced number of microbes within the gut microbiota at the time of death results in the diagenesis of less cortical tissue.

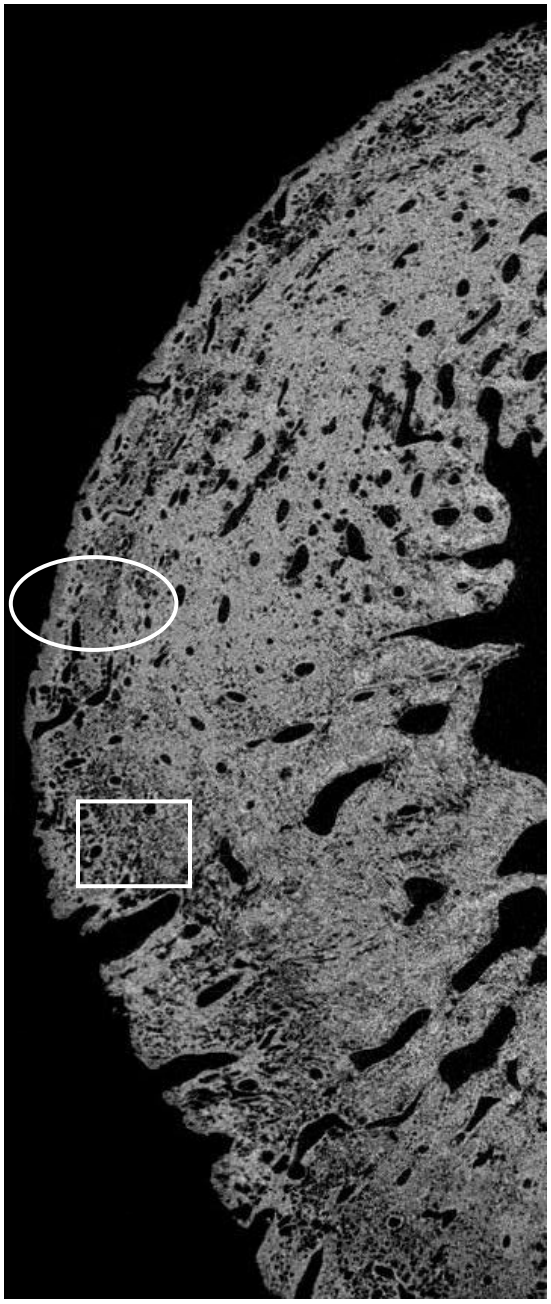

Figure 13: This image is a single transverse cross-section of the femur midshaft from Individual C (between the 38th and 40th week of gestational development at the time of death). The white line box is highlighting the region of bone with an increased concentration of microbial tunnels. In contrast, the white oval is highlighting a region of bone with inconsistent density, where the lighter coloration located at the edge of the bone and throughout the center of the cortical tissue is separated by a delineated section of cortical tissue with decreased density due to microbial tunnels.

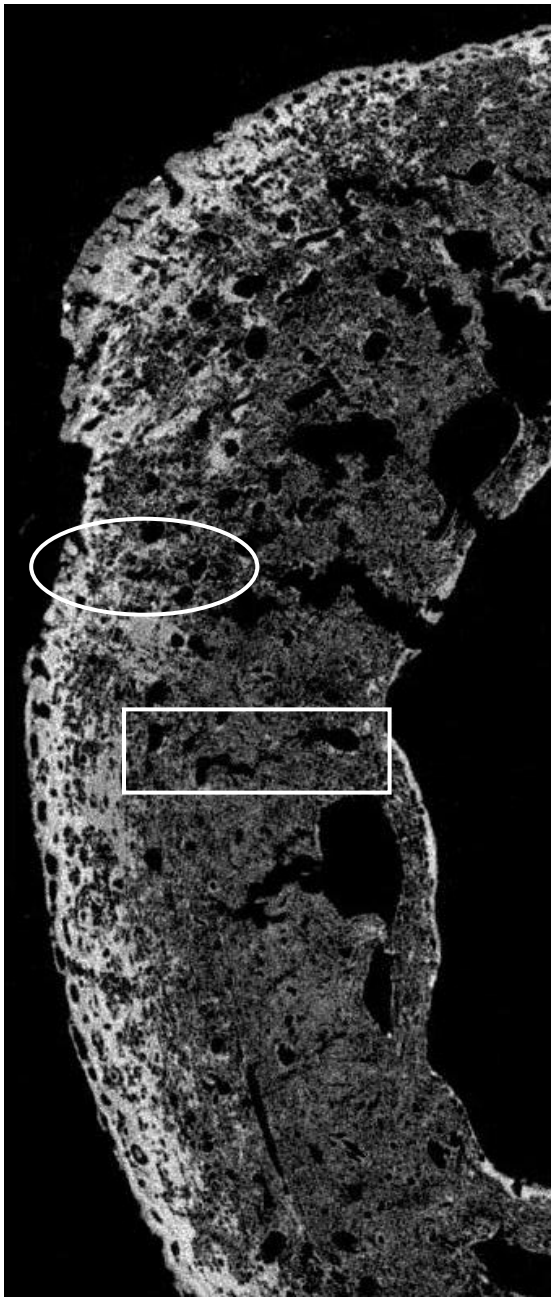

Figure 14: This image is a single transverse cross-section of the femur midshaft from Individual G (approximately two and a half years old at the time of death). The white line box is highlighting the region of bone with an increased concentration of microbial tunnels. In contrast, the lighter coloration located at the edge of the bone is indicating greater bone density. The white oval is highlighting a region of bone with inconsistent density, where the lighter coloration located at the edge of the bone is highly contrasted from the center of the cortical tissue with decreased density due to microbial tunnels.

5.5 Morphological Analyses: Cluster Formation

Cluster formation was expected to be more prominent within older individuals as these individuals would have had a higher gut bacterial load at the time of death. However, the presence of cluster formation did not change significantly between the various micro-CT scans captured. Regardless of age and whether or not microbial tunneling was the result of endogenous gut bacteria or environmental microbes, cluster formations were identified in similar quantities across individual bones and between individuals. It is therefore likely that cluster formation is not contingent on contextual circumstances (i.e., bacterial load or diagenesis-causing microbes). With this, cluster analysis is not a required morphological trait to determine the presence or absence of bacterial bioerosion within a scanned skeletal element.

5.6 Morphological Analyses: Sub-Periosteal Ridge Distinction

The scoring system used for the sub-periosteal ridge distinction assessment had good replicability as demonstrated through intraobserver analysis of score precision over time. This was significant as the results from these assessments were used to determine the presence or absence of bacterial bioerosion in each micro-CT scan. However, it should be noted that sub-periosteal ridge distinction can form in different ways and was noted during this analysis. For example, even though the scan displayed in Figure 13 and the scan displayed in Figure 14 are morphologically very different, they were both scored as 3 on the sub-periosteal ridge distinction scale. This is because in Figure 13, the ridge has formed due to the increased concentration of microbial tunnels below the entire ridge of the external cortical surface, whereas, in Figure 14, the ridge has formed due to the increased concentration of porosity occurring throughout the center and

endosteal region of cortical tissue. While this assessment is important when determining whether bioerosion is the result of endogenous or environmental microbes, it is somewhat subjective as there is not one specific defining feature that can be used to identify sub-periosteal ridge development. Due to the subjective nature of sub-periosteal ridge development, it is clear that additional morphological analyses should be considered when determining the presence or absence of bacterial bioerosion.

5.7 Bacterial Bioerosion Across the Skeleton

The analysis of multiple bones from different regions of the body (i.e., cranium, vertebrae, ribs, long bones) demonstrated that bacterial bioerosion does not develop consistently across the skeleton, especially with consideration to the cranial fragments. Of the five sampled cranial fragments, one produced inconclusive results due to scanning limitations (Individual D), two do not show evidence of bacterial bioerosion (Individuals E and G), and two do show evidence of bacterial bioerosion (Individuals C and F) (see Table 15).

The two cranial fragments that do not display evidence of bacterial bioerosion were from Individual E, who was approximately ten and a half months old at the time of death, and Individual G, who was approximately two and a half years old at the time of death. However, evidence of bacterial bioerosion was identified in the scanned femora from these two individuals. Therefore, while there were, in fact, endogenous bacteria influencing the skeletal diagenesis of other skeletal elements, the cranial fragments remained free of bacterial bioerosion. In these instances, it is likely that the increased distance between the cranial bones and the digestive organs that house the gut

microbiota reduced the likelihood of the endogenous bacteria infiltrating the cortical tissue of the cranium.

The two cranial fragments that do display evidence of bacterial bioerosion are from Individual C, who was between the 38th and 40th week of gestational development at the time of death, and Individual F, who was between one and two years of age at the time of death. Given the age difference between these two individuals, it is not likely that this similarity in the presence of bacterial bioerosion is associated to age and/or bacterial load – where older individuals who maintain a higher bacterial load at the time of death are more likely to display evidence of microbial tunneling in bones further away from the digestive tract. Currently, there are no data that could explain why these two individuals display evidence of bacterial bioerosion within the cranial bones whereas Individual E and Individual G do not.

These results demonstrate that while bacterial bioerosion can develop within cranial bones, they are not optimal bones to sample when conducting this type of diagenetic research. The conditions influencing the likelihood of bacterial bioerosion development in cranial bones are unknown, and therefore, cranial fragment scans should be examined alongside scans of other skeletal elements from the same individual when conducting bacterial bioerosion assessments.

5.8 Bacterial Bioerosion Across Specific Skeletal Elements

While assessing bacterial bioerosion across specific skeletal elements, the humerus and femur from Individual F, as well as the femur of Individual G warranted further exploration. As these two individuals were the oldest in the sample, they likely

had the highest bacterial load within their digestive tracts at the time of death. It can be presumed that this increase in bacterial load would more accurately represent advanced bacterial bieorsion and therefore demonstrate a broader range of bacterial bioerosion development.

These skeletal elements were scanned at the proximal, midshaft, and distal regions in order to assess overall skeletal diagenesis. For all humeral and femoral scans, bacterial bioerosion developed relatively similarly at the proximal, midshaft, and distal regions. The humerus produced the most consistent results in terms of microbial tunnel diameter across these three regions (see Table 10 and Figure 7). The femoral scans, however, display more variation in microbial tunnel diameter, but these variations were not consistent across individuals. For example, the femur midshaft from Individual F has microbial tunnels with significantly larger diameters in comparison to the proximal and distal regions (see Table 10). In contrast, the proximal and distal regions of the femur from Individual G has microbial tunnels with significantly larger diameters in comparison to the femur midshaft (see Table 10). Currently, there is no explanation as to why this variation in bacterial bioerosion microbial tunnel diameter was observed in these femoral samples. Fortunately however, these variations did not impede the ability to determine the presence or absence of bacterial bioerosion within each scan.

The number of cluster formations identified per scan were relatively consistent. However, despite sub-periosteal ridge distinction and microbial tunnel distribution developing relatively consistently across individual bones, there was some variation in the distal femora scans from Individuals F and G. The distal region of the femur from Individual F was scored as 1 for sub-periosteal ridge development, whereas all other

scans from the humerus and femora were scored as 3. Additionally, both distal femoral scans were described as having microbial tunnels concentrated near the endosteal surface or throughout the center of the cortical tissue. In contrast, the proximal and midshaft scans were described as having microbial tunnels extending evenly through the cortical tissue. One explanation for this variation could be the increased quantity of trabecular bone at the distal end of the femora. Trabecular bone is more porous in structure when compared to cortical bone, and this increased porosity may reduce the movement of collagenase-secreting microbes through to the sub-periosteal region of cortical tissue. Rather than the microbes extending evenly through the cortical bone, microbes may concentrate within the central labyrinth of trabecular bone and deconstruct the cells around the endosteal lacunae. Therefore, variations in the structure and thickness of these cortical tissues may impact the development of these characteristics of microbial bioerosion in different regions of the same bone. Luckily, these variations in microbial tunnel distribution and sub-periosteal ridge distinction did not impede the ability to determine if bacterial bioerosion was present.

Cortical bone is less porous than trabecular bone and offers a larger cross-sectional area with more consistent density to analyze variations in microbial tunnel development (see Figure 15). In contrast, the increased concentration of trabecular bone at the proximal and distal ends of long bones offers a smaller cross-sectional area of dense cortical bone to analyze variations in microbial tunnel development (see Figure 16 and Figure 17). While the proximal, midshaft, and distal regions of long bones can all be scanned and assessed for traces of bacterial bioerosion, the data collected through this study validate that the midshaft of the long bone is the most useful.

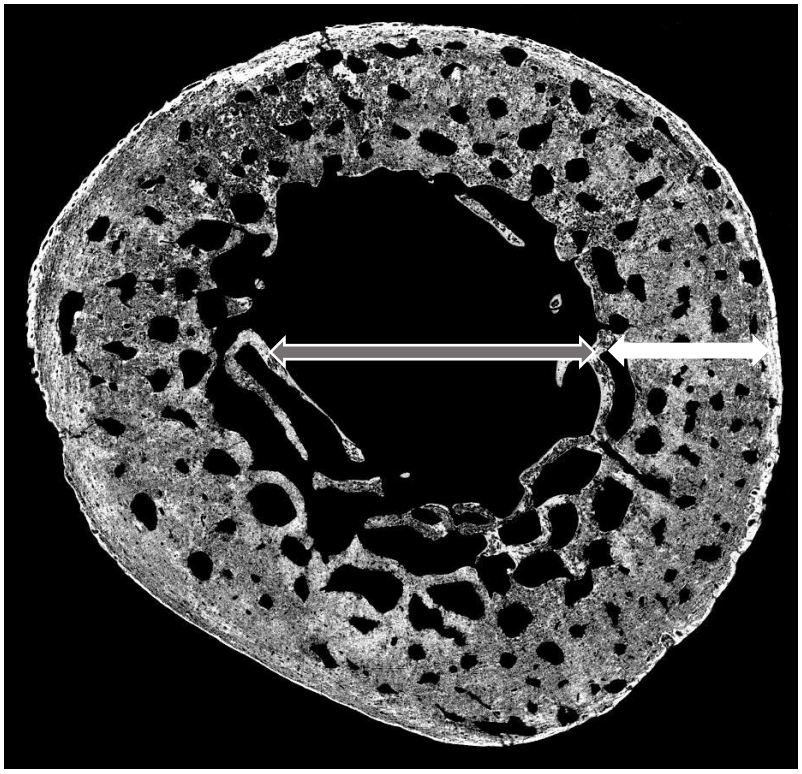

Figure 15: This image is a single transverse cross-section of the humerus midshaft from Individual F (between one and two years of age at the time of death). The grey arrow with the white outline is indicating the bone's central medullary cavity where trabecular bone can reside. In contrast, the white arrow is indicating the cortical tissue in which microbial tunnels can be easily identified. The increased thickness and density of cortical bone offers a larger cross-sectional area for analysis into microbial bioerosion development.

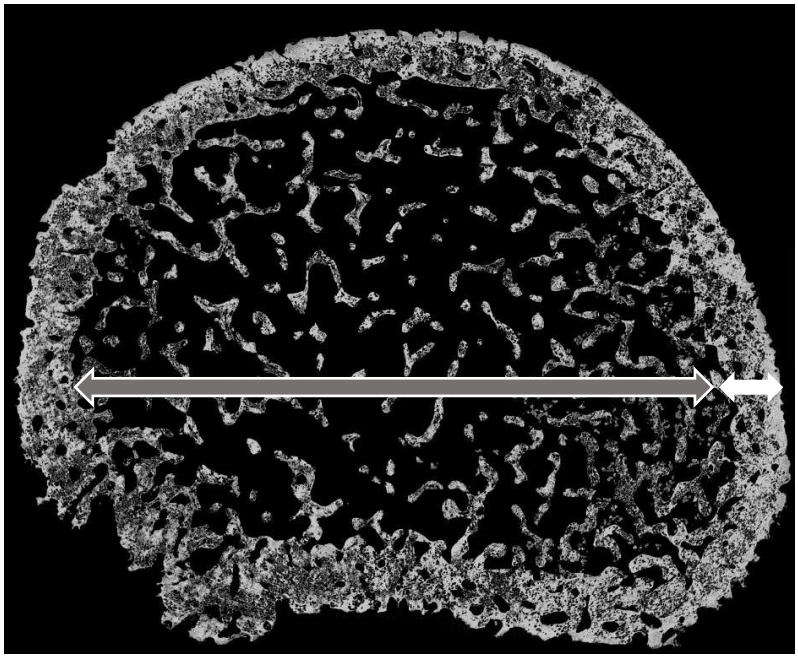

Figure 16: This image is a single transverse cross-section of the proximal humerus for Individual F (between one and two years of age at the time of death). The grey arrow with the white outline is indicating the central region of bone which is primarily comprised of trabecular tissue. In contrast, the white arrow is indicating the cortical tissue in which microbial tunnels can be easily identified. Because the proximal humerus is mostly comprised of porous trabecular tissue, the cross-sectional area of cortical tissue available to assess for evidence of bacterial bioerosion is reduced significantly – especially in comparison to the midshaft scan (see Figure 15).

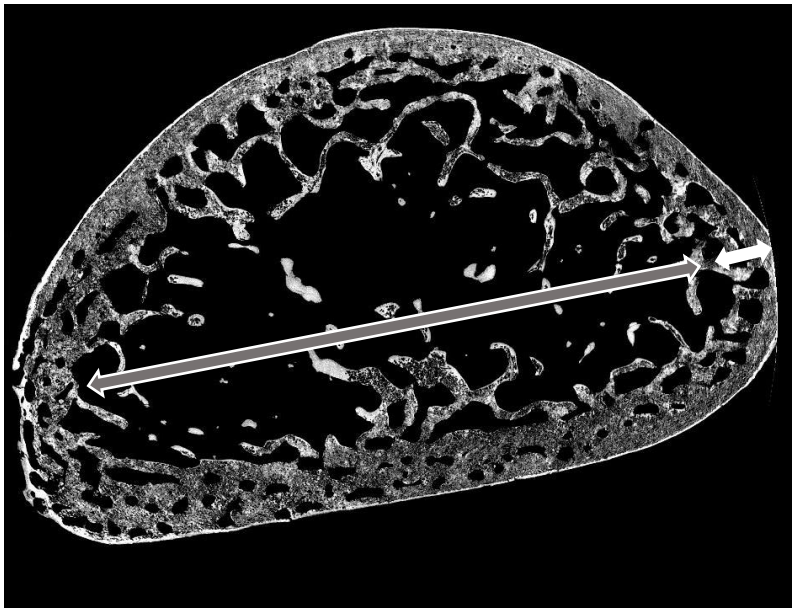

Figure 17: This image is a single transverse cross-section of the distal humerus for Individual F (between one and two years of age at the time of death). The grey arrow with the white outline is indicating the central region of bone which is primarily comprised of trabecular tissue. In contrast, the white arrow is indicating the cortical tissue in which microbial tunnels can be easily identified. Because the distal humerus is mostly comprised of porous trabecular tissue, the cross-sectional area of cortical tissue available to assess for evidence of bacterial bioerosion is reduced significantly – especially in comparison to the midshaft scan (see Figure 15).

5.9 Individual Assessments

5.9.1 Individual A

One unidentifiable long bone was scanned and microscopically assessed from Individual A. This long bone displays traces of microbial tunneling throughout the cortical tissue (see Figure 18). However, due to the fact that the microbial tunnels developed at the periosteal surface and the cortical tissue does not display greater density in the form of a sub-periosteal ridge, it was determined that these microbial tunnels were likely the result of environmental microbes, not endogenous gut bacteria.

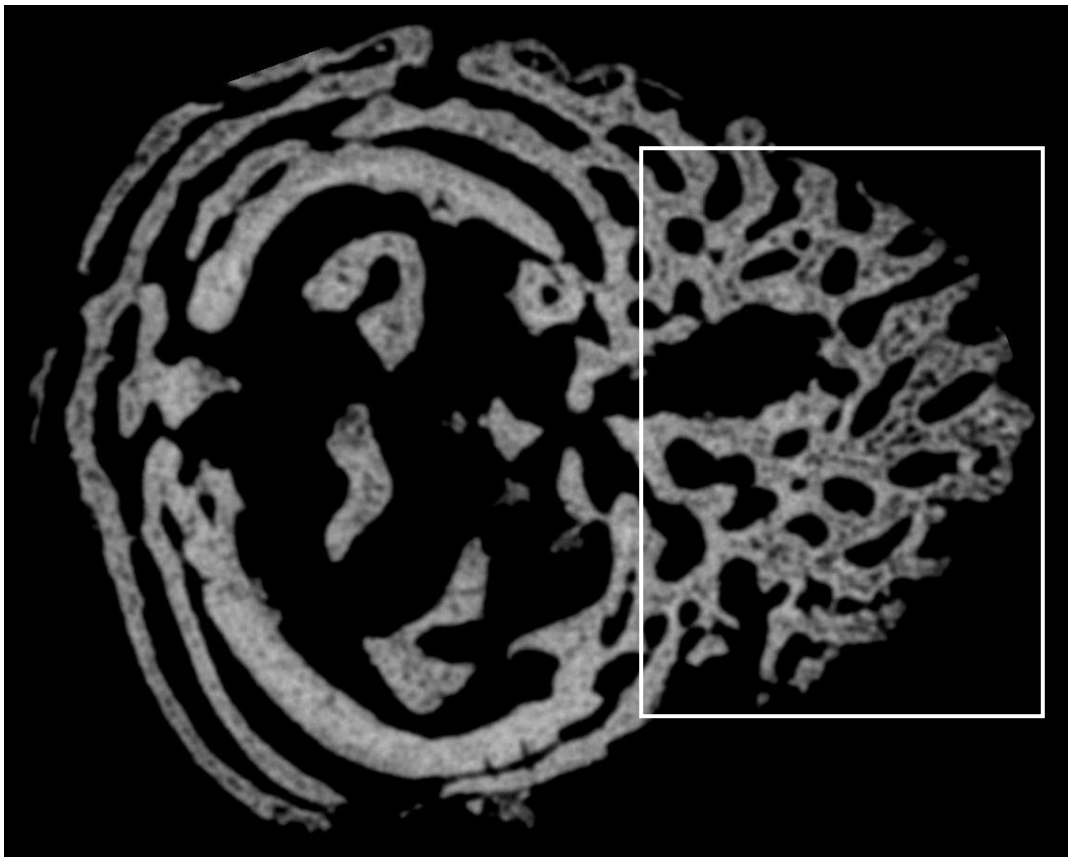

Figure 18: This image is a single transverse cross-section of long bone midshaft from Individual A (between the 14th and 16th week of gestational development at the time of death). The white line box is highlighting the region of bone with an increased concentration of microbial tunnels developing near the periosteal surface, around naturally occurring vascular canals.

Individual A likely displays microbial tunnels extending across a large area of the cortical tissue because there is extensive porosity on the cortical surface (see Figure 19). As previously discussed, bioerosion in the form of collagen resorption (whether due to endogenous bacteria or environmental microbes) is more successful when microbes infiltrate the naturally occurring pore systems and enlarge the osteological lacunae throughout the cortical tissue (see Kendall et al., 2018; Turner-Walker, 2019). The evidence of increased external cortical tissue porosity along with the minimal collagen mineralization during prenatal development would have likely facilitated the infiltration of environmental bacteria at the periosteal surface, where bacteria could then transmigrate through the tissue toward the endosteal surface (e.g., the medullary cavity) (see Figure 19).

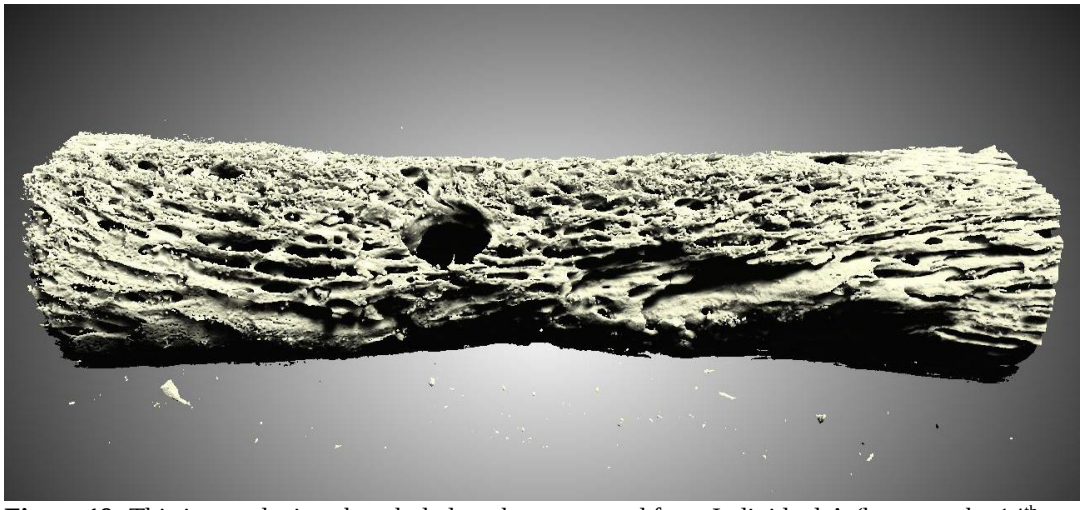

Figure 19: This image depicts the whole long bone scanned from Individual A (between the 14th and 16th week of gestational development at the time of death), demonstrating the significant porosity on the external surface of bone.

Individual A was estimated to be around the 14th and 16th week of gestational development at the time of death. Given the age of this individual and the likelihood that

the microbial tunnels present were the result of environmental microbes, this individual likely experienced prenatal death and had a sterile gut.

5.9.2 Individual B

Two ribs and one tibia were scanned and microscopically assessed from Individual B. Even though there were variations in cortical density due to microbial tunnels (see Figure 20), as well as greater density at the periosteal surface (see Figure 21), it was determined that the skeletal elements of this individual do not display evidence of bacterial bioerosion.

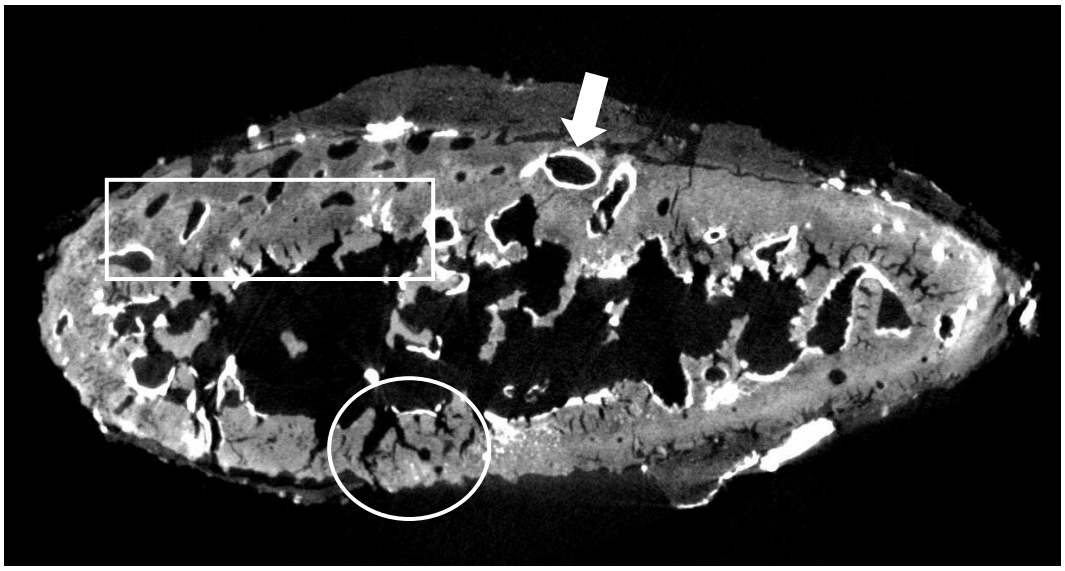

Figure 20: This image is a single transverse cross-section of superior rib from Individual B (between the 38th and 40th week of gestational development at the time of death). The development of microbial tunnel cluster formation is highlighted with the white lined box. The white arrow is indicating evidence of collagen hyper-mineralization development around a naturally occurring vascular canal, and the white circle is indicating a region of bone displaying cortical micro-fissures.

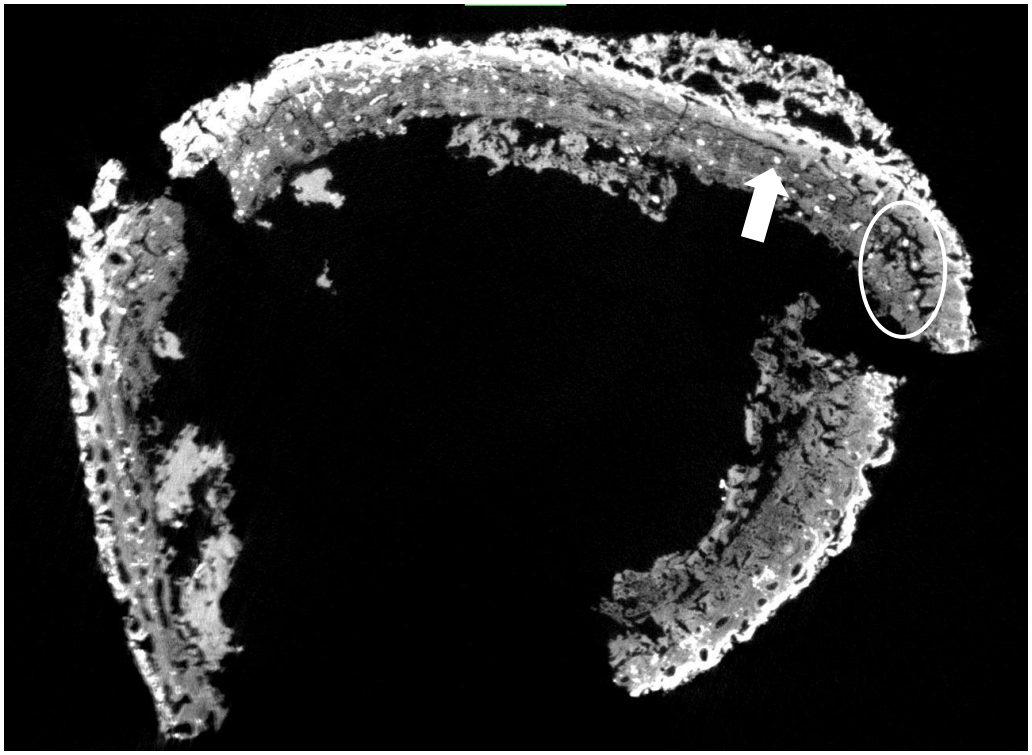

Figure 21: This image is a single transverse cross-section of tibia shaft from Individual B (between the 38th and 40th week of gestational development at the time of death). The bright white features throughout the cortical tissue represent mineral inclusions and are highlighted by the white arrow. The white oval is indicating a region of bone displaying cortical micro-fissures.

Certain degenerative features within the osteological tissue such as micro-fissures and hyper-mineralized inclusions have been associated with conditions of the burial environment (e.g., soil acidity, hydrology) (see Figure 20 and Figure 21) (Booth et al., 2016; Kendall et al., 2018). The research of Booth and colleagues (2016) discovered that fluctuations in bone density due to microbial tunneling (unaffiliated to bacterial bioerosion development) were found within bone that displays evidence of micro-fissures and hyper-mineralization. Therefore, when these two types of degenerative features are identified within bioarchaeological remains, it is likely that corresponding microbial tunnels are the result of environmental conditions rather than endogenous microbes. In conclusion, even though microbial tunnels have formed in all three bone samples from Individual B, they are not likely to be the result of endogenous microbes.

Individual B was estimated to be around the 38th and 40th week of gestational development at the time of death. Given that this individual does not display direct evidence of bacterial bioerosion it is likely that they would have experienced prenatal death or died due to obstetric complications during birth and had a sterile gut.

5.9.3 Individual C

The cranial fragment, ilium, and femur scanned from Individual C all display evidence of bacterial bioerosion. This was determined based on the analyses of microbial tunneling alongside the results from the sub-periosteal ridge distinction assessment, where ridge distinction was identified across 25% to 100% of the periosteal surface for all skeletal elements (see Figure 22).

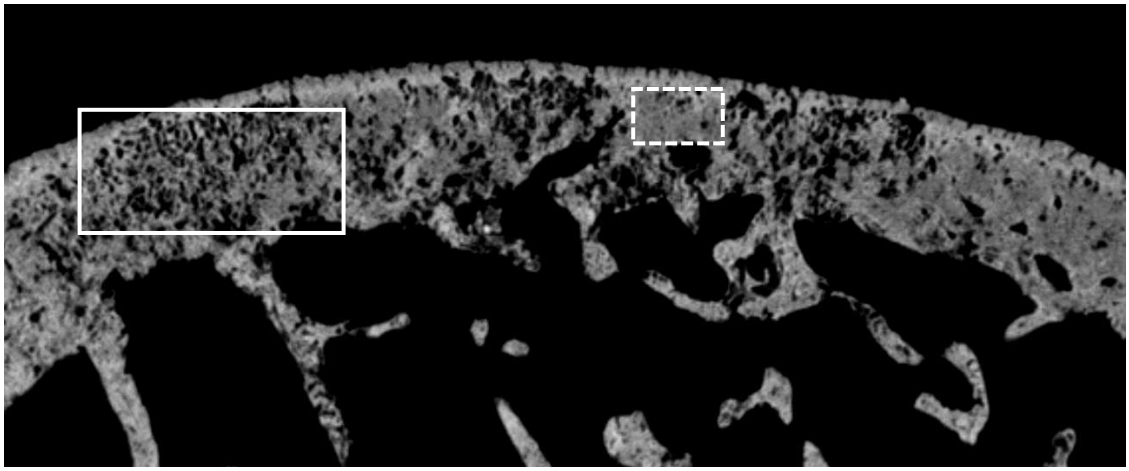

Figure 22: This image is a single transverse cross-section of ilium from Individual C (between the 38th and 40th week of gestational development at the time of death). The white line box is highlighting the region of bone with decreased density due to an increased concentration of microbial tunneling, whereas the white dotted-line box is highlighting the region of bone with typical density, unaffected by microbial tunneling.

Individual C was estimated to be around the 38th and 40th week of gestational development at the time of death. Given that the skeletal remains of this individual

display evidence of bacterial bioerosion, it is likely that they would have lived long enough to engage in at least one feeding introducing bacteria into the gut, but still died shortly after birth.

5.9.4 Individual D

A neural arch – believed to be from a cervical vertebra – was the only skeletal element scanned from Individual D that could be assessed for traces of bacterial bioerosion, as the cranial fragment produced inconclusive results due to scanning limitations. The neural arch is the posterior component of the vertebrae. It is expected that vertebrae of the inferior spinal column (i.e., the thoracic and lumbar vertebrae) would be more susceptible to bacterial bioerosion, as the digestive organs that house the gut microbiota are directly adjacent to these bones. However, as described, the neural arch of Individual D was believed to be from a cervical vertebra, which sits more superiorly within the spinal column. While this neural arch would not have been directly adjacent to the primary source of the gut microbiota, the scanned neural arch does display evidence of bacterial bioerosion based on the presence of microbial tunneling and sub-periosteal ridge distinction which was identified across 1% to 24% of the periosteal surface for the skeletal element (see Figure 23). Likely the presence of bacterial bioerosion in this neural arch reflects the close proximity of the esophagus to the spinal column, where gut bacteria could easily transmigrate into the esophagus once the lower esophageal sphincter relaxes after death (Clark et al., 1996).

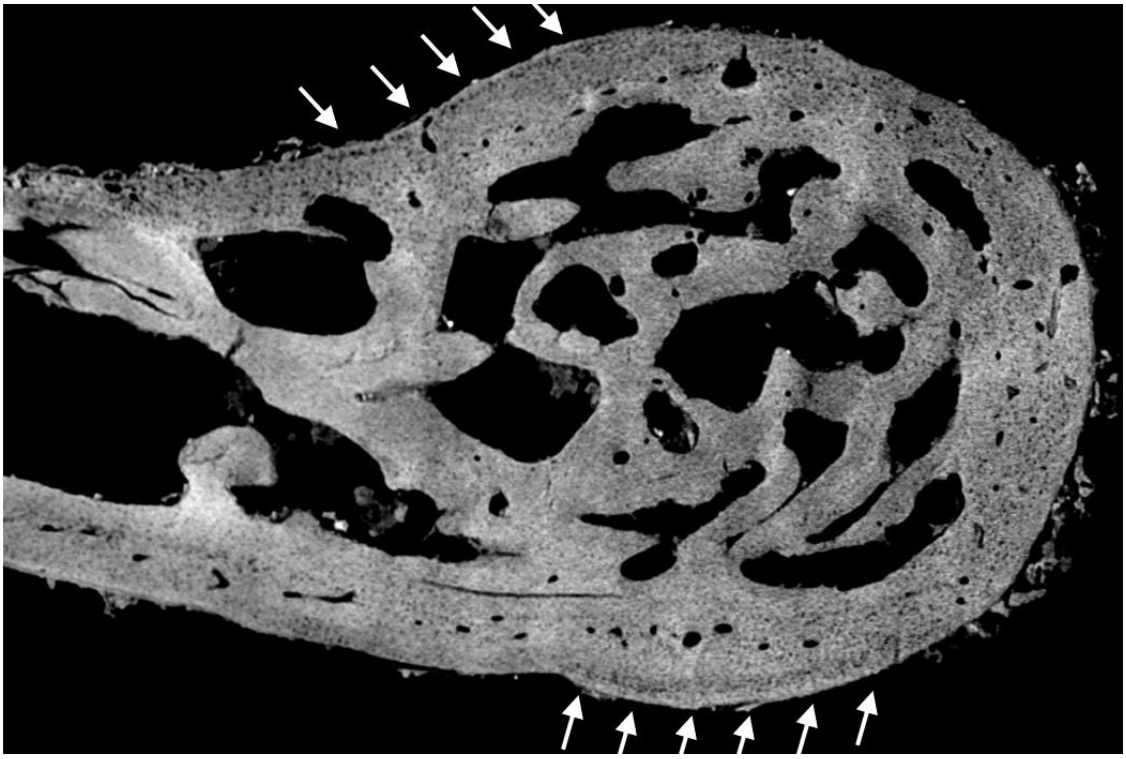

Figure 23: This image is a single transverse cross-section of cervical neural arch from Individual D (between the 38th and 40th week of gestational development at the time of death). The white arrows are indicating the region of the external bone surface with some sub-periosteal ridge distinction due to the subtle and consistent formation of microbial tunnels below the periosteal region. This sample was scored as 2 on the Ridge Distinction scale.

Individual D was estimated to be around the 38th and 40th week of gestational development at the time of death. Given that the scanned skeletal element of this individual displays evidence of bacterial bioerosion, it is likely that they would have lived long enough to engage in at least one feeding introducing bacteria into the gut, but died shortly after birth.

5.9.5 Individual E

Of the three skeletal elements scanned from Individual E, a cranial fragment and a neural arch – believed to be from either a thoracic or lumbar vertebra – do not display traces of bacterial bioerosion, whereas the midshaft of the femur does. It is possible that the cranial fragment does not display evidence of bacterial bioerosion because of the

physical distance separating the cranium and the gut. However, because the scanned neural arch is believed to be from a vertebra of the lower spinal column, it would have been directly adjacent to the primary digestive organs which house the gut microbiota. In addition to this unexpected absence of bacterial bioerosion in the neural arch, the femur midshaft scan shows evidence of a reduced bacterial load. The few microbial tunnels identified in the cortical bone of the femur were located sporadically throughout the cortical tissue and had smaller microbial tunnel diameters in comparison to what is expected in older individuals (see Figure 24).

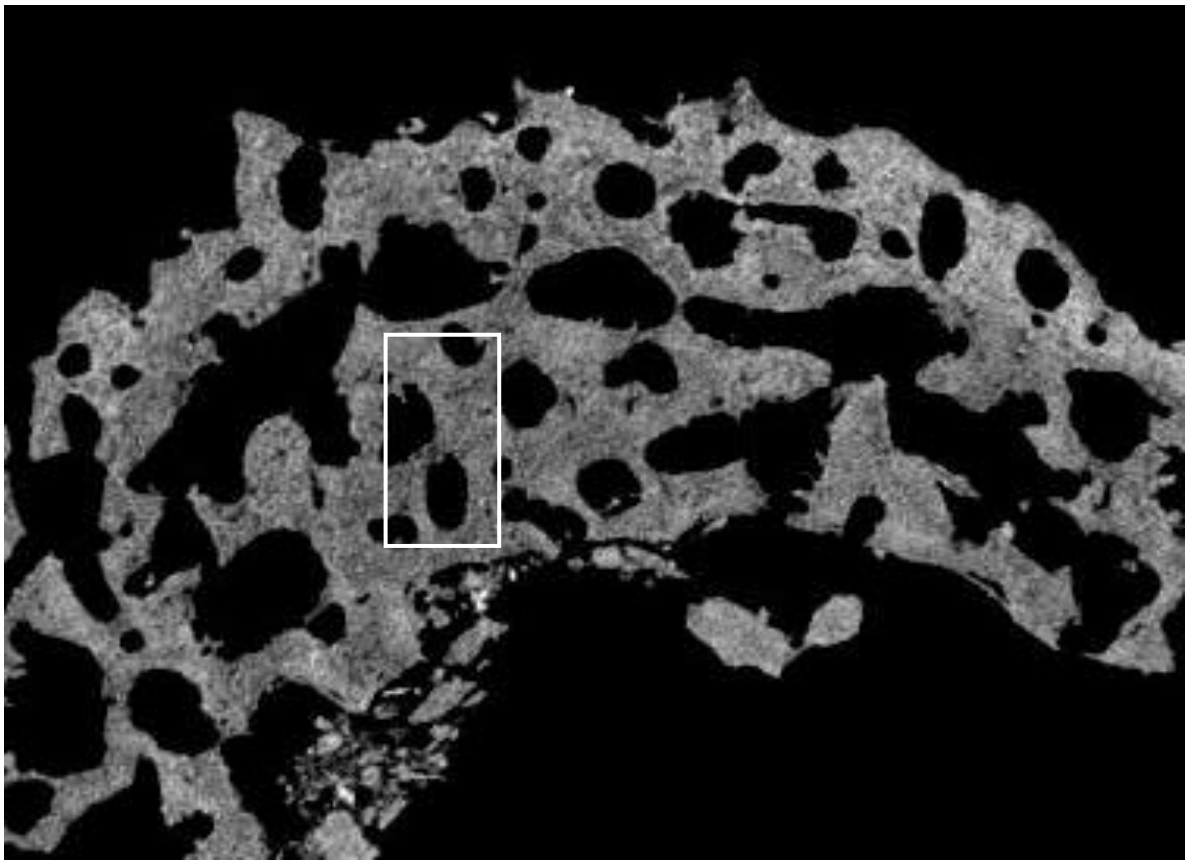

Figure 24: This image is a single transverse cross-section of femur from Individual E (approximately ten and a half months of age at the time of death). The white line box is highlighting the region of bone with decreased density around the naturally occurring vascular canals due to an increased concentration of microbial tunneling.

While an in-depth exploration into all the external factors that may have influenced the microbiome of this particular individual was beyond the scope of this thesis (see section 2.5), further investigation into these results is warranted as this individual should show clear evidence of bacterial bioerosion given their age (10.5 months). It is possible that whatever circumstance influenced the inconsistent bacterial bioerosion tunnels in the femur may have also impeded the transmigration of digestive bacteria to the cranial fragment and neural arch.

There are two possible explanations for this variation in the development of bacterial bioerosion. First, that this individual was unable to colonize healthy bacteria within their digestive tract. Second, that the geochemical conditions of the burial environment may not have facilitated typical decomposition, and incidentally influenced the transmigration of endogenous gut bacteria to the skeletal remains.

The skeletal elements of Individual E are generally well preserved; however, during macroscopic analysis of the entire skeleton, evidence of cribra orbitalia was identified on the cortical surface of the eye orbit (see Figure 25), and periosteal new bone formation was identified on the scanned femur (see Figure 26). These non-specific pathological variations are suggestive of metabolic stress which can be caused by a variety of conditions such as malnutrition, undernutrition, anemias, cancers, specific and non-specific infections, etc. (Roberts and Manchester, 2005; Yaussy and DeWitte, 2018; O'Donnell et al., 2020). While it is not possible to determine the specific etiology of these skeletal stress markers, if they were the result of inadequate nutritional health (e.g., anemia or vitamin deficiencies), a diagnosis of digestive dysbiosis could account for the

skeletal changes associated with stress as well as the reduced rates of bacterial bioerosion.

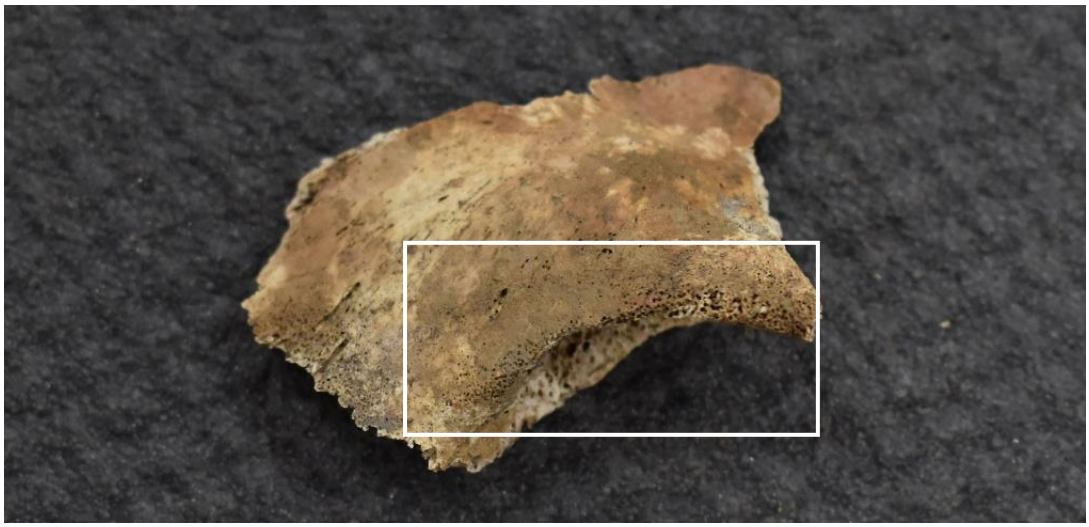

Figure 25: This image depicts the frontal bone from Individual E (approximately ten and a half months old at the time of death). The white line box is highlighting the region of the eye orbit with increased porosity, indicative of cribra orbitalia.

Figure 26: This image depicts the femur from Individual E (approximately ten and a half months old at the time of death). The white box is highlighting the external region of bone with increased porosity, indicative of periosteal new bone growth.

Dysbiosis is the imbalance of microbes within the human microbiome, such as the gut microbiota. This irregularity of the digestive microbes can result in a variety of

health conditions such as Chron's disease, colitis, irritable bowel syndrome, etc. (Beasley et al., 2015; Carding et al., 2015; Gritz and Bhandari, 2015; Henrick et al., 2018). If the individual was not able to colonize all the necessary microbes vital for healthy digestion it is possible that their digestive tract may have not been able to facilitate efficient nutrient absorption, resulting in metabolic stress. Additionally, if the specific gut microbes that prompt the development of bacterial bioerosion after death were not successfully colonized within the digestive tract, the trajectory of bioerosion development would have been negatively impacted, resulting in the reduction of microbial tunnel development.

While this diagnosis may explain the pathological skeletal changes observed and the irregular bacterial bioerosion development, it is problematic. Currently, there are no data that outline the specific types of bacteria that prompt the development of bacterial bioerosion development within the bone. Therefore, it is not possible to determine how the lack of specific digestive bacteria could influence both healthy digestion and skeletal diagenesis. Additionally, it cannot be assumed that the pathological skeletal changes and irregular bacterial bioerosion development are related. It is possible that this individual experienced metabolic stress during life, and after death, the burial environment (e.g., soil acidity or hydrology) influenced skeletal diagenesis.

5.9.6 Individual F

Individual F was between the ages of one and two at the time of death. Nine scans of five skeletal elements from Individual F were analyzed for this thesis, including a cranial fragment, rib, ilium, humerus, and femur. The results of the ilium scan were inconclusive due to scanning limitations; therefore, only the eight scans from the other

four skeletal elements could be assessed. Individual F was the second oldest individual analyzed, and it was presumed that they would have had an increased bacterial load at the time of death. As expected, all viable scans analyzed display evidence of bacterial bioerosion extending across much of the cortical tissue. Microbial tunnels were also present in addition to sub-periosteal ridge distinction which was identified across 1% to 100% of the periosteal surface for all skeletal elements.

5.9.7 Individual G

Individual G was approximately two and a half years old at the time of death. Four scans of two skeletal elements from Individual G were analyzed. This included one cranial fragment and one femur. Though the cranial fragment does not display microbial tunnels, evidence of bacterial bioerosion was identified in all three femur scans. Individual G was the oldest individual assessed for this thesis, and it was hypothesized that they would have had an increased bacterial load at the time of death. As expected, the femoral scans all display evidence of bacterial bioerosion extending across a large cross-sectional area of the cortical tissue. Microbial tunnels were also identified, as well as sub-periosteal ridge distinction across 60% to 100% of the periosteal surface for all skeletal elements (see Figure 14).

The femur of Individual G has the largest microbial tunnel diameters of all the scans assessed and are relatively consistent at the proximal, midshaft, and distal regions (see Table 10). Though this scanned femur has the largest microbial tunnel diameters of all the scans, the microbial tunnel diameter mean and median for each region assessed ranged between 36.51 and 48.14 µm. While it is possible that the increased microbial tunnel diameter is the result of increased cortical thickness common in older individuals,

we cannot exclude the possibility that the increased microbial tunnel diameters are also reflective of bacterial load. Future research assessing the variation in microbial tunnel diameter in correlation to cortical thickness may be useful in determining the true cause of these increasing microbial tunnel diameter trends.

5.10 Limitations and Considerations for Future Research

5.10.1 Inability to Assess Specific Forms of Bacterial Bioerosion

Traditionally, bacterial bioerosion and the form of microbial tunnels present within cortical tissue have been studied through the application of histological methods (see Jans, 2008, Turner-Walker 2008, 2012 and 2019, White and Booth, 2014, and Booth 2015 and 2017). This method of analysis is destructive and not preferred when conducting bioarchaeological research, but it is beneficial in the assessment of bioerosion as the shape of the microbial tunnels can be explored thoroughly. However, recently there has been some debate as to whether the different forms of bacterial bioerosion (i.e., linear-longitudinal, lamellate, or budded) are the result of different types of bacteria or the result of osteological micro-architecture and local burial environments (see Turner-Walker, 2019). If the different shapes of bacterial bioerosion tunnels are not unique to specific strains of bacteria, arguably there would be less of a need to determine which specific forms of bacterial bioerosion are present within cortical tissue. This would be beneficial as it would reduce the time and resources necessary to complete this type of research and more importantly, would not require destructive methods of analysis. However, until this hypothesis can be tested, the morphological data regarding microbial tunnel formation (i.e., microbial tunnel diameter, formation with consideration

to the osteological lacunae, overall shape) captured from histological analysis will remain an important consideration when exploring microbial tunnel development.

The employed method of analysis for this thesis primarily focused on measuring microbial tunnel diameter in order to explore patterns of bacterial bioerosion and determine if bacterial bioerosion was present or absent within the scanned cortical tissue. While this approach produced valuable results in terms of bacterial bioerosion development, the missing contextual data regarding microbial tunnel morphology did limit analytical interpretations. Morphological analysis of microbial tunnels could be explored by isolating porosity throughout the cortical tissue as a region of interest on the Dragonfly 2022.2 computer imaging software. This would allow the examiner to assess the shapes of the microbial tunnels as they extend through the cortical tissue and visualize the morphological structures taking shape. There was an attempt to conduct research in this way; however, it was not possible due to limitations in the Dragonfly 2022.2 program utilized at the time of data collection.

5.10.2 Lack of Standardized Methods

Though the method used in this thesis can be used to determine the presence or absence of bacterial bioerosion, it is somewhat subjective in terms of the standards used when capturing micro-CT scans and image rendering. For example, images of the scanned neural arch from Individual E were rendered with two different windowing and leveling settings. Figure 27 was analyzed with windowing and leveling settings of 100 and 1,200 because those are generally optimal for analyzing microstructures of osteological tissue. Under these rendering conditions, microbial tunnels were not easily identified. In contrast, the same scan was reanalyzed with the windowing and leveling

settings of 300 and 1,000 (Figure 28). Under these rendering conditions microbial tunnels were easily identified. While both image slices can be assessed, this slight change to the image rendering settings produced significantly different visualizations of the microstructures within the cortical bone, and must be recognized as a subjective limitation in the application of micro-CT technology. These types of visualization limitations were encountered in this study, and all attempts were made to account for greyscale varisitons by using similar windowing and leveling settings; however, image capture consistency across all scans was not attainable. Therefore, it is suggested to pair micro-CT analyses with additional histological methods because these methods have traditionally been used in tandem and offer more structured procedures to analyze morphology of bacterial bioerosion development.

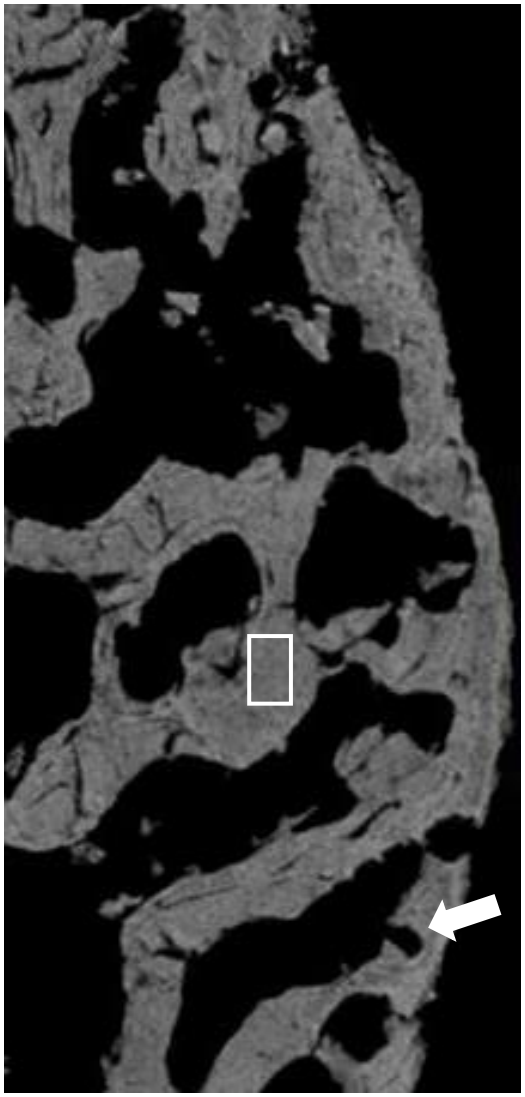

Figure 27: This image is a single transverse cross-section of the neural arch from Individual E (approximately ten and a half months of age at the time of death). The windowing and leveling settings were 100-1,200. The white arrow is indicating a naturally occurring vascular canal, not to be mistaken for bacterial bioerosion. The white line box is highlighting the region of bone with relatively consistent density. The overall light coloration of the cortical tissue is reflective of relatively consistent density of the bone.

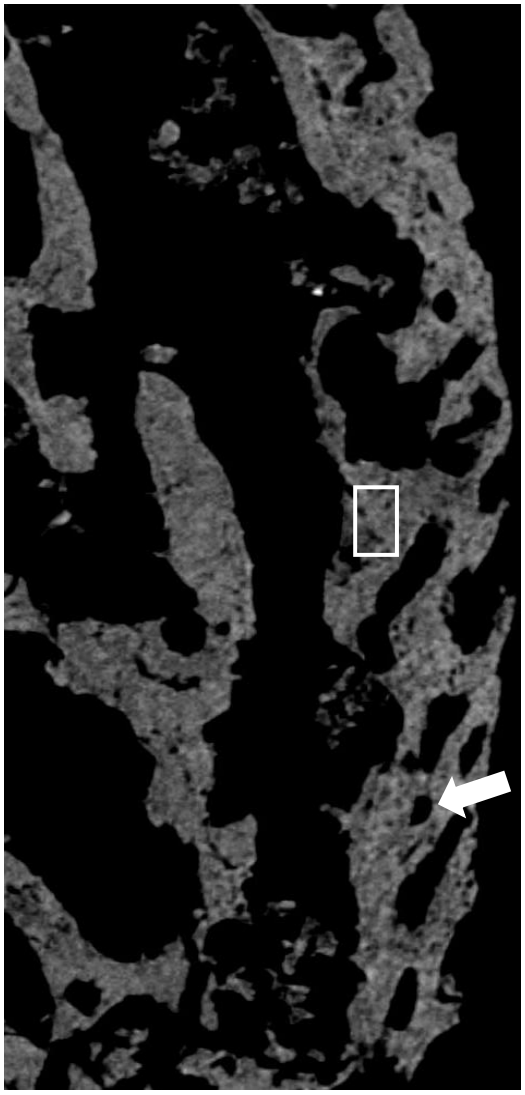

Figure 28: This image is a single transverse cross-section of neural arch from Individual E (approximately ten and a half months of age at the time of death). The windowing and leveling settings were 300-1,000. The white arrow is indicating a naturally occurring vascular canal, not to be mistaken for bacterial bioerosion. The white line box highlighting the region of bone with inconsistent density. The irregular coloration of the cortical tissue indicates the presence of microbial tunnels.

5.11 Summary

This chapter explored the significance of the patterns identified while assessing traces of bacterial bioerosion. Initial macroscopic findings demonstrate that bacterial bioerosion development may relate to the state of cortical preservation. For example, the skeletal elements with the lowest MPI score had irregular patterns of microbial tunneling; therefore, it may be beneficial for future studies to include and consider MPI assessment when selecting skeletal elements for bacterial bioerosion assessment.

In contrast to expected results, the patterns of microbial tunnel distribution and cluster formation did not seem to correlate to specific skeletal elements or differences in developmental age. However, microbial tunnel distribution as it relates to the periosteal surface was used to determine whether microbial tunnels were the result of endogenous gut bacteria or environmental microbes.

When assessing bacterial bioerosion development across different developmental ages, older individuals had a larger distribution of microbial tunnels across the cortical tissue, whereas in younger individuals these microbial tunnels were concentrated in specific regions. This pattern is likely the result of bacterial load rather than age, where an increased numbers of microbes within the gut microbiota will result in an increased spread of bacterial bioerosion throughout the cortical tissue.

Until now, patterns of bacterial bioerosion development across the skeleton were relatively unknown; however, through this analysis, two interesting patterns emerged. First, microbial tunnels diameter is not explicitly related to age, but rather tends to stay consistent in the same types of skeletal elements, except the femora. Arguably then,

skeletal diagenesis may be contingent on the amount of cortical tissue and collagen available to microbes (endogenous or otherwise) to decompose after death. Second, skeletal elements that are further from the digestive tract (e.g., the cranial bones) are less likely to be affected by bacterial bioerosion because of their physical distance from the digestive organs which house endogenous gut bacteria. While these types of skeletal elements can display traces of bacterial bioerosion, they are not ideal when analyzing remains for this type of skeletal diagenesis.

CHAPTER 6 – Conclusion

6.1 Introduction

Since the middle of the 19th century, bacterial bioerosion has been explored through the application of histological thin section analysis. However, thin section analysis is destructive and not always possible when conducting bioarchaeological research. This thesis focused on utilizing microscopic Computed Tomography (micro-CT) technology independently from traditional methods to assess bacterial bioerosion in the skeletal remains of non-adult individuals. The method created to assess evidence of bacterial bioerosion for this study has demonstrated the value in non-destructive radiological imaging, as well as contributed to the growing body of research regarding skeletal diagenesis.

6.2 Revisiting the Research Questions

1. Can micro-CT methods be used independently from histological analysis to accurately assess and identify bacterial bioerosion in osteological tissue?

> While the analytical steps used throughout this thesis varied from the traditional thin-section analyses, traces of bacterial bioerosion were confidently identified in eighteen of twenty-six micro-CT scans, affecting five of seven individuals. When determining the presence or absence of bacterial bioerosion based on micro-CT scans alone, there are three primary considerations that should be made. First, during sample selection the state of intact cortical preservation should be considered, as cortical preservation can at times influence the trajectory of bacterial bioerosion development. If implementing the

Microscopic Preservation Index (MPI) scoring system, skeletal elements with an MPI value of 2 or higher should be selected, as the bones assessed for this thesis with a minimum MPI value of 2 displayed evidence of bacterial bioerosion. Second, after microbial tunnels are identified within the cortical tissue of a scanned skeletal element, an assessment of sub-periosteal ridge development must be made with consideration to where the microbial tunnels are developing (i.e., along the external periosteal surface or throughout the internal cortical tissue). If scanned elements do not display traces of a sub-periosteal ridge but have microbial tunneling extending through the periosteal surface, the microbial tunnels are likely the result of environmental microbes. In contrast, if scanned elements display traces of a sub-periosteal ridge and do not have microbial tunneling extending through the periosteal surface, the microbial tunnels are likely the result of endogenous microbes. Finally, there must be an analysis of internal cortical preservation with consideration of osteological micro-fissures and hyper-mineralized inclusions. These two morphological features are generally the result of environmental conditions influencing skeletal diagenesis, which can also result in microbial tunnels that are not associated with endogenous bacteria. Therefore, if these features are identified in the cortical tissue alongside microbial tunneling, the microbial tunnels are likely the result of environmental microbes. When accounting for these three characteristics, it is possible to use micro-CT technology independently from traditional histological methods to analyze bone for evidence of bacterial bioerosion.

2. Is the development of bacterial bioerosion in cortical bone associated with factors such as cortical preservation or age?

Bacterial bioerosion can at times develop unpredictably in association with factors such as cortical preservation and age. Because skeletal diagenesis and bone decomposition are contingent on the burial environment, conditions such as soil acidity and hydrology can all influence microbial tunnel development (see Hedges, 2002; Szostek et al., 2011; Delannoy et al., 2018; Kendall et al., 2018; Kontopoulos et al., 2019; Turner-Walker, 2012). This applies to the development of microbial tunnels resulting from environmental or endogenous microbes. Of the two skeletal elements that had the lowest MPI score and microbial tunnels with smaller diameter sizes than expected, Individual B does not display evidence of bacterial bioerosion in any scanned skeletal elements, whereas Individual E does display evidence of bacterial bioerosion in one (but not all) of the scanned skeletal elements. In this comparison, poor cortical preservation due to environmental factors may have impacted the development of microbial bioerosion or at least the ability to visualize it through CT imaging. Therefore, conditions of the burial environment and their impact on cortical preservation are of paramount importance when analyzing patterns of skeletal diagenesis of any kind. Unfortunately, due to the nature of this skeletal collection and how it was excavated, soil samples were not obtained for all individuals and environmental conditions such as soil acidity could not be assessed.

When considering pore distribution and age, younger individuals typically display microbial tunnels extending across a smaller cross-sectional area of cortical tissue in comparison to older individuals. Arguably, this trend is related to bacterial load where older individuals have more bacteria to tunnel across a larger proportion of the cortical tissue. With respect to microbial tunnel diameter, the same types of skeletal elements typically display microbial tunnels with similar diameter sizes, except for the femur. When comparing all the femora data, microbial tunnel diameter typically increased in older individuals. Since the cortical thickness of the femur increases drastically within the first few years of life in comparison to other skeletal elements, it is likely that the rate of bioerosion is contingent on the quantity of cortical tissue that can be infiltrated by bacteria and the amount of collagen fibrils therein which can be resorbed by endogenous or environmental microbes. Therefore, as the cortical thickness of all skeletal elements increases with age, microbial tunnel diameter may also increase.

3. Does bacterial bioerosion develop consistently within specific skeletal elements or across the entire skeleton?

Bacterial bioerosion does not develop consistently across single skeletal elements or the entire skeleton. For the long bones that were scanned multiple times, traces of bacterial bioerosion were identified in all regions; however, the microbial tunnel diameter, pore distribution, and sub-periosteal ridge scores all fluctuated. Therefore, while the presence or absence of bacterial bioerosion can be determined using a single micro-CT scan, research into the patterns of

bacterial bioerosion development requires multiple scans from different regions of the same skeletal element. While it is possible for bacterial bioerosion to develop in any given bone after putrefactive decomposition, it is less likely that endogenous bacteria will infiltrate the cortical tissue of skeletal elements further from the digestive tract (e.g., the cranial bones). Therefore, multiple skeletal elements closer to the digestive organs should be selected when conducting research regarding bacterial bioerosion.

6.3 Future Research

There are three potential avenues of future research that could enhance the understanding of bacterial bioerosion development. First, further research should be conducted to better understand the role of cortical thickness in bacterial bioerosion development. While increasing microbial tunnel diameter appears to be associated with increased cortical thickness in the femur, it was not possible to determine if this trend applied to other skeletal elements. Comparing microbial tunnel diameter data from newborns and infants to microbial tunnel diameter data from adolescents and adults may provide further insight to bacterial bioerosion as it relates to the quantity of cortical tissue assessed.

Second, additional research into bacterial bioerosion development with consideration of additional microscopic and macroscopic analyses should be considered. As demonstrated in the case of Individual E, skeletal stress markers observed in conjunction with data suggesting a reduced bacterial load may reflect a more specific diagnosis of health conditions during life. This in turn would create a more complete depiction of patterns of health within past populations. Additionally, there is limited data

addressing the role health conditions that reduce cortical density (e.g., osteoporosis) may have on the development of bacterial bioerosion. Incorporating more contextual data to the analyses of bacterial bioerosion will allow for further exploration of the lived experience as well as enhance what we know of patterns in skeletal diagenesis.

Finally, it was noted that there are variations in bacterial bioerosion across the skeleton. However, it was not possible to explore the explicit reason as to why these variations occurred. It is possible that both bacterial load and distance of skeletal elements from the digestive tract may influence the patterns of bioerosion. Therefore, by conducting further research examining multiple skeletal elements across various regions of the skeleton from both younger and older individuals, it may be possible to identify how these factors influence bacterial bioerosion development.

6.4 Research Contributions

This thesis demonstrated the applicability of micro-CT technology to the assessment of bacterial bioerosion development in human skeletal remains. If the methods discussed throughout this thesis are applied to future research, it may be possible to non-destructively explore patterns of skeletal diagenesis and recreate a more contextual depiction of patterns of health within past populations. While there is still a need to standardize these methods, this study highlights how micro-CT technology can be used to enhance our understanding of bacterial bioerosion development, as microbial tunnel diameter and morphological features of microbial tunnel formation can offer important insights into skeletal diagenesis research. Moreover, this thesis directly contributes to the growing body of research regarding bacterial bioerosion development, cortical preservation, and the interpretive possibilities that bioerosion data can provide.

Finally, this research was the first of its kind conducted in the Canadian Maritimes and provides useful data regarding skeletal diagenesis in an 18th and 19th century Halifax population that could not have been identified through macroscopic analyses alone.

BIBLIOGRAPHY

Abel RL, Laurini CR, Richter M. 2012. A palaeobiologist's guide to 'virtual' micro-CT preparation. Palaeontologia Electronica 15(2):1-16.

Agarwal SC. 2016. Bone morphologies and histories: Life course approaches in bioarchaeology. Am J Phys Anthropol 159(S61):130-149.

AlQahtani SJ, Hector MP, Liversidge HM. 2010. Brief communication: The London atlas of human tooth development and eruption. Am J Phys Anthropol 142 (3):481-490.

Althani AA, Marei HE, Hamdi WS, Nasrallah GK, Zowalaty MEE, Khodor SA, Al-Asmakh M, Abdel-Aziz H, Cenciarelli C. 2015. Human microbiome and its association with health and disease. J Cell Physiol 231(8):1688-1694.

Beasley DE, Koltz AM, Lambert JE, Fierer N, Dunn RR. 2015. The evolution of stomach acidity and its relevance to the human microbiome. PLOS 10(7): e0134116.

Bell LS, Skinner MF, Jones SJ. 1996. The speed of post mortem change to the human skeleton and its taphonomic significance. For Sci Int 82(2):129-140.

Bell LS. 2012. Identifying Postmortem Microstructural Change to Skeletal and Dental Tissue using Backscattered Electron Imaging. In: Bell LS (editor). Forensic Microscopy for Skeletal Tissues: Methods in Molecular Biology 915. Totowa: Humana Press. p 173-190.

Benezra A, DeStefano J, Gordon JI. 2012. Anthropology of microbes. Proc Nat Acad Sci USA 109(17):6378-6381.

Black RE, Victora CG, Walker SP, Bhutta ZA, Christian P, Onis M, Ezzati M, Granthan-McGregor S, Katz J, Martorell R, Uauy R, Maternal and Child Nutrition Study Group. 2013. Lancet 382: 427-451.

Blake KAS. 2017. The Biology of the Fetal Period: Interpreting Life from Fetal Skeletal Remains. In: Han S, Betsinger TK, Scott AB, editors. The Anthropology of the Fetus: Biology, Culture, and Society. Brooklyn: Berghahn Books. p 34-58.

Bogin B. 1998. Evolutionary hypotheses for human childhood. Am J Phys Anthropol 104(S25):63-89.

Bolles, AL. 2016. The Curious Relationship of Feminist Anthropology and Women's Studies. In: Lewin E, Silverstein LM, editors. Mapping Feminist Anthropology in the Twenty-First Century. New Jersey: Rutgers University Press. p 84-104.

Booth TJ. 2015. An investigation into the relationship between funerary treatment and bacterial bioerosion in European archaeological human bone. Archaeometry 58(3):484-499.

Booth TJ, Redfern RC, Gowland RL. 2016. Immaculate conceptions: Micro-CT analysis of diagenesis in Romano-British infant skeletons. J Archaeol Sci 74:124-134.

Booth TJ. 2017. The Rot Sets In: Low-Powered Microscopic Investigation of Taphonomic Changes to Bone Microstructures and its Application to Funerary Contexts. In: Thompson T, Errickson D, editors. Human Remains: Another Dimension: The Application of Imaging to the Study of Human Remains. London: Elsevier Academic Press. p 7-28.

Brönnimann D, Portmann C, Pichler SL, Booth TJ, Röder B, Vach W, Schibler J, Rentzel P. 2018. Contextualizing the dead – Combining geoarchaeology and osteo-anthropology in new multi-focus approach in bone histotaphonomy. J Archaeol Sci 98:45-58.

Bushong SC. 2013. Essential Concepts of Radiologic Science. In: Bushong SC, editor. Radiologic Sciences for Technologists: Physics, Biology, and Protection: 10th edition. St. Louis: Elsevier Mosby. p 2-25.

Buzug T. 2008a. Fundamentals of X-Ray Physics. In: Buzug T, editor. Computed Tomography: From Photon Statistics to Modern Cone-Beam CT. Heidelberg: Springer Berlin. p 15-73.

Buzug T. 2008b. Milestones in CT In: Buzug T, editor. Computed Tomography: From Photon Statistics to Modern Cone-Beam CT. Heidelberg: Springer Berlin. p 75-99.

Cahill B, DeWolfe L, Alary M, Chard EA, Yorke L. 2008. The Blue Banner: The Presbyterian Church of Saint David and Presbyterian Witness in Halifax. Montreal, QC: McGill-Queen's University Press.

Campbell DA. 1905. Pioneers of Medicine in Nova Scotia. Halifax, NS: Maritime Medical News.

Carding S, Verbeke K, Vipond DT, Corfe BM, Owen LJ. 2015. Dysbiosis of the gut microbiota in disease. Microb Ecol Health Dis 26(1):26191.

Caruso V, Marinoni N, Diella V, Possenti E, Mancini L, Cantaluppi M, Berna F, Cattaneo C, Pavese A. 2021. Diagenesis of juvenile skeletal remains: A multimodal and multiscale approach to examine the post-mortem decay of children's bones. J Archaeol Sci 135: 105477.

Christensen AM, Passalacque NV, Bartelink EJ. 2019a. Forensic Taphonomy. In: Brown EA, Lima L, editors. Forensic Anthropology: Current Methods and Practice: Second Edition. London: Elsevier Academic Press. p 145-182.

Christensen AM, Passalacque NV, Bartelink EJ. 2019b. Skeletal Examination and Documentation Methods. In: Brown EA, Lima L, editors. Forensic Anthropology: Current Methods and Practice: Second Edition. London: Elsevier Academic Press. p 77-114.

Christensen AM, Passalacque NV, Bartelink EJ. 2019c. Age Estimation. In: Brown EA, Lima L, editors. Forensic Anthropology: Current Methods and Practice: Second Edition. London: Elsevier Academic Press. p 307-349.

Clark MA, Worrell MB, Pless JE. 1996. Postmortem Changes in Soft Tissues. In: Haglund WD, Sorg MH, editors. Forensic Taphonomy: The Postmortem Fate of Human Remains. Boca Raton: CRC Press. p 151-164.

Conlogue GJ, Nelson AJ, Lurie AG. 2020. Computed Tomography (CT), Multi-detector Computed Tomography (MDCT), Micro-CT, and Cone Beam Computed Tomography (CBCT). In: Beckett RG, Conlogue GJ, editors. Advances in Paleoimaging: Applications for Paleoanthropology, Bioarchaeology, Forensics, and Cultural Artifacts. Boca Raton: CRC Press: Taylor & Francis Group. p 112-176.

Corley AG. 2021. Linking armed conflict to malnutrition during pregnancy, breastfeeding, and childhood. Global Food Sec 29:100531.

Cunningham C, Scheuer L, Black S. 2016. Developmental Juvenile Osteology: Second Edition. London, UK: Elsevier Academic Press.

Damann FE, Carter DO. 2013. Human Decomposition Ecology and Postmortem Microbiology. In: Pokines J, Symes SA, editors. Manual of Forensic Taphonomy: First Edition. Boca Raton: CRC Press: Taylor & Francis Group. p 37-50.

Davis MacIntyre & Associates Ltd. 2017a. Grafton Street Methodist Burying Ground: Volume 1: Historic Background Study. Halifax, NS: Department of Communities, Culture and Heritage.

Davis MacIntyre & Associates Ltd. 2017b. Grafton Street Methodist Burying Ground: Volume 2: Archaeological Mitigation. Halifax, NS: Department of Communities, Culture and Heritage.

Davis MacIntyre & Associates Ltd. 2018. Grafton Street Methodist Burying Ground: Volume 3: 2017 Monitoring and Mitigating. Halifax, NS: Department of Communities, Culture and Heritage.

Delannoy Y, Colard T, Cannet C, Mesli V, Hédouin V, Penel G, Ludes B. 2018. Characterization of bone diagenesis by histology in forensic context: A human taphonomic study. Int J Legal Med 132: 219-227.

Dunn AB, Jordan S, Baker BJ, Carlson NS. 2017. The maternal infant microbiome: Considerations for labour and birth. MCN Am J Matern Child Nurs 42(6):318-325.

Eriksen AMH, Nielsen TK, Matthiesen H, Carøe C, Hansen LH, Gregory DJ, Turner-Walker G, Collins MJ, Gilbert MTP. 2020. Bone biodeterioration: The effect of marine and terrestrial depositional environments on early diagenesis and bone bacterial community. PLOS 15(10): e0240512.

Fazekas IGy, Kósa F. 1978. Forensic Fetal Osteology. Budapest, HUN: Akadémiai Kiadó.

Ferretti P, Pasolli E, Tett A, Asnicar F, Gorfer V, Fedi S, Armanini F, Truong DT, Manara S, Zolfo M, Beghini F, Bertorelli R, Sanctis VD, Bariletti I, Canto R, Clementi R, Cologna M, Crifò T, Cusumano G, Gottardi S, Innamorati C, Masé C, Postai D, Savoi D, Duranti S, Lugli GA, Mancabelli L, Turroni F, Ferrario C, Milani C, Mangifesta M, Anzalone R, Viappiani A, Yassour M, Vlamakis H, Xavier R, Collado CM, Koren O, Tateo S, Soffiati M, Pedrotti A, Ventura M, Huttenhower C, Bork P, Segata N. 2018. Mother-to-infant microbial transmission from different body sites shapes the developing infant gut microbiome. Cell Host Microbe 24(1):133-145.

Fingard J, Guildford J, Sutherland D. 1999. Halifax: The First 250 Years. Halifax, NS: Formac Publishing Company. p 23-42.

Finley SJ, Benbow ME, Javan GT. 2015. Microbial communities associated with human decomposition and their potential use as postmortem clocks. Int J Leg Med 129:623-632.

Galligani P, Sartori J, Barrientos G. 2019. Bacterial bioerosion in human and animal bones from subtropical environments (Northern Pampa/ Middle Paraná River Basin, Repblica Argentina). J Archaeol Sci: Rep 25:561-574.

Garnett R. 2020. A comprehensive review of dual-energy and multi-spectral computed tomography. Clin Imaging 67:160-169.

Geronimus AT. 2013. Deep integration: Letting the epigenome out of the bottle without losing sight of the structural origins of population health. Am J Pub Health 103(1):56-63.

Geva A, Schechner YY, Chernyak Y, Gupta R. 2018. X-ray Computed Tomography Through Scatter. Proceedings of the European Conference on Computer Vision. European Conference on Computer Vision, Munich, Germany, September 8-14, 2018. Switzerland: Springer Nature. p 34-50.

Gluckman PD, Buklijas T, Hanson MA. 2016. The Developmental Origins of Health and Disease (DOHaD) Concept: Past, Present, and Future. In: Rosenfeld CS, editor. The Epigenome and Developmental Origins of Health and Disease. Lodon: Elsevier Academic Press. p 1-15.

Gowland R, Halcrow S. 2020. Introduction: The Mother-Infant Nexus in Archaeology and Anthropology. In: Gowland R, Halcrow S, editors. The Mother-Infant Nexus in Anthropology: Small Beginnings, Significant Outcomes. Bioarchaeology and Social Theory. Switzerland: Springer Nature. p 1-15.

Goldman HM, McFarlin SC, Cooper DML, Thomas CDL, Clement JG. 2009. Ontogenetic patterning of cortical bone microstructure and geometry at the human mid-shaft femur. Anat Rec 292(1):48-64.

Gosman JH, Hubbell ZR, Shaw CN, Ryan TM. 2013. Development of cortical bone geometry in the femoral and tibial diaphysis. Anatom Rec. 296(5):774-787.

Griffiths NES. 1992. The Contexts of Acadian History, 1686-1784. Montreal, QC: McGill-Queen's University Press.

Gritz EC, Bhandarhi V. 2015. Corrigendum: The human neonatal gut microbiome: a brief review. Front Pediatr 3(60). DOI: 10.3389/fped.2015.00060.

Guy H, Masset C, Baud CA. 1997. Infant taphonomy. Int J Osteoarchaeol 7:221-229.

Hackett CJ. 1981. Microscopic focal destruction (tunnels) in exhumed human bones. Med Sci Law 21(4):243-265.

Hales CN, Barker DJP. 1992. Type 2 (non-insulin-dependent) diabetes mellitus: the thrifty phenotype hypothesis. Diabetologia 35:595-601.

Hanrahan M. 2008. Resisting colonialism in Nova Scotia: The Kesukwitk Mi'kmaq, centralization, and residential schooling. Nat Stud Rev 17(1):25-44.

Hedges REM. 2002. Bone Diagenesis: An Overview of Processes. Aechaeometry 4(3):319-328.

Hemer KA, Booth TJ, Raffone C, Mann C, Corkhill CL, Willmott H. 2021. 'Among his fellows cast': A histotaphonomic investigation into the impact of the Black Death in England. J Archaeol Sci: Rep 39:103161.

Henrick Bm, Hutton AA, Palumbo MC, Casaburi G, Mitchell RD, Underwood MA, Smilowitz JT, Frese SA. 2018. Elevated fecal pH indicates a profound change in the breastfed infant gut microbiome due to reduction of Bifidobacterium over the past century. Am Soc Microbiol 3(2):e00041-18.

Hollund HI, Jans MME, Collins MJ, Kars H, Joosten I, Kars SM. 2012.What happened here? Bone histology as a tool in decoding the postmortem histories of archaeological bone from Castricum, the Netherlands. Int J Osteoarchaeol 22(5):537-548.

Hurrell MA, Butler APH, Cook NJ, Butler PH, Ronaldson JP, Zainon R. 2012. Spectral Hounsfield units: a new radiological concept. Eur Radiol 22:1008-1013.

Jans MME. 2008. Microbial bioerosion of bone – a review. In: Wisshak M, Tapanila L, editors. Current Developments in Bioerosion. Berlin: Springer. p 397-413.

Jans MME. 2013. Microscopic Destruction of Bone In: Pokines J, Symes SA, editors. Manual of Forensic Taphonomy: First Edition. Boca Raton: CRC Press: Taylor & Francis Group. p 19-36.

Jiang Y, Zhao J, Liao E-Y, Dai R-C, Wu X-P, Genant HK. 2005. Application of micro-CT assessment of 3-D bone microstructure in preclinical and clinical studies. J Bone Miner Metab 23:122-131.

Kendall C, Eriksen AMH, Kontopoulos I, Collins MJ, Turner-Walker G. 2018. Diagenesis of archaeological bone and tooth. Palaeogeogr, Palaeoclimatol, Palaeoecol 491:21-37.

Kennedy KM, Gerlach MJ, Adam T, Heimesaat MM, Rossi L, Surette MG, Sloboda DM, Braun T. 2021. Fetal meconium does not have a detectable microbiota before birth. Nat Microbiol 6:865-873.

Knight R, Callewaert C, Marotz C, Hyde ER, Debelius JW, McDonald D, Sogin ML. 2017. The microbiome and human biology. Annu Rev Genom Hum Genet 18:65-86.

Knoop KA, Holtz LR, Newberry RD. 2018. Inherited nongenetic influences on the gut microbiome and immune system. Birth Def Res 110(20):1494-1503.

Kontopoulos I, Penkman K, Liritzis I, Collins MJ. 2019. Bone diagenesis in a Mycenaean secondary burial (Kastrouli, Greece). Archaeol Anthropol Sci 11:5213-5230.

Landis JR, Koch GG. 1977. The measurement of observer agreement for categorical data. Int Biometric Soc 33(1):159-174.

Lewis M. 2018. Biology and Significance of the Nonadult Skeleton. In: Lewis M, editor. Paleopathology of Children: Identification of Pathological Conditions in the Human Skeletal Remains of Non-Adults. London: Elsevier Academic Press. p 1-12.

MacLean J. 1907. William Black: The Apostle of Methodism in the Maritime Provinces of Canada. Halifax, NS: Methodist Book Room.

Maresh MM. 1970. Measurements From Roentgenograms. In: McCammon RW, editor. Human Growth and Development. Springfield: Thomas. p 157-200.

McGuigan P. 2007. Historic South End Halifax. Halifax, NS: Nimbus Publishing Limited.

Milovanovic P, Vukovic Z, Antonijevic D, Djonic D, Zivkovic V, Nikolic S, Djuric M. 2017. Porotic paradox: Distribution of cortical bone pore sizes at nano- and micro-levels in healthy vs. fragile human bone. J Mater Sci: Mater Med 28:71.

Monk C, Georgieff MK, Osterholm EA. 2013. Research Review: Maternal prenatal distress and poor nutrition – mutually influencing risk factors affecting infant neurocognitive development. J Child Psychol Psychiatry 54(2):115-130.

Nielsen-Marsh C, Hedges REM. 2000. Patterns of diagenesis in bone I: The effects of site environment. J Archaeol Sci 27(12):1139-1150.

O'Donnell L, Hill EC, Anderson ASA, Edgar HJH. 2020. Cribra orbitalia and porotic hyperostosis are associated with respiratory infections in a contemporary mortality sample from New Mexico. Am J Phys Anthropol 173(4):721-733.

Patterson S. 2009. Eighteenth-Century treaties: The Mi'kmaq, Maliseet, and Passamaquoddy experience. Nat Stud Rev 18(1):25-52.

Pinheiro J. 2006. Decay Process of a Cadaver. In: Schmitt A, Cunha E, Pinheiro J, editors. Forensic Anthropology and Medicine: Complimentary Sciences from Recovery to Cause of Death. Totowa: Humana Press. p 85-116.

Prats-Munoz G, Galtés I, Armentano N, Cases S, Fernández PL, Malgosa A. 2013. Human soft tissue preservation in the Cova des Pas site (Minorca Bronze Age). J Archaeol Sci 40(12):4701-4710.

Redfern RC, Gowland RL. 2011. A Bioarchaeological Perspective on the Pre-Adult Stages of the Life Course: Implications for the Care and Health of Children in the Roman Empire. In: Harlow M, Loven LL, editors. Families in the Roman and Late Antique World. London: Continuum International. p 111-140.

Roberts C, Manchester K. 2005. The Archaeology of Disease. Ithaca, NY: Cornell University Press.

Rutherford JN. 2012. The Primate Placenta as an Agent of Developmental and Health Trajectories Across the Life Course. In: Clancy KBH, Hinde K, Rutherford JN, editors. Building Babies: Primate Development in Proximate and Ultimate Perspective. New York: Springer. p 27-53.

Rutherford JN, Tardif SD. 2009. Developmental plasticity of the microscopic placental architecture in relation to litter size variation in the common marmoset monkey (*Callithris jacchus*). Placenta 30(1):105-110.

Sasso GD, Maritan L, Usai D, Angelini I, Artioli G. 2014. Bone diagenesis at the micro-scale: Bone alteration patterns during multiple burial phases at Al Khiday (Khartoun, Sudan) between the Early Holocene and the II century AD. Palaeogeogr, Palaeoclimatol, Palaeoecol 416:30-42.

Scheuer L, Black S, Schaefer MC. 2010. Juvenile Osteology: A Laboratory and Field Manual: First Edition. Burlington, MA: Elsevier Academic Press.

Shimabuku DM, Hall GF. 1981. St. Paul's Cemetery Halifax, Nova Scotia, Canada: Description and Interpretation of Gravestone Designs and Epitaphs. Halifax, NS: St. Mary's University.

Szostek K, Stepanczak B, Szczepanek A, Kepa M, Glab H, Jarosz P, Wlodarczak P, Tunia K, Pawlyta J, Paluszkiewicz C, Tylko G. 2011. Diagenetic signals from ancient human remains – bioarchaeological applications. Mineralogia 42(2-3): 93-112.

Thayer ZM, Rutherford J, Kuzawa CW. 2020. The Maternal Nutritional Buffering Model: an evolutionary framework for pregnancy nutritional intervention. Evol Med Pub Heal 2020(1): 14-27.

Timmerman HM, Rutten NBMM, Boekhorst J, Saulniew DM, Kortman GAM, Contractor N, Kullen M, Floris E, Harmsen HJM, Vlieger AM, Kleerebezem M, Rijkers GT. 2017. Intestinal colonisation patterns in breastfed and formula-fed infants during the first 12 weeks of life reveal sequential microbiota signatures. Sci Rep 7:8327.

Turner-Walker G, Syversen U. 2002. Quantifying histological changes in archaeological bones using BSE-SEM image analysis. Archaeometry 44(3):461-468.

Turner-Walker G. 2008. The Chemical and Microbial Degradation of Bones and Teeth. In: Pinhasi R, Mays S, editors. Advances in Human Palaeopathology. Chichester: John Wiley & Sons. p 2-30.

Turner-Walker G. 2012. Early bioerosion in skeletal tissue: Persistence through deep time. N Jb Geol Palaont Abh. 265(2): 165-183.

Turner-Walker G. 2019. Light at the end of the tunnels? The origins of microbial bioerosion in mineralized collagen. Palaeogeor, Palaeoclimatol, Palaeoecol. 529(1):24-38.

Valentine CJ, Wagner CL. 2013. Nutritional management of the breastfeeding dyad. Ped Clin North Am 60(1): 261-274.

Viera AJ, Garrett JM. 2005. Understanding interobserver agreement: the kappa statistic. Fam Med 37(5):360-363.

Weber GW. 2015. Virtual Anthropology. Am J Phys Anthropol 156(59):22-42.

Wedl C. 1864. Ueber einen im Zahnbein und Knochen keimenden Pilz. Akad Wiss Wien, math-natw K1 (I) 50:171-193.

White TD, Black MT, Folkens PA. 2012. Bone Biology and Variation. In: Brown L, editor. Human Osteology: Third Edition. London: Elsevier Academic Press. p 25-42.

White L, Booth TJ. 2014. The origin of bacteria responsible for bioerosion to the internal bone microstructure: Results from experimentally-deposited pig carcasses. For Sci Int. 239:92-102.

Whitehead RH. 2013. Black Loyalists: Southern Settlers of Nova Scotia's First Free Black Communities. Halifax, NS: Nimbus Publishing Limited.

Whitfield HA. 2006. Blacks on the Border: The Black Refugees in British North America, 1815-1860. Lebanon, NH: University Press of New England.

Yaussy SL, DeWitte SN. 2018. Patterns of frailty in non-adults from medieval London. Int J Paleopathol 22:1-7.

Appendix A

Table 16: Microscopic CT image capture

Date	Sample Name	Sample Scanned	Region Scanned	kV	Current	Watts	Voxel	Target	# of Projections	Frames	Scan Time
2021-08-16 Total Scans: 5	Individual F	Rib	Region lateral to rib tubercle	80	116	8.8	9				
		Ilium	Region distal to auricular surface	87	97	8.4	9.5				
		Humerus	Proximal end of diaphysis				9.75				
		Humerus	Midshaft								
		Humerus	Distal end of diaphysis								
2021-08-17 Total Scans: 8	Individual F	Cranial fragment	Ridge of unidentified cranial fragment	78	96	7.5	9.5	Molybdenum	3141	1	53 Minutes
	Individual D	Neural arch	Mass that would articulate lateral to centrum				6.75				
		Cranial fragment	Lateral ridge of frontal bone				7				
	Individual B	Tibia	Midshaft (more proximal)				6				
		Rib (inferior)	Region lateral to rib tubercle				6				
	Individual F	Femur	Proximal end of diaphysis				9.5				
		Femur	Midshaft								
		Femur	Distal end of diaphysis								
2021-08-18 Total Scans: 8	Individual B	Rib (superior)	Midsection between sternal and costal end	92	72	6.6	5	Molybdenum	3141	1	53 minutes
	Individual C	Ilium	Auricular surface	76	97	7.4	9				
		Cranial fragment	Ridge of unidentified cranial fragment				7				
		Femur	Midshaft				5				
	Individual E	Cranial fragment	Ridge of unidentified cranial fragment				7.75		1571	8	4 hours 21 minutes
		Neural arch	Mass that would articulate lateral to centrum				6				
		Femur	Mid- proximal diaphysis				6.25				
		Femur	Mid- distal diaphysis				6.25				
2021-08-19 Total Scans: 5	Individual A	Longbone	Midshaft	71	122	8.7	4	Molybdenum	3141	1	53 minutes
	Individual G	Cranial fragment	Ridge of unidentified cranial fragment				9.5				
		Femur	Proximal end of diaphysis				7.75		1571	8	4 hours 21 minutes
		Femur	Midshaft								
		Femur	Distal end of diaphysis								

Table 17: Microscopic CT image rendering

Individual	Element Scanned	Voxel Size (µm)	Windowing and Leveling
Individual A	Longbone	4	250-1100
Individual B	Rib One (Inferior)	6	800-2690
	Rib Two (Superior)	5	370-4930
	Tibia Midshaft	6	450-17200
Individual C	Cranial Fragment	7	450-1200
	Ilium	9	200-1800
	Femur Midshaft	5	200-2300
Individual D	Cranial Fragment	7	Inconclusive scan
	Neural Arch	6.75	365-760
Individual E	Cranial Fragment	7.5	200-2900
	Neural Arch	6	300-1000
	Femur Midshaft (Superior Region)	6.25	200-1800
	Femur Midshaft (Inferior Region)	6.25	600-1800
Individual F	Cranial Fragment	9.5	400-1800
	Rib	9	300-1800
	Proximal Humerus	9.75	160-1200
	Humerus Midshaft	9.75	140-500
	Distal Humerus	9.75	140-500
	Ilium	9.5	Inconclusive scan
	Proximal Femur	9.75	400-1800
	Femur Midshaft	9.75	400-1800
	Distal Femur	9.75	400-1800
Individual G	Cranial Fragment	9.5	260-1600
	Proximal Femur	7.75	100-2200
	Femur Midshaft	7.75	200-1800
	Distal Femur	7.75	200-2200

Table 18: Systematic assessment of microbial tunnel diameter (measured in µm)

Sub-Section of Bone Quadrant	Pore	Bone Quadrant			
		Anterior	Medial	Posterior	Lateral
Subsection 1 of Quadrant	1	13.39	8.95	21.53	19.3
	2	14.72	14.14	30.35	26.89
	3	26.18	19.11	17.78	24.57
	4	25.64	23.02	11.91	64.57
	5	19.99	24.6	7.01	8.63
	6	12	11.4	5.95	64.71
	7	24	26.08		16.62
	8	10.66	19.11		28.11
	9	12.65	15.66		43.69
	10	8.53	17.03		10.92
	Mean	16.78	17.91	15.75	30.8
Subsection 2 of Quadrant	1	5.96	30	24.77	9.69
	2	9.7	8.06	38.29	32.76
	3	10.15	17.03	19.32	13.92
	4	10.99	18.44	18.16	21.84
	5	18.94	20.62	6.6	10.92
	6	22.7	14.32	21.53	20.14
	7	32.1	20.8	21.46	7.72
	8	24.32	15	31.37	22.01
	9	27.48	22.21	6.6	13.07
	10	15.2	16.72	8.26	12.25
	Mean	17.75	18.32	19.64	16.43
Subsection 3 of Quadrant	1	10.74	12.37	57.51	8.19
	2	19.99	20.09	33.02	17.48
	3	14.42	8.28	19.88	13.86
	4	17.38	21.67	29.84	10.92
	5	20.39	8.12	21.47	22.61
	6	25.32	9.86	12.02	13.72
	7	19.99	16	24.77	10.96
	8	21.32	26.44	6.61	
	9	17.38	27.95	23.47	
	10	25.36	9.74	13.31	
	Mean	19.23	16.05	24.19	13.96
Subsection 4 of Quadrant	1	24.03	20.67	15.03	16.14
	2	13.33	23.25	36.11	24.72
	3	19.81	8.12	13.41	14.7
	4	27.99	21.12	17.95	22.01
	5	16.27	10.4	16.43	30.89
	6	60.8	20.09	18.55	56.27
	7	23.31	9.88	30.51	19.87
	8	15.54	46.54	25.12	29.16
	9	36.86	9.88	28.26	12.81
	10	17.38	14.97	38.11	16.86
	Mean	25.53	18.49	23.95	24.34
Subsection 5 of Quadrant	1	9.42	29.95	8.94	23.33
	2	25.47	42.27	16.66	27.14
	3	18.52	44.37	52.48	25.9
	4	22.07	16.96	22.26	13.92
	5	24.46	15.32	20.8	18.31
	6	25.04	11.37	18.33	13.65
	7		13.97	13.38	12.21
	8		19.83	16.92	32.98
	9		15.32	16.68	60.99
	10		19.01	13.18	8.12
	Mean	20.83	22.84	19.96	23.66

Subsection 6 of Quadrant	1	29.59	16.57	52.12	23.16
	2	13.59	11.49	22.14	9.69
	3	5.96	19.56	27.37	5.92
	4	10.16	26.64	24.5	6.1
	5	12.07	52.39	11.62	19.12
	6	14.66	27.03	15.29	44.21
	7	18.66	17.57	45.29	22.64
	8	25.47	33.44	17.64	25.9
	9	35.99	11.49	8.3	5.46
	10	25.88	16	21.57	12.6
	Mean	19.2	23.22	24.58	17.48
Subsection 7 of Quadrant	1	13.33	35.95	18.33	27.03
	2	19.22	4.92	8.3	30.62
	3	8.53	16.35	30.06	23.16
	4	25.36	4.92	32.86	19.34
	5	29.59	11.84	17.64	15.44
	6	5.76	18.7	5.98	27.84
	7	31.32	27.49	30.28	32.12
	8	21.49	10.14	8.31	16.84
	9	25.04	23.1	9.68	22.51
	10	19.63	20.22	23.59	
	Mean	19.93	17.36	18.5	23.88
Subsection 8 of Quadrant	1	13.09	8.87	19.99	23.16
	2	12.07	13.29	24.94	40.59
	3	10.75	19.83	11.61	39.08
	4	25.47	7.7	38.21	27.3
	5	15.99	17.18	23.59	10.92
	6	21.07	16.49	14.27	8.19
	7	18.86	33	26.56	42.47
	8	25.88	20.66	18.56	21.62
	9	14.66	6.69	11.13	7.72
	10	13.59	19.45	13.28	5.46
	Mean	17.14	16.32	20.21	22.64
Subsection 9 of Quadrant	1		18.72	30.47	25.76
	2		41.5	15.03	19.3
	3		6.41	59.1	8.19
	4		28.59	16.35	10.21
	5		24.21	20.19	32.21
	6		34.09	22.57	17.48
	7		17.77	20.19	24.42
	8		37.97	16.92	21.84
	9		16.35	5.01	22.01
	10		24.59	16.88	11.25
	Mean		25.02	22.27	19.27
Subsection 10 of Quadrant	1		6.41	21.25	
	2		31.9	9.68	
	3		18.7	16.59	
	4		20.2	21.83	
	5		13.6	17.32	
	6		26.49	27.37	
	7		31.45	13.38	
	8		17.73	15.74	
	9		13.29	14.84	
	10		39.98	15.75	
	Mean		21.98	17.38	
Subsection 11 of Quadrant	1			23.29	
	2			23.47	
	3			5.98	
	4			16.6	
	5			19.98	
	6			23.59	
	7			43.94	
	Mean			22.41	
Mean Pore Diameter		19.55	19.75	20.95	21.62

Table 19: Random assessment of microbial tunnel diameter (measured in µm)

Pore	Pore Measurment
1	40.51
2	13.32
3	14.89
4	27.46
5	13.32
6	21.06
7	75.34
8	27.45
9	61.4
10	6.66
11	77.66
12	18.84
13	13.32
14	26.64
15	24.01
16	18.84
17	47.08
18	14.89
19	6.66
20	28.25
Mean	28.88

Table 20: Systematic metric diameter assessment: anterior quadrant

Sub-Quadrant Comparisons	t	df	p
1-2	-0.283	18	0.78
1-3	-0.971	18	0.344
1-4	-1.767	18	0.094
1-5	-1.22	14	0.243
1-6	-0.658	18	0.519
1-7	-0.924	18	0.368
1-8	-0.135	18	0.894
2-3	-0.475	13.51	0.642
2-4	-1.475	18	0.157
2-5	-0.754	14	0.463
2-6	-0.353	18	0.728
2-7	-0.563	18	0.58
2-8	-0.188	18	0.853
3-4	-1.436	18	0.198
3-5	-0.601	14	0.558
3-6	-0.008	18	0.994
3-7	-0.229	18	0.822
3-8	0.933	18	0.363
4-5	0.76	14	0.46
4-6	1.166	18	0.259
4-7	1.069	18	0.299
4-8	1.743	18	0.098
5-6	0.368	14	0.718
5-7	0.225	14	0.825
5-8	1.251	14	0.232
6-7	-0.178	18	0.861
6-8	0.589	18	0.563
7-8	0.87	18	0.396

Table 21: Systematic metric diameter assessment: medial quadrant

Sub-Quadrant Comparisons	t	df	p
1-2	-0.161	18	0.874
1-3	0.625	18	0.54
1-4	-0.145	18	0.886
1-5	-1.185	18	0.252
1-6	-1.228	18	0.235
1-7	0.152	18	0.881
1-8	0.523	18	0.607
1-9	-1.848	18	0.081
1-10	-1.097	18	0.287
2-3	0.755	18	0.46
2-4	-0.043	18	0.966
2-5	-1.081	13.012	0.3
2-6	-1.128	18	0.274
2-7	0.264	18	0.795
2-8	0.652	18	0.523
2-9	-1.731	18	0.101
2-10	-0.98	18	0.34
3-4	-0.566	18	0.578
3-5	-1.523	18	0.145
3-6	-1.555	18	0.137
3-7	-0.333	18	0.743
3-8	-0.077	18	0.94
3-9	-2.153	18	0.045
3-10	-1.468	18	0.159
4-5	-0.836	18	0.414
4-6	-0.887	18	0.387
4-7	0.237	18	0.815
4-8	0.499	18	0.624
4-9	-1.438	18	0.204
4-10	-0.719	18	0.481
5-6	-0.07	18	0.945
5-7	1.118	18	0.278
5-8	1.448	18	0.165
5-9	-0.43	18	0.672
5-10	0.173	18	0.864
6-7	1.163	18	0.26
6-8	1.483	18	0.155
6-9	-0.346	18	0.734
6-10	0.243	18	0.811
7-8	0.262	18	0.796
7-9	-1.652	18	0.116
7-10	-1.021	18	0.321
8-9	-2.064	18	0.054
8-10	-1.384	18	0.183
9-10	0.466	18	0.527

Table 22: Systematic metric diameter assessment: posterior quadrant

Sub-Quadrant Comparisons	t	df	p
1-2	-0.744	14	0.469
1-3	-1.286	14	0.219
1-4	-1.742	14	0.103
1-5	-0.73	14	0.478
1-6	-1.359	14	0.196
1-7	-0.535	14	0.601
1-8	-0.974	14	0.342
1-9	-0.982	14	0.343
1-10	-0.457	14	0.655
1-11	-1.138	11	0.279
2-3	-0.815	18	0.426
2-4	-0.988	18	0.336
2-5	-0.065	18	0.949
2-6	-0.892	18	0.384
2-7	0.244	18	0.81
2-8	-0.136	18	0.894
2-9	-0.467	18	0.646
2-10	0.616	18	0.546
2-11	-0.518	15	0.612
3-4	0.045	18	0.964
3-5	0.717	18	0.483
3-6	-0.062	18	0.951
3-7	1.025	18	0.319
3-8	0.76	18	0.457
3-9	0.299	18	0.768
3-10	1.43	18	0.17
3-11	0.275	15	0.787
4-5	0.839	18	0.413
4-6	-0.121	18	0.905
4-7	1.264	18	0.223
4-8	0.959	18	0.35
4-9	0.312	18	0.759
4-10	2.027	18	0.058
4-11	0.313	15	0.759
5-6	-0.789	18	0.44
5-7	0.292	18	0.774
5-8	-0.054	18	0.958
5-9	-0.388	18	0.703
5-10	0.628	18	0.538
5-11	-0.421	15	0.68
6-7	1.105	18	0.284
6-8	0.843	18	0.41
6-9	0.363	18	0.721
6-10	1.529	18	0.144
6-11	0.339	15	0.74

7-8	-0.407	18	0.689
7-9	-0.673	18	0.51
7-10	0.313	18	0.758
7-11	-0.739	15	0.471
8-9	-0.389	18	0.702
8-10	0.917	18	0.371
8-11	-0.458	15	0.654
9-10	1.014	18	0.324
9-11	-0.021	15	0.984
10-11	-1.251	15	0.23

Table 23: Systematic metric diameter assessment: lateral quadrant

Sub-Quadrant Comparisons	t	df	p
1-2	2.087	11.491	0.06
1-3	2.515	10.391	0.03
1-4	0.85	18	0.407
1-5	0.888	18	0.386
1-6	1.774	18	0.093
1-7	1.027	10.675	0.327
1-8	1.032	18	0.316
1-9	1.676	11.468	0.121
2-3	0.752	15	0.464
2-4	-1.683	18	0.11
2-5	-1.338	18	0.197
2-6	-0.23	18	0.821
2-7	-2.427	17	0.031
2-8	-1.204	13.698	0.249
2-9	-0.83	18	0.417
3-4	-2.04	15	0.059
3-5	-1.612	15	0.128
3-6	-0.825	12.516	0.425
3-7	-3.585	14	0.003
3-8	-1.769	11.646	0.103
3-9	-1.621	15	0.126
4-5	0.109	18	0.914
4-6	1.231	18	0.234
4-7	0.1	17	0.922
4-8	0.278	18	0.784
4-9	1.081	18	0.294
5-6	1	18	0.331
5-7	-0.041	17	0.968
5-8	0.151	18	0.881
5-9	0.814	18	0.426
6-7	-1.426	17	0.172
6-8	-0.866	18	0.398
6-9	-0.393	18	0.699
7-8	0.247	12.228	0.809
7-9	1.458	17	0.163
8-9	0.656	13.66	0.523

CURRICULUM VITAE

Nicole Marie Breedon

Education:

2020- 2022	Master of Arts in Anthropology University of New Brunswick Fredericton, New Brunswick
2016-2018	Completion of Bachelor of Arts (Hons.) in Forensic Science and Anthropology Trent University Peterborough, Ontario
2013-2016	Partial completion of Bachelor of Arts (Hons.) in Anthropology University of Manitoba Winnipeg, Manitoba

Conference Presentations:

Breedon N. 2022. The Bare Bones: Exploring bacterial decomposition in an 18^{th}-19^{th} century Halifax cemetery. Graduate Research Conference, Fredericton, New Brunswick.

Academic Awards:

2021	University of New Brunswick Department of Anthropology Graduate Scholarship - $8, 500
2020	University of New Brunswick Department of Anthropology Graduate Scholarship - $10, 500
2013	University of Manitoba Entrance Scholarship – $1, 000